Investigations of sputtered (Ba,Sr)TiO3 thin films for tunable microwave applications

Lihui Yang

THESE

Présentée à

L'Université de Valenciennes
Et du Hainaut Cambrésis.

Pour obtenir le grade de
Docteur de l'Université

Spécialité : ELECTRONIQUE

Par

Lihui YANG

INVESTIGATIONS OF SPUTTERED $(Ba,Sr)TiO_3$ THIN FILMS FOR TUNABLE MICROWAVE APPLICATIONS

ETUDE DE FILMS DE BST ACCORDABLES DEPOSES PAR PULVERISATION CATHODIQUE POUR DES APPLICATIONS MICRO ONDES

Soutenue le 28 Juin 2010
Devant la commission d'examen :

Rapporteurs

M. R. Plana, Directeur de Recherche LAAS, Toulouse
M. G. Tanné, Professeur, Lab-STICC, BREST

Examinateurs

M. Dong Xianlin, Prof. SICCAS, Directeur de thèse
M. Wang Genshui, Prof. SICCAS, Co-directeur de thèse
M. D. Lippens, Prof. IEMN
M. Velu Gabriel, MdC habilité,
LEMCEL M. Légier Jean-Francois,
MdC IEMN
M. Rémiens Denis, Prof. IEMN – DOAE, Directeur de thèse

Acknowledgements

Since the September of 2007, it was my pleasure to come to the prestigious Institute of Electronics, Microelectronic and Nanotechnology (IEMN) in Villeneuve d'Ascq by the recommendation of my supervisors Prof. Xianlin Dong and Prof. Genshui Wang, and with the help of my supervisor in France Prof. Denis Rémiens, who fought for the fellowship from the French Government for me. During my five years of PhD studies, I have interacted so many people who have offered generous assistances on both emotional and academic states.

First, it is my pleasure to express my deepest gratitude and respect to Prof. Xianlin Dong for his invaluable guidance, helpful suggestions and endless support. His personal and academic virtue shaped my academic personality and changed my approach to scientific study. I am grateful to him for allowing me some freedom to pursue research topics of my own interest. Without his generous help and guidance, I cannot finish my PhD study. I really feel lucky to have the chance to carry out PhD study under his supervision.

At the same time I am profoundly grateful to my supervisor in France Prof. Denis Rémiens for his support, encouragement, interest and trust during the days in France. I have learned a lot not only in academic but also in life from him. Without his generous help, guidance, and discussions, I am sure that I could not finish my dissertation smoothly.

I sincerely wish to acknowledge Prof. Genshui Wang. It is he who introduced me to the field of ferroelectric thin films, and who provided me with a good opportunity to study abroad in order to train myself. He is always caring about me and gives me numerous suggestions and constructive criticisms through mail during the period of my stay in France.

I am also thankful to Prof. Yongling Wang for his supports and instructions on this work. His wide knowledge, serious research attitude and enthusiasm in work deeply impressed me and taught me what a true scientific research should be.

I particularly thank Assoc. Prof. Ruihong Liang for her kind help in arranging my daily life especially at the beginning of my study in France, for her great patience to explain the use of the experimental set-ups, for providing informative literature and helpful discussions and also for her interesting introductions to French culture and folklore.

Many thanks to my colleagues, Dr. Freddy Ponchel and Mr. Jean-Fançois Legier. They provided many helps and suggestions in the microwave measurements and characterizations. Thanks to Mr. Christophe Biyoval and Ms. Sylvie Lepilliet for their assistance in SEM investigations and low temperature measurements.

I would like to thank Ms. Fabis Daniele for generous helps on life issues, including scholarship and lodgment during my stay in France.

I would like to thank former and present members in Prof. D. Rémiens's group, Dr. Caroline Soyer, Dr. Sama Nossikpendou, Dr. Sebastien Quignon, Dr. Jean Midy, Mr. Jean Costecalde, Mr. Correntin Verrue, for various successful collaborations and French language learning.

I also would like to thank previous and current members in Prof. Xianlin Dong's Group, Zhiyong Zhou, Tao Zeng, Shutao Chen, Si Chen Yuanyuan Zhang, Gang Yu, Ningbo Feng, Hengchang Nie, Shuai Zhang, Hongling Zhang, Sheng Cao, Wei Liu, Shaobo Guo, Zheng Huang, Xiuyun Lei, Kui Li, Li Wang, Gang Du and Pierre Guerder for their fruitful supports and friendship.

I also thank to Ling Peng, Hui Liu, Jinlin Gong, Jian Liu, Zhengqiang Li, Nanying Zhao, Luanluan Xue, Ling Shang, Haipo Wang, Shengxiang Wang, Quan Xu, Nan Meng and Qiao Lu, who I met during my study in France. Your friendship is invaluable to me. Moreover, I would like to thank all my other friends, no matter whether old or new, far away or nearby, to offer various helps to me. Thank you all.

I wish to thank the technical personnel at the factory in SICCAS for a vey professional work in machining the ceramics targets used in the experiments.

I would like to thank the members of the Department of Graduate Education, especially Mr. Zhiwei Zhou, Ms. Zeng Tang, Ms. Caifei Lu, Ms. Xueying Zhao, Ms. Huijuan Shao, Ms. Xinhong Lu and all heads at Shanghai Institute of Ceramics for their warmly support and help.

Financial supports from the French Government and Chinese Academy of Sciences are gratefully acknowledged.

Finally, but definitely not the least, great thanks to my family, my father, mother, elder sister for their endless love, unwavering encouragement and care.

Abstract

This thesis discussed the deposition and characterization of perovskite (Ba,Sr)TiO_3 thin films using radio-frequency (RF) magnetron sputtering with the goal of studying the feasibility of fabricating high quality BST films in an economical manner for tunable microwave devices.

We optimized the sputtering parameters to synthesize perfectly (001)-and (111)-oriented $Ba_{0.6}Sr_{0.4}TiO_3$ (BST) thin films directly on Pt(111)/TiO_x/SiO_2/Si substrates without buffer layers and to achieve best possible dielectric properties for tunable microwave devices. The O_2/(Ar+O_2) mixed ratios (OMR) during deposition were found to have significant effects on the crystallographic orientation, microstructure and dielectric properties of the prepared BST films. The samples with OMR=0 % showed perfect (001) orientation, while those with OMR ranging from 10 % to 50 % showed preferential (111) orientation. Electrical measurements showed that high tunability of 52 % and 68 % can be achieved for (001)-and (111)-oriented BST films, respectively, measured at 10 kHz and 400 kV/cm applied field.

The effects of ultrathin TiO_x (0~12 nm) seeding layers on the degree of texturing, surface morphology and dielectric behaviors on BST thin films have also been studied. The ultrathin TiO_x layer was found to act as an initial template for the BST films in the first nucleation stage, resulting in a significant influence on crystalline orientation and electrical characteristics of the resultant BST films. With increasing the TiO_x layer thickness from 0 to 1.2 nm, the orientation of the BST films switched from (001) to (111) preferred orientation, and highly (111)-oriented BST film was obtained as TiO_x layer thickness was ~ 5 nm. As a result, the BST(111)/TiO_x(5 nm) film exhibited a shifted Curie temperature (*Tc*=275 K) and an enhanced tunability of 61.16 % at 400 kV/cm, when compared with (001)-oriented BST without TiO_x layer (*Tc*=250 K and tunability=50.05 %).

It would be desirable for the ferroelectric thin films to have moderate dielectric constant while having low losses in order to obtain high figure of merit, hence

composite thin films of high tunability films such as perfectly BST(111) films with low loss material like $Bi_{1.5}Zn_{1.0}Nb_{1.5}O_7$ (BZN) were prepared. We have therefore studied the effects of thickness of BZN layer on dielectric properties of BST (111) films. It was observed that the BZN layer thicknesses play an important role in improving the dielectric properties. A significant improvement in the figure of merit (~46.8) was obtained for BZN(50 nm)/BST(450 nm) bilayered films at frequency of 10 kHz and 400 kV/cm bias field.

Our studies showed that perfectly BST (111) films on Pt(111)/TiO_x/SiO_2/Si substrates exhibited excellent dielectric properties, which have more advantages for microwave tunable devices application than (001)-oriented BST films. Thus, we further investigated the variations in the permittivity with film thickness and measurement temperature of perfectly BST (111) thin films with thicknesses ranging from 45 to 800nm. Our results revealed that BST (111) films had unusual Curie point independent of thickness, about 305±5 K. A model incorporating a bulk film and an interfacial capacitance was employed to explain the thickness-dependent permittivity at the given temperature.

To test BST thin films for practical purpose, the material should be characterized at microwave frequencies, since tunable devices are operated at in the microwave range (300 MHz to 300 GHz). Epitaxial (111)-oriented BST thin films on Al_2O_3 (0001) substrates have been grown by inserting an ultrathin TiO_x (~1.2 nm) seeding layer. Microwave properties of the epitaxial and polycrystalline BST thin films were evaluated up to 40 GHz. The dielectric dispersion demonstrated that the complex permittivity ($\varepsilon=\varepsilon'-j\varepsilon''$) is well described by a Curie-von Scheidler power law with an exponent of 0.40. Moreover, the high permittivity (~428) combined with a high tunability (~40.88 %, 300 kV/cm) up to 40 GHz suggest that epitaxial (111)-oriented BST thin film could be well suited for tunable microwave devices.

Finally, microwave properties of BZN/BST bilayered thin films directly deposited on high resistivity (HR)-Si substrates toward 50 GHz were also investigated. As expected, the BZN helped in tailoring the dielectric constant and reducing the loss

tangent significantly. The BZN/BST/HR-Si heterostructured films have moderate permittivity (~224), low microwave loss (~0.167) and a high tunability (~7.7 %, 200 kV/cm) until 50 GHz, which demonstrated a great promise application for integration into tunable microwave devices.

Résumé

Cette thèse étudie le dépôt et la caractérisation du (Ba,Sr)TiO_3 en couches minces sous forme pérovskite, en utilisant la pulvérisation cathodique magnétron par radio-fréquences (RF), avec pour but d'étudier la faisabilité de la fabrication de films de BST de haute qualité de manière économique pour des applications dans le domaine des dispositifs micro-ondes accordables.

Nous avons optimisé les paramètres de pulvérisation pour synthétiser parfaitement des couches minces de $Ba_{0.6}Sr_{0.4}TiO_3$ (BST) orientées (001) et (111) directement sur des substrats Pt(111)/TiO_x/SiO_2/Si, sans couche tampon et pour obtenir les meilleures propriétés diélectriques possibles pour les dispositifs micro-ondes accordables. Il a été observé que le taux O_2/(Ar+O_2) (OMR) utilisé pour la pulvérisation avait des effets significatifs sur l'orientation des cristaux, la microstructure et les propriétés diélectriques des films de BST produits. Les échantillons produits avec un OMR de 0 % avaient une orientation (001) parfaite, alors qu'une variation de l'OMR de 10 % à 50 % a favorisé une orientation (111). Les mesures électriques ont permis d'observer qu'une haute accordabilité de 52 % et 68 % pouvait être atteinte pour les films de BST orientés (001) et (111) respectivement, mesurée à 10 kHz par l'application d'un champ de 400 kV/cm.

Nous avons aussi étudié l'effet de couches d'ensemencement ultrafines de TiO_x (0~12 nm) sur l'orientation, la morphologie de la surface et le comportement diélectrique des couches minces de BST. Il a été montré que la couche ultrafine de TiO_x agissait comme un modèle initial pour les films de BST lors du premier stade de nucléation, ce qui résulte en une influence significative sur l'orientation cristalline et les caractéristiques électriques du film de BST résultant. En élevant l'épaisseur de la couche de TiO_x de 0 à 1.2 nm, l'orientation privilégiée des films de BST est passée de (001) à (111), et un film de BST hautement orienté (111) a été obtenu lorsque l'épaisseur de la couche de TiO_x atteignait ~5 nm. En conséquence, le film BST(111)/TiO_x(5 nm) montrait une température de Curie supérieure (Tc=275 K) et

une accordabilité améliorée de 61.16 % à 400 kV/cm, à comparer avec le BST orienté (001) sans couche de TiO_x (*Tc*=250 K et accordabilité de 50.05 %).

Il serait souhaitable que les couches minces ferroélectriques aient une constante diélectrique modérée combinée avec de faibles pertes pour pouvoir obtenir de grandes figures de mérite, d'où la préparation de couches minces composites entre de hautes accordabilités comme celle du film de BST(111) et de faibles pertes comme celle du $Bi_{1.5}Zn_{1.0}Nb_{1.5}O_7$ (BZN). Nous avons donc étudié l'effet de l'épaisseur de la couche de BZN sur les propriétés des films de BST (111). Il a été observé que l'épaisseur de la couche de BZN jouait un rôle important dans l'amélioration des propriétés diélectriques. Une amélioration significative de la figure de mérite (~46.8) a été obtenue pour la double couche BZN (50 nm)/BST(450 nm) à une fréquence de 10 kHz et un champ de 400 kV/cm.

Notre étude a montré que les films de BST parfaitement orientés (111) sur des substrats Pt(111)/TiO_x/SiO_2/Si possédaient d'excellentes propriétés diélectriques, ce qui est plus intéressant pour les applications dans les dispositifs micro-ondes accordables que les films de BST orientés (001). Nous avons donc de plus étudié les variations de la permittivité avec l'épaisseur du film et la température de mesure sur les films de BST parfaitement orientés (111) avec une épaisseur variant de 45 à 800 nm. Nos résultats révèlent que les films BST (111) possèdent une température de Curie inhabituelle et indépendante de l'épaisseur, valant environ 305±5 K. Un modèle incorporant les propriétés intrinsèques d'un film et une capacitance interfaciale a été utilisé pour expliquer la dépendance de la permittivité à l'épaisseur à une température donnée.

Puisque les dispositifs accordables fonctionnent aux fréquences micro-ondes (300 MHz à 300 GHz), il est nécessaire de caractériser le matériau à ces fréquences, pour tester la possibilité d'utiliser les films de BST en pratique. Les couches minces de BST épitaxiales (111) sur des substrats de Al_2O_3 (0001) ont été produites en insérant une couche d'ensemencement ultrafine de TiO_x (~1.2 nm). Les propriétés micro-ondes des couches minces de BST épitaxiales et polycristallines ont été

évaluées jusqu'à 40 GHz. La dispersion diélectrique a montré que la permittivité complexe ($\varepsilon=\varepsilon'-j\varepsilon''$) est bien décrite par une loi de puissance de Curie-von Scheidler avec un exposant de 0.40. De plus, la haute permittivité (~428) combinée avec une haute accordabilité (~40.88 %, 300 kV/cm) jusqu'à 40 GHz suggère que les couches épitaxiales de BST orientées (111) pourraient être adaptées à des applications dans les dispositifs micro-ondes accordables.

Finalement, les propriétés micro-ondes des doubles couches BZN/BST directement placées sur du Si de haute résistivité (HR) ont été également étudiées jusqu'à 50 GHz. Comme attendu, le BZN a aidé à adapter la constante diélectrique et à réduire significativement les pertes tangentielles. Les films hétérostructurés BZN/BST/HR-Si ont une permittivité modérée (~224), de faibles pertes micro-ondes (~0.167) et une haute accordabilité (~7.7 %, 200 kV/cm) jusqu'à 50 GHz, ce qui se révèle prometteur pour l'application dans les dispositifs micro-ondes accordables.

TABLE OF CONTENTS

CHAPTER 1

Introduction

Introduction

The recognition of the potential usefulness of ferroelectric materials in tunable high-frequency devices dates back over 40 years. However, due to various reasons related to both device electronics and materials technology, it is only in the past decade that intensive development efforts are being made in this direction. The main driving force for this resurgent interest is the potential for substantial miniaturization of microwave components and systems (accompanied also by a large cost reduction) and the potential for integration with microelectronic circuits due to the development of thin and thick film ferroelectric technology. The focus of the research work is the development of tunable dielectric materials for frequency agile radio frequency and microwave devices, such as tunable filters, voltage controlled oscillators, varactors, delay lines and phase shifters operating in the microwave regime. Ferroelectrics such as $(Ba,Sr)TiO_3$ (BST) have emerged as leading candidates for such applications due to their highly nonlinear dielectric response to an applied electric field, especially in the vicinity of the paraelectric-to-ferroelectric phase transformation temperature. The major challenge in designing material systems for tunable devices is simultaneous requirements of high tunability coupled with low dielectric loss. A significant effort has been put towards BST materials with the goal of fabricating high quality BST films in an economical manner for tunable microwave device applications.

Among the various techniques available for fabrication, the radio frequency (RF) magnetron sputtering offers an effective way for obtaining high quality films over a wide range of materials with thicknesses up to about 5 μm. It exhibits several important advantages such as high deposition rate, high quality films, ability to coat heat-sensitive substrate and extremely high adhesion of films and this led to the development of a number of commercial applications ranging from microelectronics fabrication through to simple decorative coatings.

Although the BST materials for tunable devices are being developed, many issues regarding BST capacitors should be solved. Since one of the important applications of ferroelectric thin films is to integrate with Si technology, hence

Pt/TiO_x/SiO_2/Si substrate will be a good substrate, in which the Pt also serves as the bottom electrode. However, it will be difficult in controlling orientation of BST on Pt due to the dissimilarity in structure and big lattice mismatch between them. Another, mixing of a low loss dielectric and a ferroelectric result in an overall low loss without deteriorating strongly the tunablity of the composite presents a formidable challenge. The general phenomenon that films often exhibit lower permittivity and tunablity than bulk materials of a similar composition still lacks of investigation. Finally, few reports focus on the evaluations of the performance of the materials at GHz frequency.

In this thesis, we present the details investigations on the microwave dielectric materials, mainly BST and other related materials, deposited by RF magnetron sputtering for tunable microwave applications.

CHAPTER 2

Backgrounds and Literature Review

2.1 Ferroelectrics

2.1.1 Historical Perspective of Ferroelectrics

A subset of polar materials was first observed by Valasek in 1921 in single crystals of Rochelle salt, $KNa(C_4H_4O_6) \cdot 4H_2O$.[1] The hysteretic behavior observed between polarization and applied electric field was analogous to the magnetism verses magnetic field behavior in ferromagnetic materials which were previously understood. Therefore the phenomenon was termed "ferroelectricity." The earliest research identified only two types of ferroelectric materials, tartrates such as Rochelle salt (*e.g.* sodium ammonium tartrate tetrahydrate $NaNH_4(C_4H_4O_6)\cdot 4H_2O$ in 1928[2] and lithium ammonium tartrate monohydrate $LiNH_4(C_4H_4O_6)\cdot H_2O$ in 1951[3]), and potassium dihydrogen phosphate (e.g. KH_2PO_4 in 1935[4]) and its isomorphs (*e.g.* ammonium dihydrogen phosphate $NH_4H_2PO_4$ in 1938[5]). These materials' water solubility made them impractical for use in electronic devices and the ferroelectric phenomenon could only be observed at low temperatures.

In 1940, the first refractory oxide ferroelectric with room temperature ferroelectricity was discovered in the perovskite barium titanate, $BaTiO_3$, by Thurnauer and Deaderick at the American Lava Co.[6] Publication of the high permittivity of $BaTiO_3$ in the open literature came from the U.S.[7,8] and Europe[9,10] in concurrent independent reports and the determination that the high permittivity was due to ferroelectricity in $BaTiO_3$ was given by von Hippel of the Laboratory for Insulation Research at MIT.[11] The discovery of ferroelectric barium titanate represented a breakthrough in ferroelectric research and fueled development of high permittivity devices. Piezoelectric transducers were facilitated by the discovery of the ferroelectric perovskite solid solution lead zirconate titanate, $Pb(Zr,Ti)O_3$ or PZT,[12] and the existence of a temperature independent polymorphic phase boundary at Zr:Ti mole ratios of 52:48.[13] To date, perovskite based ferroelectrics are the mostly widely utilized class of solid-state materials for high capacitance density capacitors and high strain/sensitivity transducers. Despite the large number of publications each year, their potential for commercial electronics is yet to be exhausted.

2.1.2 Phase Transitions in Ferroelectrics

A necessary criterion for classification for ferroelectricity is the existence of a phase transition from a low temperature low symmetry ferroelectric phase to a higher symmetry non-polar paraelectric phase above a transition temperature called the Curie Temperature (T_C). The temperature dependence of permittivity for a ferroelectric is given by Fig. 2.1.

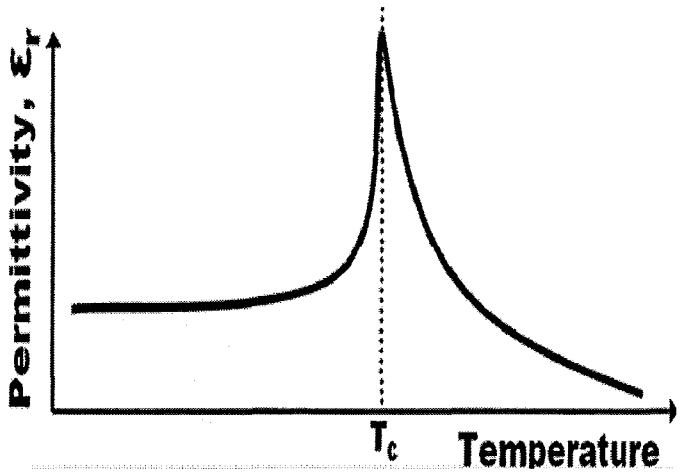

Fig. 2.1. Temperature response of permittivity for a single crystal mono-domain ferroelectric

Above T_C, the permittivity falls off with the temperature according the Curie-Weiss law:

$$\kappa = \frac{\varepsilon}{\varepsilon_0} = \frac{C}{T-\theta}, \tag{2.1}$$

where C is constant, T is temperature, θ is the Curie-Weiss temperature, and ε reaches maximum at T_C, the transition temperature. $\theta=T_C$ and ε declines steeply for $T< T_C$. For 1st order transition $\theta<T_C$ and ε discontinuously decreases at this temperature. For barium titanate, no exact indisputable value for C has been determined yet, all measurements are on the order of 10^5 and the Currie-Weiss temperature θ is typically 10 °C lower than the transition temperature.[14] Curie-Weiss behavior is valid for many other non-linear dielectrics, for example, strontium titanate ($SrTiO_3$), which is considered an incipient ferroelectric since the predicted transition temperature is less

than 0 K. The Curie-Weiss constants have been measured for $SrTiO_3$ to be C slightly less than 10^5 and $\theta \sim 20$ °C. [15,16]

Near and at the transition temperature, T_C, anomalies in dielectric, elastic, optical, and thermal properties are observed. The transitions can be of first or second order. These classifications constitute a transition that occurs discontinuously in first order cases, or smoothly over a range of temperatures in the second order scenario. Both scenarios were modeled by Devonshire in 1954. This phenomenological theory is based on the thermodynamic function for a ferroelectric system. The equations of state for ferroelectric crystals relate the system free energy to polarization based on the influences of temperature, stress and external electric fields. The results of these calculations show that polarization has equivalent minima at $P \neq 0$ at temperatures below T_C supporting the observation of spontaneous polarization. Results of the calculations show for a second order transition the minima slowly collapse toward $P = 0$ yet for a first order transition free energy minima move very little yet a localized reduction of the free energy appears at $P = 0$ and becomes a global minima at $T \geq T_C$.[17] First order ferroelectric transitions are associated with discontinuous changes in polarization, latent heat, and specific heat. Most perovskite oxide ferroelectric show first order transition behavior. Devonshire's description adequately describes the behavior of measured parameters though the phase transition yet a more complete understanding of the physical phenomenon can be proposed using the dynamics of lattice vibrations. The transverse optical vibration mode in perovskites showing displacive transitions is associated with the vibration of the B-site cation and is defined as the "soft mode". As the temperature is lowered from a temperature above the transition temperature this mode decreases in frequency (increases in wavelength) at the Brillouin Zone center at zero wave number.

$$\varpi_{TO}^2 = K(T - T_0), \tag{2.2}$$

Here ω_{TO} is the angular frequency of the transverse optical mode or soft mode, T_0 is the temperature where the frequency of the mode falls to zero, and K is a constant that

determines how fast the frequency falls with T. The non-zero frequency of the soft mode above the transition shows that the cations are free to vibrate around their respective unit cell centers and therefore the time and spatially averaged charge density is located at the unit cell center, thus polarization cannot be supported. As the soft mode frequency falls to zero the mode is frozen and all cations vibrate in phase over a longer distance within the crystal. This can interpreted as an overall spontaneous polarization since at a low enough temperature (where frequency goes to zero, or wavelength goes to infinity) all cations are displaced away from the center of the unit cell at any point in time. The permittivity is a result of the linear combination of all displacements which can be described by all the optic modes at $k = 0$ yet the soft mode contributes the most significantly to the permittivity in ferroelectrics as seen in Eq. (2.3).

$$\varepsilon = \frac{1}{\varpi_S^2}, \tag{2.3}$$

As the temperature is lowered below the transition temperature the soft mode decreases in wavelength leading to vibrations including longer-range coordination of polarizing displacements and the permittivity increases. At the transition temperature the permittivity peaks and spontaneous polarization is supported. If hysteretic behavior is to be avoided then a device can be operated just above the transition temperature while still taking advantage of high permittivity.

2.1.3 Theory of Dielectric Response of Ferroelectrics

Ferroelectrics are known for their high permittivity and high non-linear dielectric response dependent electric field. The typical ε-E curve is shown in Fig. 2.2. The feature of this ε-E curve is called dielectric tunability, which has been widely investigated for potential applications in tunable devices.

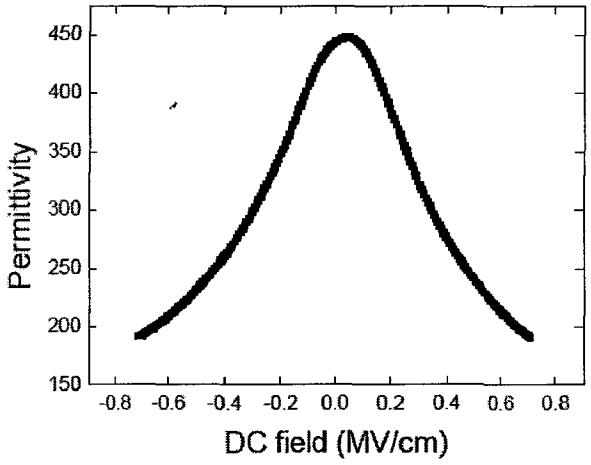

Fig. 2.2. The typical ε-E curve for ferroelectrics

Dielectric permittivity. The origin of the high dielectric permittivity of ferroelectrics in the paraelectric phase is a delicate compensation of various kinds of microscopic forces that maintain the material in a non-poled state in the absence of a microscopic electric field. Because of this compensation, the restoring force opposing the poling action of the applied field is relatively weak. This result in a high dielectric permittvity of the material.[18] In the ferroelectric phase, the newly appeared spontaneous polarization is not very stable either. This makes the dielectric permittivity high in the ferroelectric phase. In addition to this, the permittivity may be further increased by contributions stemming from ferroelectric domains.

The most straightforward description of the dielectric response of ferroelectrics is given by the conventional Landau theory and is based upon an expansion of the Helmholtz free energy F with respect to the vector macroscopic polarization P. For the situation where the polarization is collinear with the macroscopic electric field E in the material, the first two terms of this expansion read:

$$F = \frac{\alpha}{2}P^2 + \frac{\beta}{4}P^4, \tag{2.4}$$

The equation of state $\partial F / \partial P = E$ then leads to a relation between the polarization and electric field:

$$E = \alpha P + \beta P^3, \tag{2.5}$$

Eq. (2.5) enables us to present to the relative dielectric permittivity of the material in the form:

$$\varepsilon = \frac{1}{\varepsilon_0}\frac{\partial P}{\partial E} = \frac{1}{\varepsilon_0}\frac{1}{\alpha + 3\beta P^2} = \varepsilon(0)\frac{1}{1+3\beta\varepsilon(0)\varepsilon_0 P^2}, \tag{2.6}$$

where $\varepsilon(0) = (\varepsilon_0\alpha)^{-1}$ and $\varepsilon_0 = 8.85\times10^{-12} F/m$. This expression describes the dielectric permittivity both in the absence of a bias field and under it. In the first case, one sets P=0 in Eq. (2.6) to obtain:

$$\varepsilon = \varepsilon(0) = \frac{1}{\varepsilon_0\alpha}, \tag{2.7}$$

whereas, for the situation under the bias, one sets P=P_{dc} in Eq. (2.6) (P_{dc} is the polarization induced by the bias field).

According to the Lanau theory, the coefficient of α is assumed to be a linear function of temperature and vanishes at the Curie-Weiss temperature θ, the ferroelectric instability temperature of the material

$$\alpha = \alpha_L = \frac{1}{\varepsilon_0}\frac{T-\theta}{C}, \tag{2.8}$$

An essential feature of displacive ferroelectrics is the typical value of the Curie-Weiss constant C of about 10^5 K. Such a value of C implies high values of the dielectric permittivity even far from the Curie-Weiss temperature.

Tunability. The dependence of the dielectric permittivity on the applied dc bias electric field E_0 can be determined from Eq. (2.6). These are two parameters used for characterization of this dependence: tunability

$$n = \frac{\varepsilon(0)}{\varepsilon(E_0)}, \tag{2.9}$$

and relativity tunability:

$$n_r = \frac{\varepsilon(0) - \varepsilon(E_0)}{\varepsilon(0)} = \frac{n-1}{n}, \tag{2.10}$$

The aforementioned trend — the higher permittivity $\varepsilon(0)$, the higher the tunability (for a given value of the bias field E_0) can be clearly traced. In the limit of weak nonlinearly, i.e. at $n_r<<1$, this trend is really strong. Indeed, in this case, according to (2.6), we have:

$$n = \frac{\varepsilon(0)}{\varepsilon(E_0)} = 1 + 3\beta\varepsilon(0)\varepsilon_0 P_{dc}^2 \approx 1 + 3\beta(\varepsilon(0)\varepsilon_0)^3 E_0^2, \tag{2.11}$$

That means that the relative tunability is a very fast function of $\varepsilon(0)$, specifically, $n_r \propto \varepsilon(0)^3$. With increasing bias fields this dependence slows down. In the limit of ultrahigh fields where $n >> 1$, one readily finds $\varepsilon(E_0) \approx \beta^{-1/3} E_0^{-2/3}/(3\varepsilon_0)$. This implies $n \propto \varepsilon(0)$. It is instructive to give an expression for the field E_n needed to achieve a given tunability n:

$$En = \frac{\sqrt{n-1}(2+n)}{\varepsilon_0\sqrt{27\beta\varepsilon_0}} \frac{1}{\varepsilon(0)^{3/2}}, \tag{2.12}$$

Thus, it is seen that a high dielectric permittivity of the material is really essential for its tunable behavior.

For the description of the dielectric non-linearity at an arbitrary dc field, one can use Eq. (2.6) where the polarization P is calculated from the solution of cubic Eq. (2.5). A convenient form for calculation of the dependence of the permittivity on the dc bias field has been suggested by Vendik:[19]

$$\varepsilon(T, E_0) = \frac{\varepsilon_{00}}{[(\xi^2 + \eta^3)^{1/2} + \xi]^{2/3} + [(\xi^2 + \eta^3)^{1/2} - \xi]^{2/3} - \eta}, \tag{2.13}$$

$$\varepsilon_{00} = \frac{T}{\theta}; \quad \eta = \varepsilon_{00}\alpha\varepsilon_0;$$

$$\xi = \xi_B = \frac{E_0}{E_N}; \tag{2.14}$$

$$E_N = \frac{2}{\sqrt{27\beta\varepsilon_{00}^3}}.$$

The field dependence of dielectric permittivity discussed above is illustrated in Fig. 2.3 for two values of $\varepsilon(0)$ and the value of $\beta = 8 \times 10^9$ JC^{-4} m^{-5} (typical for $SrTiO_3$). The regimes of small and high tunability are shown together with the asymptotic dependences of $\varepsilon(E)$ in these regimes.

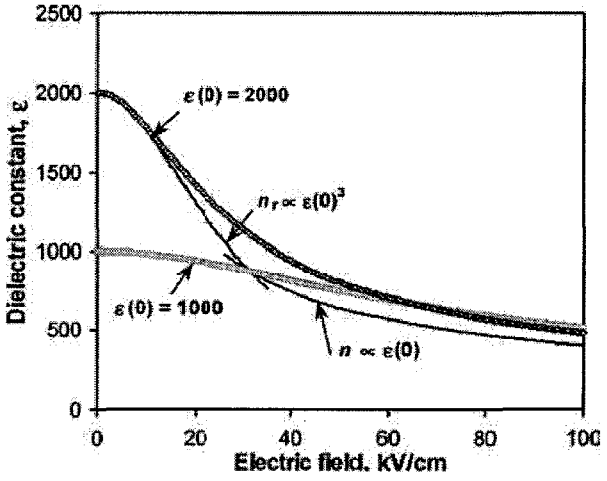

Fig. 2.3. Field dependence of the dielectric permittivity according to Eq. (2.13) plotted for $\beta = 8\times10^9$ JC^{-4} m^5 and for the values of $\varepsilon(0)$ 2000 and 1000. The regimes of small and high tunability are shown together with the asymptotic dependences of $\varepsilon(E)$ in these regions

Dielectric loss tangent. Of equal importance to the tunability is dielectric loss tangent. The reduction of loss tangent is the central motivation for choosing a paraelectric phase. All losses can be divided into intrinsic losses or extrinsic origins. Intrinsic loss is due to the interaction of the AC field with the lattice vibrations, or phonons, present in the material. Extrinsic loss arises from interactions of the electric field with defects. These defects can not be avoided entirely and can be exacerbated by the processing, stoichiometry and microstructure. The following discussion follows the concepts outlined in extensive reviews on the subject for displacive ferroelectric materials.[18,20-22]

Intrinsic contributions to loss involve the interaction of phonons, typically the transverse optical lattice vibrations of the soft mode, of frequency, ω_{TO}, with the

oscillating electric field of frequency, ω. For displacive ferroelectrics in the paraelectric phase there is a large disparity in frequency between the soft mode and electric field frequencies. Conservation laws are difficult to satisfy when $\omega_{TO}>>\omega$ and only three types of interactions are likely to occur and contribute to loss: 3-quantum, 4-quantum, and quasi-Debye interactions. For a two-phonon mechanism, interactions with an oscillation field can only occur when the two phonon differ very little in frequency; a situation which only occurs when there is degeneracy between the various branches of the soft mode. This degeneracy arises from the centro-symmetric symmetry associated with the paraelectric phase. The function dependence of loss with respect to ω, T, ε for a displacive ferroelectric in the paraelectric phase is given below:

$$\tan\delta \equiv \frac{\varepsilon''}{\varepsilon'} \propto \varpi T^2 \varepsilon^{3/2}, \tag{2.15}$$

Figure 2.4 shows actual data for $SrTiO_3$ measured at high frequency. In this case, the reduction in permittivity as temperature increases from 0 K causes a drop in loss tangent via the $\varepsilon^{3/2}$ dependence. Above 150 K, the loss begins to increase, and is associated with the T^2 dependency in Eq. (2.15).

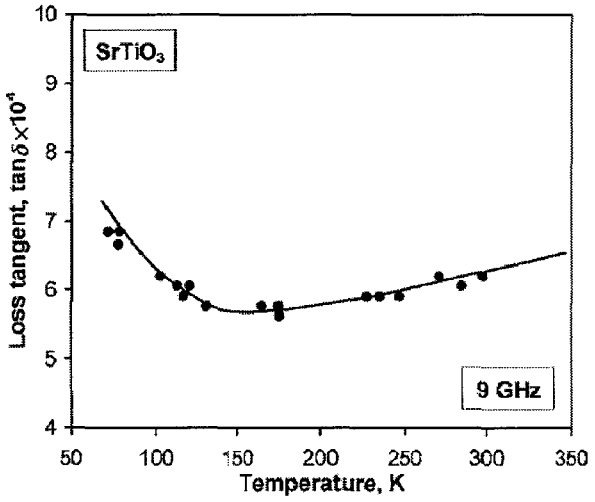

Fig. 2.4. Experimental data for the temperature dependence the 3-quantum loss mechanism in $SrTiO_3$. Figure is adapted from Tagantsev *et al.* [18] based on data from Buzin.[23]

Conservation laws are less restrictive and insensitive to crystal symmetry when 3 phonons interact with an electric field. In the high temperature limit $T \geq \hbar\omega_{TO}K_B^{-1}$, which is valid at near and above room temperature, the functional dependence of this mechanism is identical to Eq. (2.15) yet the magnitude is smaller than the 3-quantum (or two phonon) case. The quasi-Debye mechanism is only valid for non-centrosymmetric crystals and operates in paraelectric crystals only when the electric field induces dipoles and crystal distortions. When the electric field is applied, a phonon dispersion relaxation occurs and the phonon distribution deviates from the equilibrium value. The dependence is a complex function depending on the phonon damping constant, the amount of electric field applied to break the centrosymmetric symmetry, and exact phonon distribution. In the case of a displacive ferroelectric the contribution is an order of magnitude greater than 3 and 4 quantum mechanisms. Figure 2.5 (b) shows the results of a quasi-Debye calculation of loss verses applied biasing field and AC field frequency.

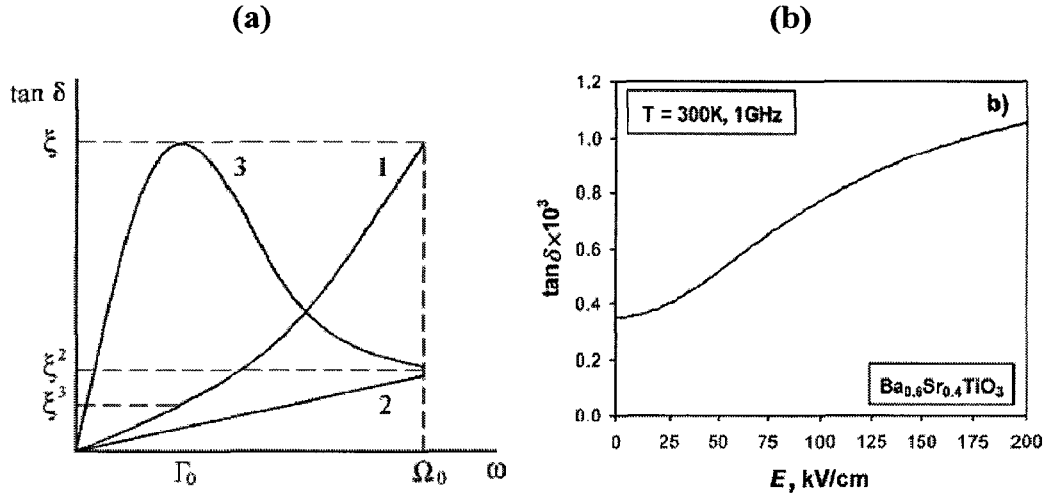

Fig. 2.5. Figure adapted from Tagantsev *et al.*[18] Plot a) gives a schematic comparison between 1) 3 quantum interactions, 2) 4 quantum interactions and 3) quasi-Debye contributions to loss. Plot b) gives the calculated functional dependence and magnitude of the quasi-Debye loss for paraelectric $Ba_{0.6}Sr_{0.4}TiO_3$ tested at 300 K and 1 GHz (actual data from Sengupta *et al.* [24])

Figure 2.5 (a) gives a comparison of the pertinent intrinsic loss mechanisms for a paraelectric material. The overall intrinsic loss the linear superposition of all

significant mechanisms and therefore the intrinsic loss of these materials should be no greater than $\tan\delta \sim 10^2$.

The losses typically measured in ferroelectric crystals is often an order of magnitude or greater than the expected intrinsic values. This disparity can be attributed to extrinsic sources. Extrinsic losses include those caused by charged defects, quasi-Debye losses incurred by the random local polar regions caused by defects, structural imperfections, and microstructure, and those based on universal relaxation. Entropic considerations and limitations of processing of electroceramic materials predicts finite point defect concentrations which by necessity exist in equilibrium with compensating electronic and ionic charge carriers. These defects routinely occur in the ppm to ppt level. Additionally, the purity levels of raw materials impart substantial concentrations of isovalent and aliovalent impurity cations and anions. The discrete and often mobile charges associated with impurities also contribute to losses in paraelectric materials. These losses increase according to the square of the electro-active defect's charge and directly proportional to their number density in the lattice.

$$\tan\delta \propto Z^2 N_{defects}, \tag{2.16}$$

This loss mechanism increases proportionally with the permittivity thus complicating the optimization for high tunability and low loss yet in paraelectric materials the permittivity quickly drops with the application of an electric biasing field.

$$\tan\delta \propto \varepsilon \propto 1/E, \tag{2.17}$$

This allows identification of different regions in the characteristic ε-E curve for a paraelectric crystal. At low bias fields the loss is dominated by extrinsic effects that are present in real materials and the high field regions show intrinsic permittivity and loss from intrinsic mechanisms. Structural defects such as planar defects (i.e. surfaces, grain boundaries, stacking faults, twinning, etc.), line defects (i.e. dislocations), and neutral point defects can impart localized regions which assume polar characteristics. These randomly distributed and aligned polar regions reduce local symmetry and

therefore lead to quasi-Debye losses. The loss mechanism is identical as described above yet they are caused by extrinsic defect and hence considered an extrinsic loss mechanism. This loss also contributes mainly to the high permittivity region of a ε-E curve following the following relation where $<P_{loc}>$ is the average polarization of the polar regions in the material.

$$\tan\delta \propto \varepsilon^{3/2} < P_{loc}^2 >, \tag{2.18}$$

At microwave frequencies between 10^1-10^2 GHz the ionic mechanism responsible for the high permittivity can relax. Little theory has been established on exactly what frequency this should occur and much of the knowledge about this relaxation is gleaned experimentally.[25] In most experimentally observed samples, the extrinsic losses dominate thus obfuscate the onset of relaxation in the microwave frequency regime.

Figure of Merit (FOM). For tuning applications, both tunability and tan δ must be considered when comparing the relative merits of different film compositions and varactor configurations. A figure of merit, K, is given by:

$$\text{K=tunability/tan } \delta, \tag{2.19}$$

Where tan δ is measured under zero dc bias.

For high frequency tunable device such as phase shifter, high permittivity is not desired due to the device impedance matching purposes, which lead to less efficient power transfers in the device and thereby degrading the device performance. Thus, it is important to select materials with low microwave loss and high dielectric tunability, so that the figure of merit is high. Also, other desirable material's characteristics are high breakdown voltage and low water absorption, which are a function of density.

2.1.4 Ferroelectric Thin Films

Ferroelectric ceramic bulk and single crystal materials have found a wide application in electronic industry over the past 50 years due to their unique properties such as high dielectric constants, high piezoelectric constants, and electromechanical

coupling, high pyroelectric coefficient. They have been used as capacitors, sonar and ultrasonic transducers, communication filters, positive temperature coefficient (PTC) sensors and switches.[26]

Over the past 20 years, ferroelectric thin films have been extensively investigated for their potential applications in devices such as dynamic random access memory (DRAM)[27-30], non-volatile ferroelectric memory [27,29, 31-34],and microelectromechanical systems (MEMS)[35], ferroelectric varactors, phase shifters, tunable filters, and voltage-controlled oscillators[27]. A conventional DRAM comprises a transistor connected to an integrated capacitor. The capacitor occupies most of the space of a DRAM. Replacing the existing dielectric silicon dioxide (ε=4) in capacitor with ferroelectric thin film (ε>100) can significantly reduce the size of capacitor and the DRAM. Barium strontium titanate is considered the best dielectric material for DRAM.[27-31] NVFRAM can make use of the property of tunable remnant polarization of ferroelectric thin film. NVFRAM is expected to compete strongly with electrically erasable programmable read-only memory (EFPROM) and magnetic storage media on account of their fast switching speed (less than 6.5 ns) and low powder requirement[27,34]. The main ferroelectric candidates for NVFRAM are lead zirconate titanate (PZT), and strontium bismuth tantalite (SBT).[27,29,31-34,36]

Since the 1980s, several techniques have been developed to deposit ferroelectric thin films. These methods can be classified into three types:

- Physical vapor deposition (PVD), *e.g.* RF magnetron sputtering[36] and pulsed laser deposition (PLD).[33]
- Chemical vapor deposition (CVD), *e.g.* metal-organic chemical vapor deposition (MOCVD).[29,37]
- Chemical solution deposition, *e.g.* Sol-gel.[38]

The advantages and disadvantages of these techniques are summarized in Table 2.1.

Table 2.1 Advantages and disadvantages of conventional thin film techniques

Method	Advantages	Disadvantages
PVD	High quality thin film	Costly equipment
(Sputtering, PLD)	Epitaxial thin film	Lattice defects
	CMOS compatible	High temperature
CVD	High deposition rate	Costly equipment
(MOCVD)	Scalability	Precursor availability
	CMOS compatible	High temperature
CSD	Composition control	Scalability
(Sol-gel)	Low cost	Undeveloped for industry
	Substrates in any shape	High temperature

2.1.5 Applications of Ferroelectric Thin Films in Tunable Devices

The strong renewed interest in tunable dielectrics for microwave applications has been promoted by the recent expansion in microwave communications. Ferroelectric thin films, demonstrate a spontaneous electric polarization at temperatures below a critical value known as the Curie temperature. It is desirable to operate devices slightly above this temperature, where the dielectric constant is high, dielectric loss are comparatively lower, and hysteresis effects are less pronounced. In the sub-Curie temperature region of operation, these ferroelectrics exhibit a dielectric non-linearity with the apply of a dc electric field (i.e. dielectric permittivity can be fast controlled by electric bias field).[39,40] This feature makes them particularly attractive for use as frequency agile tunable microwave electronic components, including phase shifters, varactors, tunable filters, and antennas.

Microwave ferroelectric phase shifters are the most widely studied tunable ferroelectric components. Their importance stems from the role they could play in phased array antennas. A phased array antenna consists of thousands of radiating elements which should be served by thousands of phase shifters. The phase shifters

are used to modify and control the width and angle of the steered radar beam. At present, each phase shifter is a housed microwave semiconductor module. The use of ferroelectric films enables the integration of the phase shifters with the microwave circuits on one substrate thus substantially reducing the size, mass, and cost of the antennas. A simple coplanar line structure patterned on a ferroelectric thin film coated substrate makes a phase shifter [Fig. 2.6 (a)] in which the phase velocity of the electromagneticwave that passes through the line is controlled by the applied dc electric field, U_{dc} (via changing the permittivity of the film, which in turn controls the wave velocity).[41] It is also possible to tune the phase velocity of the electromagnetic wave passed through the coplanar line by loading this line with tunable ferroelectric capacitors (by contrast to the previous case where the coplanar line is homogeneously loaded with a ferroelectric film).[42]

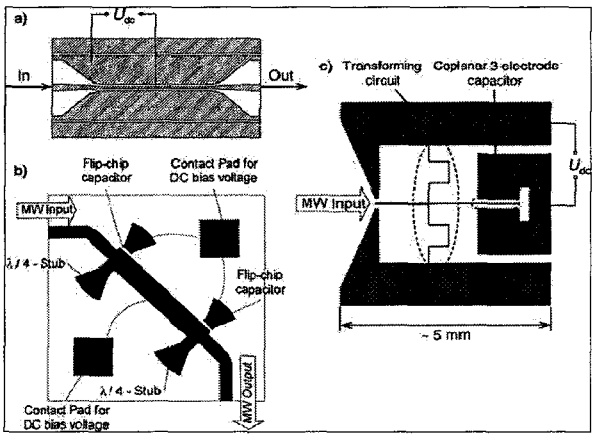

Fig. 2.6. Ferroelectric microwave phase shifters: (a) Coplanar line analog phase shifter [41], (b) Periodically loaded line phase shifter,[40] (c) Reflection type digital phase shifter. [39]

Another possibility is the so-called digital phase shifter which is used only at two values of the tuning voltage providing a fixed phase shift (e.g. 45° or 90°). Examples of this kind of phase shifters are presented in Figs. 2.6 (b) and (c). Fig. 2.6 (b) shows a layout of a periodically loaded line digital phase shifter with two planar capacitors connected in parallel to the line as flip chip elements.[41] Another solution is presented in Fig. 2.6 (c) [39] showing a phase shifter that consists of a transforming circuit that is terminated by a coplanar 3-electrode capacitor. The advantage of the digital phase

shifters compared to those based on the simple coplanar line is that the former can be better optimized. Namely, better impedance matching with the 50 Ω external wave impedance and lower amplitude modulation distortions at switching can be reached in the digital phase shifters.

The Figure of Merit (F_{ph}) of microwave phase shifters is the ratio of the phase shift produced by the phase shifter ($\Delta\varphi_{ph}$) to its insertion loss (L_{dB}). The upper bound of the figure of Merit F_{ph} for an optimally designed one-bit digital phase shifter (not taking into account conductor and interconnections losses) can be determined as:[40]

$$F_{ph}^{max} = 6.6\frac{\Delta\varphi/2}{\sin(\Delta\varphi/2)}\sqrt{K}, \qquad (2.20)$$

where K is the commutation quality factor of the ferroelectric capacitor used in the circuit and φ is the desired phase shift. Values of F_{ph} in the range of 30–100 (for frequencies of 1–30 GHz) were reported[39,41-43], for phase shifters based on ferroelectric films with tunability 1.5-2, loss tangent 0.02-0.05, and with copper or gold as the conducting layers.

2.2 Suitable Materials for Tunable Applications

The perovskite family provides the suitable materials for tunable microwave dielectrics, *e.g.* $SrTiO_3$ (STO), $KTaO_3$, $CaTiO_3$, and several solid solutions, *e.g.* (Ba,Sr)TiO_3, (Pb,Sr)TiO_3 etc. and their doped and modified compositions (for the frequency and field agile microwave electronics). Table 2.2 lists some of commonly used and potential ferroelectric materials for such applications and their characteristics. Electrically tunable microwave components based on the thin films of STO and BST have been demonstrated in past few years.[44,45] Much work on tunable microwave devices has been done using the STO thin film, which requires cryogenic operation.[46] The STO films show tunable characteristics at large field at room temperature.[47] Thus for room temperature application, BST and related thin films are preferred. Properties and literature survey of commonly studied BST, and another possible candidate material, $Bi_{1.5}Zn_{1.0}Nb_{1.5}O_7$, are presented in the next section.

Table 2.2 Properties of most commonly used and potential ferroelectrics.

Material	Structure	Working temp	Dielectric Permittivity	Dielectric loss	Tunability	Remarks
Materials Currently used						
$SrTiO_3$	Perovskite	4~100K	~20,000 (~2,000 in film)	$\sim 10^{-4}$ (10^{-2}~10^{-3} in film)	95% (79% in film)	FOM ~200(~20 in film); incipient ferroelectric; 110 K phase transition.
$Sr_{1-x}Ba_xTiO_3$, e.g. (x=0.5)	Perovskite (solid solution)	RT	~2,000 (~200 in film)	$\sim 10^{-2}$ (10^{-2}~10^{-3} in film)	87% (50% in film)	Property varies by composition; Oxygen deficiency; large temp dependency.
Candidate FE materials						
$KTaO_3$	Perovskite	4~100K	~4,500 (4.2K, 10kHz)	10^{-3}~10^{-4}	~63%	Highly suitable for liquid phase epitaxy; incipient ferroelectric; no twinning or ferroic transitions; better control of stoichiometry
$K(Ta_{1-x}Nb_x)O_3$, e.g., x~0.35	Perovskite (solid solution)	RT	~240 at RT (~200 in film)	10^{-2}~10^{-3}	-	Stoichiometric film can be made; LPE and lift-off tech useful.
$(Sr_xBa_{1-x}Nb_2)O_6$, e.g., x~0.5	Tungsten Bronze solid solution	<400K	300-500 (at 100 MHz)	10^{-2}~10^{-3}	-	Film can be made; LPE suitable; high quality material synthesis is possible
$(Ba_{2-x}Sr_xK_{1-y}Na_yNb_5)O_{15}$, (BSKNN)	Tungsten Bronze solid solution	<470K	100-600 (at 100 kHz)	10^{-3}	-	Interesting and high performance compositions

2.2.1 Fundamentals of $Ba_xSr_{1-x}TiO_3$ Material Properties

The solid solution of barium strontium titanate has been studied intensively in past years for its potential application in novel electronic devices. $Ba_xSr_{1-x}TiO_3$ (BST) undergoes a ferroelectric phase transition at Curie temperature (T_C) that depends on the Ba:Sr ratio.[48] The phase diagram of BST solid solution is shown in Fig. 2.7.

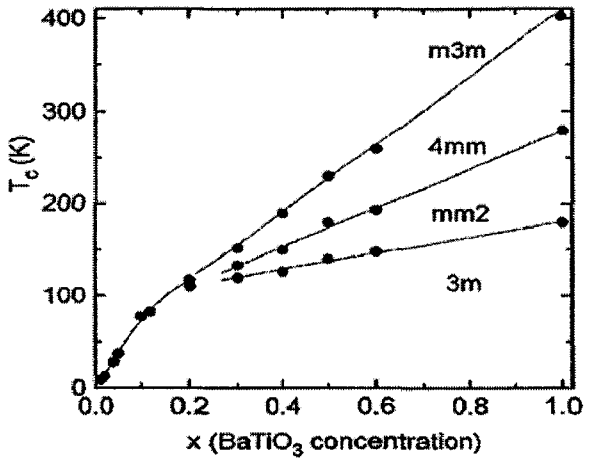

Fig. 2.7. Phase diagram of $BaTiO_3$-$SrTiO_3$ system[49]

Below T_C, BST is true ferroelectric (FE) with re-orientable, spontaneous polarization. BST exhibits a large electric field dependent dielectric constant (tunability).[50] It is well known that the tunability is enhanced for BST in the FE phase (below and near T_C), however, the dielectric losses are usually higher below the T_C, due to domain and wall motion in FE phase. For the tunable microwave devices applications in paraelectric region, just above the Curie point is preferable, where the dielectric constant is high, dielectric loss are comparatively lower, and hysteresis effects are less pronounced. $Ba_xSr_{1-x}TiO_3$ with Ba content x~0.5 is used in the development of microstrip phase shifters, which has a Curie point just below 0°C, which allows normal operation above the Curie point in the paraelectric region.

2.2.1.1 Bulk $Ba_xSr_{1-x}TiO_3$

Towards the goal of affordable high performance electronic beam steering of antennas at microwave frequencies, FE materials such as BST have been of recent

interest. In particular, the composition-dependent T_C and the non-linear field dependent dielectric permittivity of BST make it attractive for tunable devices, such as voltage-controlled oscillators, tunable filters, and phase shifters[51,52]. Phase shifters using BST, which has high tunability, low loss tangent, and high power handling capability, are promising as a replacement for traditional ferrite and semiconductor device phase shifters. Conventionally, BST is used as a bulk material to form the entire substrate that results in high control voltages[53]. Flaviis *et al.* used BST ceramics in ferroelectric microstrip based phase shifter and demonstrated a phase shifter of 165° with the reduced required voltage to change dielectric constant and losses below 3 dB at 2.4 GHz[53]. In the effort of improving properties of BST, Chen *et al.*[54] prepared BST (x=0.6) composite ceramics with non-ferroelectric low loss materials (Mg_2SiO_4, MgO) and showed the improvement in dielectric constant and loss tangent.

There are several disadvantages of using bulk ceramics in high frequency applications. In general, very high voltages are required to apply large electric fields in the material and additionally bulk based devices are heavy. From the point of view of device integration, as well as the ability to achieve substantial fields with reasonable applied voltages, incorporation of BST in thin film form to the microwave components is rather desirable.

2.2.1.2 $Ba_xSr_{1-x}TiO_3$ Thin Films

In the last few years, thin films of ferroelectric materials have attracted attention because of their potential applications in microwave components. The integration of thin films is necessary not only to reduce size and weight of the devices, but also to have configurations that are compatible with existing planar microwave circuits. Thin films offer additional advantage over bulk materials for the high frequency applications, since large electric field (0-200 kV/cm) can be applied in thin films (~0.5 um) using low bias voltages (0-10 V). Although much research has been done to develop BST thin films for tunable microwave dielectric devices, but high dielectric losses and low tunability of these films at high frequencies have restricted its practical

application. It remains a challenge to synthesize the thin film with higher dielectric tunability, moderate dielectric constant and low loss tangent. Development of BST thin film of suitable compositions having the above stringent properties will permit the development of low-cost phase shifters, tunable oscillators, and tunable filters.

The dielectric and ferroelectric properties of $Ba_xSr_{1-x}TiO_3$ are known to depend dramatically on the film composition. For microwave applications, large dielectric tunability and low dielectric loss tangent are the two critical parameters needed for optimal device performance. The choice of Ba/Sr ratio in the $Ba_xSr_{1-x}TiO_3$ films for microwave applications depends on the intended temperature of operation of the device. As mentioned before, the Curie temperature of the $Ba_xSr_{1-x}TiO_3$ system changes linearly with Sr contents on $BaTiO_3$. Among the $Ba_xSr_{1-x}TiO_3$ films, compositions with $0.4 \leq x \leq 0.6$ are the compositions studied by most of the researchers[55,56] for room temperature tunable dielectric applications as their T_C lies around room temperature. Moreover, modifications to the structure and properties of $Ba_xSr_{1-x}TiO_3$ thin films can also be done by fabricating thin films with different compositional layers.[57,58] If the multilayer film has smooth chemical gradients normal to the substrate, it is called a compositionally graded $Ba_xSr_{1-x}TiO_3$ thin film. Mantese and co-workers have reported on the fabrication and characterization of compositionally graded BST thin films.[59,60] According to their observations, graded $Ba_xSr_{1-x}TiO_3$ thin films have demonstrated new and interesting properties like polarization offset, charge pumping effects etc. The most important advantage of compositionally graded BST thin film is the superior temperature stability of its dielectric properties.

Degree of orientation of the films was also found to affect the dielectric properties of $Ba_xSr_{1-x}TiO_3$ films. For example, Carter *et al.* showed that parallel-plate varactors of highly (100) oriented BST (x=0.8) layers (0.5-μm-thick) fabricated by PLD have a 40 % tunability with five volts dc bias at 2 GHz, and tan δ values from 0.067 to 0.10.[61] Wang *et al.*[62] fabricated (111) oriented BST (x=0.6) films on Pt/Si(001) substrate by RF magnetron sputtering and showed high tunability of 49.4 %, at 455

kV/cm. To achieve high tunability and low loss tangent, the FE thin films are usually grown on epitaxially on single crystalline substrates with low dielectric constant and dielectric loss, such as $LaAlO_3$ (LAO) (ε_r=25, tan δ=6×10^{-5}) and MgO (ε_r=9.5, tan δ=3.3×10^{-5}). Epitaxial films are typically comprised of 50-70 nm grains that are epitaxially oriented relative to the substrate and have very smooth surfaces, with RMS roughnesses 0.3-0.5 nm.[47,63] C. L. Chen *et al.* observed high dielectric constant, high tunability and low losses in PLD grown epitaxial thin films, which suggested that epitaxial films can improve the dielectric properties of the films for room temperature tunable microwave elements.[56] However, it is not easy to grow epitaxial BST films onto substrates with large lattice mismatch, such as MgO (6.4 % between MgO and BST60). Chen *et al.*[64,65] and Gao *et al.*[66] have examined the interface between epitaxial BST(x=0.6) films on MgO and LAO substrates. As grown films on MgO had high degree of orientation and crystallinity with flat sharp interface, many period edge dislocations were observed,[67] which indicated that the lattice mismatch strains were completely released at the interface with such dislocations. Twins exist in LAO substrate surface, which were found beneficial to release the strain energy between the BST film and LAO substrate,[66] so that the total energy in this system can be reduced during film growth. The tunability of BST films strongly depends on the state of the strain that arises from the lattice parameter mismatch between film and the substrate. To improve the epitaxial quality of the BST thin films, post-annealing process is usually required. Deposition of ferroelectric films directly on dielectric substrates (such as LAO) also enables the additional option of post-annealing the films at higher temperatures. Al-Shareef *et al.* and Raymond *et al.*[68,69] demonstrated that increasing the post-annealing temperature of BST and STO films to 1100 °C caused substantial increases in grain size and tunability.

In case of epitaxial films, it has been demonstrated that the microwave properties of BST films are greatly affected by the stress and strain. Knauss *et al.*[70] demonstrated that post-annealing BST thin films on LAO substrate at 900 °C substantially decreased strain in the films, which led to higher tunabilities, and the permittivity

versus temperature profiles which more closely resembled bulk behavior. The tunability in that case increased from 20 % to 32 % for BST (x=0.35) films on LAO substrates after annealing treatment.[70] Carlson *et al.*[55] reported that annealing the film at higher temperatures relaxes the residual compressive stresses and thereby improve tunability from 36 % to 52 % of BST (x=0.60) film deposited on LAO substrate. Kim *et al.* measured the microwave properties of BST (x=0.40) films on MgO substrate at 10 GHz and showed that the tunability and figure of merit increased to 50 % and 7, respectively, when stress in the film was minimum.[71] Chang *et al.* observed reduction in the dielectric constant and losses by using an optimized buffer layer between the film and the substrate to reduce (or relieve) strain in the BST film due to lattice mismatch.[72]

Doping has been found to have a significant effect on the microwave dielectric properties of the $Ba_xSr_{1-x}TiO_3$ thin films. Acceptor ions (such as Fe^{3+}, Mn^{2+}, Mn^{3+}) provide electron traps, but they may cause oxygen vacancies and holes to compensate their effective negative charge, whereas donor ion (such as W^{6+}) reduce the oxygen vacancies, but they may generate (Ba,Sr) vacancies and free electrons to compensate their effective positive charge.[73] Several researchers have shown that the addition of some dopants (with small concentrations) such as Fe^{3+}, Mn^{2+}, Mg^{2+},Ni^{2+}, and La^{2+} could dramatically reduce the dielectric loss tangents of the BST thin films.[74-76] Usually it has been observed that with the reduction in the losses of the BST thin films is accompanied by the reduction in tunability. Kim *et al.* observed that with 1 mol % Ni-doped BST thin films tunability and losses were reduced to 54.2 %, and 0.0183, respectively as compared to 63 % and 0.0275 that in pure BST film, so that FOM of 1 mol % Ni-doped film was 30 as compared 23 for pure BST film measured at 100 kHz.[77] Up to 5 mol % Mg doping in BST (x=0.6) films Joshi *et al.* observed the reduction in tunability to 17.2 % and losses to 0.007 as compared to 28 % and 0.013 for pure BST on Pt substrates.[75] With further Mg doping the losses increased as observed in case of La doping. Cole *et al.* prepared 1, 5, and 10 mol % La doped BST (x=0.6) films.[78] Among those films, 1 mol % La doped film showed lowest losses of

0.019 with 19 % tuning, and with further increase in dopant concentration tunability decreased drastically and losses were increased.[78]

Recently, there have been a few efforts of introducing low loss materials like MgO, Al_2O_3 to make high quality composite thin films. For example, Chong *et al.* prepared doped $Ba_{0.5}Sr_{0.5}TiO_3$ targets with 10-40 % Al_2O_3 and deposited the thin film by PLD technique.[79] With the increase in the Al_2O_3 contents in the target, dielectric constant, dielectric loss, and tunability was found to decrease and reached to 870, 0.11, and 15.9 respectively for 40 % doped BST films measured at 7.7 GHz. The FOM increased from 7.33 for pure BST to 14.15 for 40 % Al_2O_3 doped BST film. Lee *et al.*[80] observed dielectric constant and loss tangent of 5 mol % MgO doped BST (x=0.7) films deposited by RF sputtering were 372 and 0.0037 as compared to 329 and 0.011 (at 100 kHz) for the pure BST films grown on Pt/TiN/SiO_2 coated on Al_2O_3 substrates. Considering the trade off between dielectric tunability and the values of dielectric losses, dielectric constant, and film resistivity $\tan\delta = [\rho\omega\varepsilon_0\varepsilon_r]^{-1}$, where ρ is the resistivity, and ε_r is the relative permittivity,[81] the concentrations of the dopants must be optimized to obtain the best overall properties for use in the tunable device applications. Few results are summarized in Table 2.3.

These results show that high quality thin films are obtained depend on the details of growth technique. In addition, good dielectric and insulating properties are not standalone requirements, other material properties, such as bottom electrodes, film thickness, and nature of the film-substrate interface properties etc. are also reported to influence device performance and long term reliability. To fully evaluate and understand the properties, the influence of growth conditions on the microstructural, surface morphological, and properties must be assessed and correlated with the film's dielectric and insulating properties. Moreover, most of the measurements are only done at low frequency regime. The dielectric properties of these films at microwave frequencies have rarely been reported, however in most of these studies, it was tacitly been assumed that the high frequency behavior would resemble the trend of low frequency behavior of these films. With the concept of using FE films for tunable

microwave devices, the practical implementation requires the ability to fabricate high-quality thin films and the demonstration that the microwave dielectric properties of thin films are attractive.

Table 2.3. Review of pure, doped and composite BST thin films.

	BST composition/ Substrate	Tech.	Freq.	ε	Tunability (%) (E. Field)	Loss	K-factor	Phase shift (field in kV/cm)	FOM (PS°)
Pure BST thin films	BST60 on MgO	PLD	1MHz	2290	65 (57kV/cm)	-	-	-	-
	-do-		30GHz	-	-			-	43°/dB
	BST60 on LAO		1MHz	4660	52 (57 kV/cm)	-	-		-
	BST 50 on LAO	PLD	1MHz	1430	33 (23.3 kV/cm)	0.007	47	-	-
	BST50 on LAO	PLD	100 MHz	-	42 (80 kV/cm)	0.008	52.5	-	-
	BST60 on MgO	PLD	1MHz	2000	47 (30 kV/cm)	0.008	58.7	-	-
			23.67GHz	-	-	<5dB	-	250° (400)	53°/dB
	BST70	MOCVD	50 MHz	-	60 (0.175)	~0.004	-		-
	BST40 on Pt/Si	Polymeric precursor	100 kHz	680	-	0.01	-	-	-
	BST80 on Pt/Si			749	-	0.04	-	-	-
	BST80 on LAO	Sol-gel	1MHz	4000	-	0.018	-	-	
	BST70 on LAO			-	-	-	-	-	-
	BST60 on LAO			3800	46.9 (80 kV/cm)	0.008	55	-	
	BST50 on LAO			3500		0.009	-	-	
	Compositionally graded BST with BT-BST70/Pt/Si	Sol-gel	100 kHz	520	40 (230 kV/cm)	0.03	-	-	-
Doped BST	Mg doped BST60 on Pt/Si								
	0 mol%	MOSD	100 kHz	450	28.1 (200 kV/cm)	0.013		-	-
	1 mol%		100 kHz	386	17.2 (200 kV/cm)	0.007			
	20 mol %		100 kHz	205	7.9 (200 kV/cm)	0.009			

Doped BST thin films	La doped BST60 on Pt/Si								
	0 mol%	MOSD	100 kHz	450	28.1 (200kV/cm)	>0.025	-		-
	1 mol%		100 kHz	283	12.1 (-do-)	0.019			
	5 mol%		100 kHz	204	3.49 (-do-)	0.019			
	10 mol%		100 kHz	200	1.2 (-do-)	0.030			
	BST60 on LAO	PLD	100 kHz	1736	66 (100V)	0.0153	-	-	
			10 GHz	730	58 (-do-)	0.040			
	1% Mn-BST60 on MgO		100 kHz	2093	63 (-do-)	0.0030			
			10 GHz	1820	56 (-do-)	0.006			
	BST50 on LAO	PLD	16 GH	-	-	-7.36 dB	-	204°	37.3 °/dB
	BST40 on LAO		14 GHz			-7.01 dB		274°	39.1 °/dB
	BST60 on LAO		15 GHz			-4.4 dB		121°	27.5 °/dB
	1% Mn-BST50		19.6 GHz			-1.4 dB		57°	40.7 °/dB
	1% Mn-BST60		15 GHz			-2.1 dB		114°	54.3 °/dB
	1-2 % Mn-BST50	PLD	1-10 GHz	-	30 (67 kV/cm)	0.005	-	-	-
	BST50 on LAO	PLD	14.3 GHz	-	-	-4.5 dB	-	168° (400)	37.3 °/dB
	BST40 on LAO		14 GHz			-7.01 dB		274° (400)	39.1 °/dB
	BST:1%Magnesia on MgO		16 GHz			-1.95 dB		75° (533)	38.5 °/dB
	BST60/ MgO	MOSD	10 GHz	406	-	0.025	-		
	1 mol% Mg-BST60/MgO			348	-	0.022			
	BST60/Pt/Si			450	50.1 (300 kV/cm)	0.013			
	1 mol% Mg-BST60/ Pt/Si			423	43.0 (-do-)	0.009			
	BST60	PLD	0.5 MHz	1200	23 (30 kV/cm)	-	-	-	-
	1 wt % Magnesia -BST60		-do-	926	24 (30 kV/cm)				

Composite BST thin films	BST60+40 wt% MgO (950 °C) (1100 °C)	PLD	-	-	- 2 17.7	- 0.006 0.027	-	-	-
	Al_2O_3 doped BST50 on LAO 0 wt% 10 wt% 20 wt% 30 wt% 40 wt%	PLD	7.7 GHz	 1622 1387 1311 950 870	 22 (8.7 kV/cm) 19.7 17.9 16.4 15.9	 0.030 0.021 0.015 0.012 0.011	 7.33 9.38 11.93 13.67 14.45	-	
	MgO-Mixed BST60 0 wt% 1 wt% 20 wt% 40 wt% 60 wt%	PLD	8 GHz	 800 600 250 150 100	 32 (100 kV/cm) 22 (-do-) 10 (-do-) 8 (-do-) 5 (-do-)	 0.05 0.03 0.012 0.013 0.013	-	-	-
	TiO_2 doped BST60 1 wt% 5 wt% 10 wt% 50 wt%	PLD	1MHz	-	 - - 37 (200 kV/cm) undetectable	 - - 0.001 0.006	 - - ~61.7 -	-	-

*PS= Phase shifter

2.2.2 Fundamentals of Bi_2O_3-ZnO-Nb_2O_5 Material Properties

In the 1990s, Bi_2O_3-ZnO-Nb_2O_5 ceramics attracted considerable attention as low-temperature co-fired ceramics (LTCC) for multilayer ceramic capacitors (MLCCs).[82-84] The Bi_2O_3-ZnO-Nb_2O_5 ternary system has two main phases: One phase is a cubic pyrochlore with a composition of approximately $Bi_{1.5}Zn_{1.0}Nb_{1.5}O_7$;[82,85,86] The second phase with a composition of $Bi_{2.0}(Zn_{2/3}Nb_{4/3})O_{7.0}$ has a monoclinic zirconolite-like structure.[82,85,87] The cubic phase has a high permittivity (~170) and a positive temperature coefficient of capacitance, whereas the monoclinic phase has a lower permittvity (~80) and a negative temperature coefficient of capacitance.[82,88] Both phases have very low dielectric losses.[84,89] By combining these two phase, BZN ceramics with a moderate relative permittivity (~90) and with a good temperature stability of the capacitance can be fabricated for integrated passive component applications.[82,84] Furthermore, Ren *et al.*[90] demonstrated that the permittivity of BZN cubic pyrochlore thin film was tunable by an applied electric field. The cubic pyrochlore phase is of interest because of its high permittivity, low dielectric loss, and electric field tunability that can be exploited for applications such as microwave tunable devices and circuits. In the following, the acronym BZN refers specifically to the $Bi_{1.5}Zn_{1.0}O_{7.0}$ cubic pyrochlore.

2.2.2.1 Crystal Structure of Bi_2O_3-ZnO-Nb_2O_5 System

Many ternary metallic oxides of the general formula $A_2B_2O_7$, where A and B represent metal cations, adopt the cubic pyrochlore structure.[91] This crystal structure can tolerate vacancies on both A and O sites to a certain extent. Materials with the pyrochlore structure exhibit a wide variety of interesting properties, such as ferroelectricity, electrical conductivity, and frustrated spin magnetism, and a great number of elements can substitute on the A and B-sites.[91] The $A_2B_2O_7$ pyrochlore structure is often described by the formula $A_2B_2O_6O'$, which emphasizes that the structure is built of two interpenetrating networks. The B_2O_6 octahedra share vertices to form a three dimensional network, resulting in large cavities that contain the O' and

an atoms in an A_2O' tetrahedral net.[86] Levin *et al.*[86] investigated the crystal structure of a BZN powder that contained small amounts of ZnO by neutron, electron, and X-ray diffraction, respectively. The composition of the stoichiometric pyrochlore phase was $Bi_{1.5}Zn_{0.92}Nb_{0.92}O_{6.92}$, with a lattice constant of 10.56 Å. Rietveld refinements of neutron powder diffraction patterns show that Zn^{2+} substituted on both A and B sites. Thus, the formula of BZN can be expressed as $(Bi_{1.5}Zn_{0.42})(Zn_{0.5}Nb_{1.5})O_{6.92}$.

2.2.2.2 $Bi_{1.5}Zn_{1.0}Nb_{1.5}O_7$ Thin Films

To date, several growth techniques have been employed to study BZN thin films, including metal-organic deposition (MOD),[90,92] radio-frequency (RF) magnetron sputtering,[93-95] pulsed laser deposition (PLD)[96,97] and metal-organic chemical vapor deposition (MOCVD).[98] BZN thin films show a high permittivity and low dielectric loss up to 1 MHz. The experimental results show that the permittivity of BZN does not change with film thickness for films thicker than 50 nm.[90] Moderate tunabilities are demonstrated under a large bias field for BZN thin films. In Table 2.4, we summarize the dielectric properties of BZN films reported in the literature.

Table 2.4 Summary of BZN thin films properties reported in literature

Growth method	ε_r	tan δ	Tunability/Bias field (MV/cm)	Measurement frequency
MOD[90]	~150	~0.005	46%/3*	10 kHz
Sputtering[93]	~153	~0.003	14%/1	1 MHz
Sputtering[94]	~220	~0.0005	55%/2.4	1 MHz
PLD[99]	~187	~0.002	6%/0.75	100 kHz
MOCVD[98]	~200	~0.002	8%/0.4	1 MHz

*Measured at 77 K

2.3 Motivations for the Present Study

With the rapid development of communication systems including satellite, bluetooth, 3G wireless phone, ultra-wide band and optical network, it is desirable to be able to design frequency agile RF front ends for operation in various frequency bands. Tunable RF and microwave components are thus in largely demanded due to their frequency agile characteristics. In addition, high-speed, small-size, and low-operation voltage components are required in the current and next generation communication systems. These requirements impose significant challenges on current tunable circuit technologies and illustrate the need for new materials, technologies and designs. Barium strontium titanate ($Ba_xSr_{1-x}TiO_3$ or BST), a ferroelectric film whose dielectric constant can be controlled by the application of a DC electric field, has shown great promise for the design of tunable RF and microwave circuits such as phase shifters, filters, antennas, adaptive matching circuits, and voltage controlled oscillators. The presented literature review in earlier sections elucidated the current status of BST ferroelectric thin films for tunable devices operated at microwave frequencies.

From the point of view of device integration, as well as the ability to miniaturize the device, incorporation of BST in thin film form with properties similar to bulk (high tunability and low loss) is desirable. To attain this, BST thin films should be epitaxially or highly-oriented grown on Si based substrates having sharp film-substrate interface with minimal interdiffusion. Reduction/absence of grain boundaries in textured/epitaxial films would reduce the losses, especially at microwave frequencies and it is also expected that these films would have higher tunability as compared to their polycrystalline counterpart. The growth of highly-oriented with high quality thin films using single substrate such as MgO and $LaAlO_3$ or conductive oxide (lattice matched) buffer layer has been demonstrated. However, it remains an open formidable challenge to grow highly oriented BST thin films directly on Pt coated Si substrates without any buffer layers.

It is well known that orientation and growth mode in epitaxy or well-oriented are very much determined by the involved interface and surface energies. These depend primarily on the strength and nature of the chemical bonds between film and substrate atoms on the one hand, and between film atoms on the other hand. Epitaxial relationships lower the interfacial energy. It may occur that the optimal epitaxial relationship does not sufficiently lower the energy, and another orientation may have a more advantageous energy balance due to lower surface energies. Similarly, the orientation control on bare platinum can be explained in terms of competing surface and interface energies the moment of nucleation. Unfortunately, our knowledge of the relevant surface and interface energies is not complete. We nevertheless try to explain the observed behavior with the available data.

There are several studies on the effect on dielectric properties for BST thin films, especially on lower dielectric losses by doping with Mg^{2+}, Co^{3+}, Fe^{3+} and Mn^{2+}, etc. The mechanism for this behavior is that ions with a charge less than 4^+ can substitute for Ti^{4+} and behave as electron acceptors. These acceptors prevent the reduction of Ti^{4+} to Ti^{3+} by neutralizing the donor action of oxygen vacancies. Because the electrons resulting from the generation of oxygen vacancy can hop between different titanium ions and provide a mechanism for dielectric losses, the compensation for oxygen vacancy with the correct amount of acceptor dopants helps to lower the loss tangent. However, the reduced dielectric losses of BST as a result of the addition of the nontunable and of relatively low permittivity of these oxides were at the expense of great reduction in dielectric constant, as well as dielectric tunability. Viewing this light, compositing BST films with moderate permittivity and very low loss dielectrics BZN seems promising. However, it may be challenging to retain texture growth as well as control the dielectric properties of such composite structures. Therefore, it is required to fabricate composite thin films to tailor the losses of BST films without compromising the tunability much to achieve high figure of merit suitable for microwave tunable devices. More research is clearly required to explore these alternatives.

For decades, there has been a great deal of interest in mapping and understanding changes that occur in the functional characteristics of ferroelectrics as specimen size is reduced. Particularly attention has been given to ferroelectric thin films. Establishing fundamental size limits beyond which ferroelectricity can no longer be supported has been a key quest, and has involved careful experimental characterization of ultrathin films, as well as modeling. It has been reported that the bulk properties of very high dielectric constant were frustrated showing decreasing dielectric constant, and increasing dielectric loss and leakage currents with decreasing film thickness. Exploring the issue that the dielectric properties degradation in thin film form compared to bulk is important to design novel materials with better material characteristics as well as device performance. Although BST thin films are extensively investigated for tunable microwave device application, limited attempts have been made so far to identify the variations in permittivity in highly oriented BST films with film thickness and measured temperature (low temperature) to understand the dielectric behavior of the bulk layer and the nature of the low permittivity interfacial component.

In the last decade, BST thin films have been studied extensively for their use in tunable microwave devices. Most of these studies were studied to evaluate material parameters at lower (<1 MHz) frequencies. To test these thin films for practical purpose, the material should be evaluated at microwave frequencies, since tunable devices are operated at in the microwave range (300 MHz to 300 GHz). Moreover, as mentioned earlier, growth of highly epitaxially with high quality BST films is also equally important. Furthermore, it is very difficult to prepare highly epitaxially BST films on sapphire substrate due to big lattice mismatch between BST and sapphire. There are few attempts in the literature concerning the microwave properties of epitaxial BST films on sapphire over a wide range microwave frequencies (1-40 GHz), rather than at the lower, narrower frequency ranges ($\leq$ 10 GHz).

For many practical applications, accurate characterization of the frequency dispersion of BST-based thin film on semiconductor compatible high resistivity Si

substrates, is crucial if the BST dielectric material is to be used in future high-frequency integrated circuit device application. Similarly, the limitations for high frequency applications are the low tunability and high microwave loss. Thus, introducing of a low loss dielectric BZN combined with high permittivity BST on HR-Si presents an intriguing opportunity to develop materials for tunable device applications with stringent demands focused on low dielectric losses, while still maintaining moderate tunability. Moreover, accurate characterization of microwave properties at higher frequency gives the right feedback to enhance the tunability and improve microwave loss. Very limited experimental attempts have been identified in the literature that studies the microwave properties of BST-based capacitors directly on HR-Si substrates in the high frequency domain.

Motivated by the above stated facts, following areas have been identified that need further research to synthesize barium strontium titanate and related thin films for their possible applications in microwave applications. The main objectives of this research work are stated as follows:

(1) To grow high quality textured BST thin films on Pt-coated Si substrates.

RF magnetron sputtering method is an effective technique used to deposit high quality thin films. The preparation of the film is very sensitive to process parameters. A systematic study of the effect of sputtering parameter [O_2/(Ar+O_2)] on phase formation behavior aimed towards synthesizing highly oriented and textured films needs to be carried out. Introducing seeding layer is also an effective approach to obtain highly oriented films. Hence, the first part of the thesis was devoted to indentify and optimize the process parameters as well as insert TiO_x seeding layer to obtain grain oriented highly textured, device quality BST thin films.

(2) Study the effect of thickness of BZN layer on the dielectric properties of highly oriented BST thin films.

Very low loss non-ferroelectric material, such as $Bi_{1.5}Zn_{1.0}Nb_{1.5}$ (BZN) has been found to have considerable effect of the electrical and dielectric properties of the BST

thin films. Hence the effect of making composites in the highly oriented BST thin films with optimum thickness of BZN films are needed to be studied in details.

(3) Investigate the bulk and interfacial properties for highly oriented BST films.

In a thin film, near either film-electrode interface the ionic contribution to the dielectric properties is suppressed, that is, a region a few lattice constant thick acts as a low permittivity or "dead" layer. An applied voltage is dropped across the interfacial layers and the bulk of the film in series. The effect of interfacial capacitance is more pronounced for thinner films. Thus, systematically investigation of highly oriented BST thin films with various thicknesses is necessary to study in details.

(4) Evaluation of epitaxial BST and heterostructures BZN-BST at high frequency by fabricating coplanar waveguide configurations.

Most of the earlier studies on the electrical properties of BST thin films were carried out only at low frequencies. However, high frequency properties of the films may differ from that measured at low frequencies. Hence, in order to choose the best material for room temperature microwave tunable devices, it is needed to test these thin films at high frequencies.

2.4 Reference

1. J. Valasek, "Piezo-Electric and Allied Phenomena in Rochelle Salt," *Physical Review*, **17**(4), 475-481, 1921.

2. W. Mandell, "Change in Elastic Properties on Replacing the Potassium Atom of Rochelle Salt by the Ammonium Group," *Proceedings of the Royal Society of London,* **121**, 122-130, 1928.

3. W. J. Merz, "Lithium Ammonium Tartrate Monohydrate, a New Ferroelectricity Crystal," *Physical Review*, **82**(4), 562-563, 1951.

4. G. Busch and P. Scherrer, "Eine Neue Seignette-elektrische Substanz," *Naturwissenschaften*, **23**(43), 737-737, 1935.

5. G. Busch, "New 'Rochelle-electrics'," *Helvetica Physica Acta,* **11**(4), 269-298, 1938.

6. H. Thurnauer and J. Deaderick, U.S. Patent No. 2, 429, 588 (October 21, 1941).

7. E. Wainer and A. N. Salomon. Electrical Report No. 9 Titanium Alloy Mfg. Co. (1943).

8. E. Wainer, "High Titania Dielectrics," *Transactions of the Electrochemical Society*, **89**, 331-356, 1946.

9. B. M. Wul and I. M. Goldman, "Dielectric Hysteresis in Barium Titanate," *Academie des Sciences de l'URSS - Comptes Rendus,* **51**(1), 21-23, 1946.

10. P. R. Coursey and K. C. Brand, "Dielectric Constants of Some Titanates," *Nature*, **157**, 297-298, 1946.

11. A. V. Hippel, R. G. Breckenridge, F. G. Chesley and L. Tisza, "High Dielectric Constant Ceramics," *Industrial and Engineering Chemistry,* **38**, 1097-1109, 1946.

12. G. Shirane and D. A. Takeda, "Phase Transitions in Solid Solutions of $PbZrO_3$ and $PbTiO_3$ (I) Small Concentrations of $PbTiO_3$," *Journal of the Physical Society of Japan*, **7**, 5-11, 1952.

13. B. Jaffe, R. S. Roth and S. Marzullo, "Piezoelectric Properties of Lead Zirconatelead Titanate Solid-solution Ceramics," *Journal of Applied Physics*, **25**(6), 809-810, 1954.

14. F. Jona and G. Shirane, "Ferroelectric Crystals," 1st ed. In *International Series of Monographs on Solid State Physics*, Vol. 1 Edited by R. Smoluchowski and N. Kurti. New York: Pergamon Press Inc, 1962.

15. A. D. Hilton and B. W. Ricketts, "Dielectric Properties of $Ba_{1-x}Sr_xTiO_3$ ceramics," *Journal of Physics D-Applied Physics,* **29**(5), 1321-1325, 1996.

16. N. A. Pertsev, A. G. Zembilgotov, S. Hoffmann, R. Waser and A. K. Tagantsev, "Ferroelectric Thin Films Grown on Tensile Substrates: Renormalization of the Curie-Weiss Law and Apparent Absence of Ferroelectricity," *Journal of Applied Physics*, **85**(3), 1698-1701, 1999.

17. A. F. Devonshire, "Theory of Ferroelectrics," *Advances in Physics,* **3**(10), 85-130, 1954.

18. A. K. Tagantsev, V. O. Sherman, K. F. Astafiev, J. Venkatesh, and N. Setter, "Ferroelectric Materials for Microwave Tunable Applications," *Journal of Electroceramics*, **11**, 5-66, 2003.

19. O. G. Vendik, L. T. Ter-Martirosyan, and S. P. Zubko, "Microwave Losses in Incipient Ferroelectrics as Functions of the Temperature and the Biasing Field," *Journal of Applied Physic*, **84**(2), 993-998, 1998.

20. V. L. Gurevich and A. K. Tagantsev, "Intrinsic Dielectric Loss in Crystals," *Advances in Physics*, **40**(6), 719-767, 1991.

21. X. X. Xi, H. C. Li, W. D. Si, A. A. Sirenko, I. A. Akimov, J. R. Fox, A. M. Clark and J. H. Hao, "Oxide Thin Films for Tunable Microwave Devices," *Journal of Electroceramics*, **4**(2-3), 393-405, 2000.

22. M. J. Lancaster, J. Powell and A. Porch, "Thin-film Ferroelectric Microwave Devices," *Superconductor Science & Technology*, **11**(11), 1323-1334, 1998.

23. I. M. Buzin, "Dielectric Losses of Strontium Titanatr at Vhf," *Vestnik Moskovskogo Universiteta Seriya 3 Fizika Astronomiya*, **18**(6), 70-76, 1977.

24. L. C. Sengupta, S. Stowell, E. Ngo, M. E. Oday and R. Lancto, "Barium Strontium Titanate and Non-ferroelectric Oxide Ceramic Composites for Use in Phased Array Antennas," *Integrated Ferroelectrics*, **8**(1-2), 77-88, 1995.

25. T. Tsurumi, T. Teranishi, T. Harigai, H. Kakemoto, S. Wada, M. Nakada and J.

Akedo, "Ultra Wide Band Dielectric Spectroscopy of Perovskite Dielectrics," *In Proceedings of the International Symposium on the Applications of Ferroelectrics*, Edited by D. P. Cann. Sunset Beach, NC, USA, 2006.

26. Y. Xu, "Ferroelectric Materials and Their Application," Amsterdam, London, New York, Tokyo: North-Holland, 1991.

27. M. Daglish and T. Kemmitt, "Ferroelectric Thin Film-Research, Development and Commercialisation," *IPENZ Transactions*, **27**, 21-24, 2000.

28. A. I. Kingon, S. K. Streifer, C. Basceri, and S. R. Summerfelt, "High-permittivity Perovskite Thin Films for Dynamic Random-access Memories," *Material Research Society Bulletin*, **21**, 46-52, 1996.

29. M. D. Keijser and G. J. M. Dormans, "Chemical Vapor Deposition of Electroceramic Thin Film," *Material Research Society Bulletin*, **21**, 37-43, 1996.

30. W. L. Warren, D. Dimos, and R. M. Wase, "Degradation Mechanism in Ferroelectric and High-permittivity Perovskites," *Material Research Society Bulletin*, **21**, 40-45, 1996.

31. N. Setter and R. Waser, "Electronic Materials," *Acta Materialia*, **48**(1), 151-178, 2000.

32. J. F. Scott, F. M. Ross, C. A. P. D. Araujo, and M. C. Scott, "Structure and Device Characteristics of $SrBi_2Ta_2O_9$-based Nonvolatile Radom-access Memories," *Material Research Society Bulletin*, **21**, 33-39, 1996.

33. O. Auciello and R. Ramesh, "Laser-ablation Deposition and Characterization of Ferroelectric Capacitors for Nonvolatile Memories," *Material Research Society Bulletin*, **21**, 31-36, 1996.

34. R. E. Jones and S. B. Desu, "Process Integration for Nonvolatile Ferroelectric Memory Fabrication," *Material Research Society Bulletin*, **21**, 55-58, 1996.

35. D. L. Polla and L. F. Francis, "Ferroelectric Thin Films in Microelectromechanical Systems Applications," *Material Research Society Bulletin*, **21**, 59-65, 1996.

36. O. Auciello, A. I. Kingon, and S. B. Krupanidhi, "Sputter Synthesis of Ferroelectric Films and Heterostructures," *Material Research Society Bulletin*, **21**,

25-30, 1996.

37. S. K. Dey and P. V. Alluri, "PE-MOCVD of Dielectric Thin Films: Challenges and Opportunities," *Material Research Society Bulletin*, **21**, 44-48, 1996.

38. B. A. Tuttle and R. W. Schwartz, "Solution Deposition of Ferroelectric Thin Films," *Material Research Society Bulletin*, **21**, 49-54, 1996.

39. H. Diamond, "Variation of Permittivity with Electric Field in Perovskite-like Ferroelectrics," *Journal of Applied Physics*, **32**(5), 909-915, 1961.

40. K. M. Johnson, "Variation of Dielectric Constant with Voltage in Ferroelectrics and Its Application to Parametric Devices," *Journal of Applied Physics*, **33**(9), 2826-2831, 1962.

41. H. Tamura, T. Konoike, and K. Wakino, "Geometrical Effects in Elastic/Plastic Indentation," *Journal of the American Ceramic Society*, **67**(1), 57-60, 1984.

42. K. Wakino, K. Minai, and H. Tamura, "Microwave Characteristics of (Zr, Sn)TiO_4 and BaO-PbO-Nd_2O_3-TiO_2 Dielectric Resonators," *Journal of the American Ceramic Society*, **67**(4), 278-281, 1984.

43. H. M. O'Bryan, JR., J. Thomon, JR., and J. K. Plourde, "A New BaO-TiO_2 Compound with Temperature-Stable High Permittivity and Low Microwave Loss," *Journal of the American Ceramic Society*, **57**(10), 450-453, 1974.

44. G. Subramanyam, F. W. Van Keuls, and F. A. Miranda, "A K-band Tunable Microstrip Bandpass Filter Using a Thin-film Conductor/ferroelectric/dielectric Multilayer Configuration," *IEEE Microwave Guided Wave Letters*, **8**(2), 78-80, 1998.

45. A. T. Findikoglu, Q. X. Jia, X. D. Wu, G. J. Chen and T. Venkatesan, D. W. Reagor, "Tunable and Adaptive Bandpass Filter Using a Nonlinear Dielectric Thin Film of $SrTiO_3$," *Applied Physics Letters*, **68**(12), 1651-1653, 1996.

46. A. T. Findikoglu, Q. X. Jia, and D. W. Reago, "Superconductor/Nonlinear-dielectric Bilayers for Tunable and Adaptive Microwave Devices," *IEEE Transactions on Applied Superconductivity*, **7**(2), 2925-2928, 1997.

47. C. H. Mueller, R. E. Treece, T. V. Rivkin, F. A. Miranda, H. R. Moutinho, A. S. Franz, M. Dalberth, C. T. Rogers, "Tunable $SrTiO_3$ Varactors Using Parallel Plate and

Interdigital Structures," *IEEE Transactions on Applied Superconductivity*, **7**(2), 3512-3515, 1997.

48. A. D. Hilton and B. W. Ricketts, "Dielectric properties of $Ba_{1-x}Sr_xTiO_3$ Ceramics," *Journal of Physics D: Applied Physics*, **29**(5), 1321-1325, 1996.

49. V. V. Lemanov, E. P. Smirnova, P. P. Syrnikov, and E. A. Tarakanov, "Phase Transitions and Glasslike Behavior in $Sr_{1-x}Ba_xTiO_3$," *Physical Review B*, **54**(5), 3151-3157, 1996

50. L. Davis Js, and L. G. Rubin, "Some Dielectric Properties of Barium Strontium Titanate Ceramics at 3000 Megacycles," *Journal of Applied Physics*, **24**(9), 1751-1753, 1953.

51. W. Chang, J. S. Horwitz, A. C. Carter, J. M. Pond, S. W. Kirchoefer, C. M. Gilmore, and D. B. Chrisey, "The Effect of Annealing on the Microwave Properties of $Ba_{0.5}Sr_{0.5}TiO_3$ Thin Films," *Applied Physics Letter*, **74**(7), 1033-1035, 1999.

52. K. S. Chang, M. Aronova, O. Famodu, and I. Takeuchi, S. E. Lofland, J. Hattrick-Simpers, and H. Chang, "Multimode Quantitative Scanning Microwave Microscopy of in situ Grown Epitaxial $Ba_{1-x}Sr_xTiO_3$ Composition Spreads," *Applied Physics Letters*, **79**(26), 4411-4413, 2001.

53. F. A. Flaviis, N. G. Alexopoulos, and O. M. Stafsudd, "Planar Microwave Integrated Phase Shifter Design with High Purity Ferroelectric Material," *IEEE Transactions on Microwave Theory and Techniques*, **45**(6), 963-969, 1997.

54. Y. Chen, X. L. Dong, R. H. Liang, J. T. Li, and Y. L. Wang, "Dielectric Properties of $Ba_{0.6}Sr_{0.4}TiO_3/Mg_2SiO_4$/MgO Composite Ceramics," *Journal of Applied Physics*, **98**(6), 064107-11, 2005.

55. C. M. Carlson, T. V. Rivkin, P. A. Parilla, J. D. Perkins, D. S. Ginley, A. B. Kozyrev, V. N. Oshadchy, and A. S. Pavlov, "Large dielectric constant ($\varepsilon/\varepsilon_0$>6000) $Ba_{0.4}Sr_{0.6}TiO_3$ Thin Films for High-Performance Microwave Phase Shifters," *Applied Physics Letters*, **76**(14), 1920-1922, 2000.

56. C. L. Chen, H. H. Feng, Z. Zhang, A. Brazdeikis, Z. J. Huang, W. K. Chu, C. W. Chu, F. A. Miranda, F. W. Van Keuls, R. R. Romanofsky, and Y. Liou, "Epitaxial Ferroelectric $Ba_{0.5}Sr_{0.5}TiO_3$ Thin Films for Room-temperature Tunable Element

Applications," *Applied Physics Letters*, **75**(3), 412-414, 1999.

57. S. J. Lee, S. E. Moon, H. C. Ryu, M. H. Kwak, Y. T. Kim, and S. K. Han, "Microwave Properties of Compositionally Graded (Ba,Sr)TiO_3 Thin Films According to the Direction of the Composition Gradient for Tunable Microwave Applications," *Applied Physics Letters*, **82**(13), 2133-2135, 2003.

58. M. W. Cole, E. Ngo, S. Hirsch, M. B. Okatan, and S. P. Alpay, "Dielectric Properties of MgO-doped Compositionally Graded Multilayer Barium Strontium Titanate Films,"*Applied Physics Letters*, **92**(7), 072906-072908, 2008.

59. F. Jin, G. W. Auner, R. Naik N. W. Schubring, J. V. Mantese, A. B. Catalan, and A. L. Micheli, "Giant Effective Pyroelectric Coefficients from Graded Ferroelectric Devices," *Applied Physics Letters*, **73**(19), 2838-2840, 1998.

60. M. S. Mohammed, G. W. Auner, R. Naik, J. V. Mantese, N. W. Schubring, A. L. Micheli, and A. B. Catalan, "Temperature Dependence of Conventional and Effective Pyroelectric Coefficients for Compositionally Graded $Ba_xSr_{1-x}TiO_3$ Films," *Journal of Applied Physics*, **84**(6), 3322-3325, 1998.

61. A. C. Carter, J. S. Horwitz, D. B. Chrisey, J. M. Pond, S. W. Kirchoefer, and W. Chang, "Pulsed Laser Deposition of Ferroelectric Thin Films for Room Temperature Active Microwave Electronics," *Integrated Ferroelectrics*, **17**(1-4), 273-285, 1997.

62. Y. Wang, B. T. Liu, F. Wei, Z. M. Yang, and J. Du, "Fabrication and Electrical Properties of (111) Textured $(Ba_{0.6}Sr_{0.4})TiO_3$ Film on Platinized Si Substrate," *Applied Physics Letters*, **90**(4), 042905-042907, 2007.

63. R. E. Treece, J. B. Thompson, C. H. Mueller, T. V. Rivkin, M. W. Cromar, "Optimization of $SrTiO_3$ for Applications in Tunable Resonant Circuits," *Applied Superconductivity*, **7**(2), 2363-2366, 1997.

64. C. L. Chen, J. Shen, S. Y. Chen, Z. Zhang, G. P. Luo, W. K. Chu, and C. W. Chu, "Epitaxial Growth of Ferroelectric $Ba_{1-x}Sr_xTiO_3$ Thin Films for Room Temperature Tunable Microwave Devices," *Ferroelectrics*, **252**(1), 181-189, 2001.

65. C. L. Chen, J. Shen, S. Y. Chen, G. P. Luo, C. W. Chu, F. A. Miranda, F. W. Van Keuls, J. C. Jiang, E. I. Meletis, and H. Y. Chang, "Epitaxial Growth of Dielectric $Ba_{0.6}Sr_{0.4}TiO_3$ Thin Film on MgO for Room Temperature Microwave Phase Shifters,"

Applied Physics Letters, **78**(5), 652-654, 2000.

66. H. J. Gao, C. L. Chen, B. Rafferty, S. J. Pennycook, G. P. Luo and C. W. Chu, "Atomic Structure of $Ba_{0.5}Sr_{0.5}TiO_3$ Thin Films on $LaAlO_3$," *Applied Physics Letters*, **75**(17), 2542-2544, 1999.

67. J. C. Jiang, Y. Lin, C. L. Chen, and C. W. Chu, and E. I. Meletis, "Microstructures and Surface Step-induced Antiphase Boundaries in Epitaxial Ferroelectric $Ba_{0.6}Sr_{0.4}TiO_3$ Thin Film on MgO," *Journal of Applied Physics*, **91**(5), 3188-3192, 2002.

68. H. N. Al-Shareef, D. Dimos, M. V. Raymond, R. W. Schwartz, and C. H. Mueller, "Tunability and Calculation of the Dielectric Constant of Capacitor Structures with Interdigital Electrodes," *Journal of Electroceramics*, **1-2**, 145-153, 1997.

69. M. V. Raymond, H. N. Al-Shareef, D. B. Dimos. N. Missert, C, Mueller, and D. Galt, "Sputter Deposition of $SrTiO_3$ Thin Films for Voltage Tunable Capacitors," *Integrated Ferroelectrics*, **17** (1-4), 247-256, 1997.

70. L. A. Knauss, J. M. Pond, J. S. Horwitz, D. B. Chrisey, C. H. Mueller and R. Treece, "The Effect of Annealing on the Structure and Dielectric Properties of $Ba_xSr_{1-x}TiO_3$ Ferroelectric Thin Films," *Applied Physics Letters*, **69**(1), 25-27, 1996.

71. W. J. Kim, H. D. Wu, W. Chang, S. B. Qadri, J. M. Pond, S. W. Kirchoefer, D. B. Chrisey, and J. S. Horwitz, "Microwave Dielectric Properties of Strained $(Ba_{0.4}Sr_{0.6})TiO_3$ Thin Films," *Journal of Applied Physics*, **88**(9), 54485451, 2000.

72. W. Chang, S. W. Kirchoefer, J. M. Pond, J. S. Horwitz, and L. Sengupta, "Strain-relieved $Ba_{0.6}Sr_{0.4}TiO_3$ Thin Films for Tunable Microwave Applications," *Journal of Applied Physics*, **92**(3), 1528-1535, 2002.

73. S. Aggarwal and R. Ramesh, "Point Defect Chemistry of Metal Oxide Heterostructure," *Annual Review Material Science*, **28**, 463-499, 1998.

74. M. W. Cole, C. Hubbard, E. Ngo, M. Ervin, M. Wood, and R. G. Geyer, "Structure–property Relationships in Pure and Acceptor-doped $Ba_{1-x}Sr_xTiO_3$ Thin Films for Tunable Microwave Device Applications," *Journal of Applied Physics*, **92**(1), 475-483, 2002.

75. P. C. Joshi and M. W. Cole, "Mg-doped $Ba_{0.6}Sr_{0.4}TiO_3$ Thin Films for Tunable

Microwave Applications," *Applied Physics Letters*, 77(2), 289-291, 2000.

76. W. Chang and L. Sengupta, "MgO-mixed $Ba_{0.6}Sr_{0.4}TiO_3$ Bulk Ceramics and Thin Films for Tunable Microwave Applications," *Journal of Applied Physics*, **92**(7), 3941-3946, 2002.

77. H. S. Kim, M. H. Lim, H. G. Kim, and I. D. Kim, "Characterization of Ni-Doped BST Thin Films on LSCO Buffer Layers Prepared by Pulsed Laser Deposition," *Electrochemical and Solid-State Letters*," **7**, J1, 2004.

78. M. W. Cole, P. C. Joshi, and M. H. Ervin, "La doped $Ba_{1-x}Sr_xTiO_3$ Thin Films for Tunable Device Applications," *Journal of Applied Physics*, **89**(11), 6336-6340, 2001.

79. K. B. Chong, L. B. Kong, L. F. Chen, L. Yan, C. Y. Tan, T. Yang, C. K. Ong, and T. Osipowicz, "Improvement of Dielectric Loss Tangent of Al_2O_3 Doped $Ba_{0.5}Sr_{0.5}TiO_3$ Thin Films for Tunable Microwave Devices," *Journal of Applied Physics*, **95**(3), 1416-1419, 2004.

80. S. Y. Lee, and T. Y. Tseng, "Electrical and Dielectric Behavior of MgO Doped $Ba_{0.7}Sr_{0.3}TiO_3$ Thin Films on Al_2O_3 Substrate," *Applied Physics Letters*, **80**(10), 1797-1799, 2002.

81. D. Dimos and C. H. Mueller, "Perovskite Thin Films for High-frequency Capacitor Applications," *Annual Review Material Science*, **28**, 397-419, 1998.

82. C. A. Randall, J. C. Nino, A. Baker, H. J. Youn, A. Hitomi, R. Thayer, L. F. Edge, T. Sogabe, D. Anderson, T. R. Strout, S. T. Mckinstry, and M. T. Lanagan, "Bi-Pyrochlore and Zirconolite Dielectrics for Integrated Passive Component Applications," *American Ceramic Society Bulletin*, **82**(11), 9101-9108, 2003.

83. M. Valant and P. K. Davies, "Synthesis and Dielectric Properties of Pyrochlore Solid Solutions in the Bi_2O_3-ZnO-Nb_2O_5-TiO_2 System," *Journal of Materials Science*, **34**(22), 5437-5442, 1999.

84. H. L. Du and X. Yao, "Investigation of Dielectric Properties of Bi_2O_3-ZnO-Nb_2O_5-Sb_2O_3 Based Pyrochlores," *Ferroelectrics*, **262**(1-4), 1057-1062, 2001.

85. T. A. Vanderah, I. Levin, and M. W. Lufaso, "An Unexpected Crystal-Chemical Principle for the Pyrochlore Structure," *European Journal of Inorganic Chemistry*, **14**,

2895-2901, 2005.

86. I. Levin, T. G. Amos, J. C. Nino, T. A. Vanderah, C. A. Randall, and M. T. Lanagan, "Structural Study of an Unusual Cubic Pyrochlore $Bi_{1.5}Zn_{0.92}Nb_{1.5}O_{6.92}$," *Journal of Solid State Chemistry*, **168**(1), 69-75, 2002.

87. I. Levin, T. G. Amos, J. C. Nino, T. A. Vanderah, C. A. Randall, and M. T. Lanagan, "Crystal Structure of the Compound $Bi_2Zn_{2/3}Nb_{4/3}O_7$," *Journal of Materials Research*, **17**(6), 1406-1411, 2002.

88. H. Wang, and X. Yao, "Structure and Dielectric Properties of Pyrochlore-Fluorite Biphase Ceramics in the Bi_2O_3-ZnO-Nb_2O_5 System," *Journal of Materials Research*, **16**(1), 83-87, 2001.

89. X. L. Wang, H. Wang, X. Yao, "Structrue, Phase Transformations, and Dielectric Properties of Pyrochlores Containing Bismuth," *Journal of the American Ceramic Society*, **80**(10), 2745-2748, 1997.

90. W. Ren, S. T. Mckinstry, C. A. Randall, and T. R. Shrout, "Bismuth Zinc Niobate Pyrochlore Dielectric Thin Films for Capacitive Applications," *Journal of Applied Physics*, **89**(1), 767-774, 2001.

91. M. A. Subramanian, G. Aravamudan, and G. V. S. Rao, "Oxide Pyrochlore-A Review," *Progress in Solid State Chemsitry*, **15**(2), 55-143, 1983.

92. R. L. Thayer, C. A. Randall, and S. T. McKinstry, "Medium Permittivity Bismuth Zinc Niobate Thin Film Capacitors," *Journal of Applied Physics*, **94**(3), 1941-1947, 2003.

93. Y. P. Hong, S. Ha, H. Y. Lee, Y. C. Lee, K. H. Ko, D. W. Kim, H. B. Hong, and K. S. Hong, "Voltage Tunable Dielectric Properties of rf Sputtered Bi_2O_3-ZnO-Nb_2O_5 Pyrochlore Thin Films," *Thin Solid Films*, **419**(1-2), 183-188, 2002.

94. J. W. Lu and S. Stemmer, "Low-loss, Tunable Bismuth Zinc Niobate Films Deposited by Rf Magnetron Sputtering," *Applied Physics Letters*, **83**(12), 2411-2413, 2003.

95. J. W. Lu, D. O. Klenov, and S. Stemmer, "Influence of Strain on the Dielectric Relaxation of Pyrochlore Bismuth Zinc Niobate Thin Films," *Applied Physics Letters*, **84**(6), 957-959, 2004.

96. W. Y. Fu, L. Z. Cao, S. F. Wang, Z. H. Sun, B. L. Cheng, Q. Wang and H. Wang, "Dielectric Properties of $Bi_{1.5}Zn_{1.0}Nb_{1.5}O_7$/Mn-doped $Ba_{0.6}Sr_{0.4}TiO_3$ Heterolayered Films Grown by Pulsed Laser Deposition," *Applied Physics Letters*, **89**(13), 132908-132910, 2006.

97. I. D. Kim, Y. W. Choi, and H. L. Tuller, "Low-Voltage ZnO Thin Film Transistors with High-K $Bi_{1.5}Zn_{1.0}Nb_{1.5}O_7$ Gate Insulator for Transparent and Flexible Electronics," *Applied Physics Letters*, **87**(4), 043509-043511, 2005.

98. S. Okaura, M. Suzuki, S. Okamoto, H. Uchida, S. Koda, and H. Funakubo, "MOCVD Growth of $Bi_{1.5}Zn_{1.0}Nb_{1.5}O_7$ (BZN) Epitaxial Thin Films and Their Electrical Properties," *Japanese Journal of Applied Physics*, **44**(9B), 6957-6959, 2005.

99. L. Z. Cao, W. Y. Fu, S. F. Wang, Q. Wang, Z. H. Sun, H. Yang, B. L. Cheng, H. Wang, and Y. L. Zhou, "*C*-axial Oriented $(Bi_{1.5}Zn_{0.5})(Zn_{0.5}Nb_{1.5})O_7$ Thin Film Grown on Nb Doped $SrTiO_3$ Substrate by Pulsed Laser Deposition," *Journal of Physics D: Applied Physics*, **40**, 1460-1463, 2007.

CHAPTER 3
Experimental Procedures

In this chapter, ceramic target preparation, thin film deposition technique and their characterization techniques used in the present study are described.

3.1 Preparation of Sputtering Ceramic Target

In this thesis, ceramic targets including $Ba_xSr_{1-x}TiO_3$ and $Bi_{1.5+x}ZnNb_{1.5}O_7$ were used for sputtering. Details of ceramic targets preparation can be found in the following section.

3.1.1 Preparation of $Ba_xSr_{1-x}TiO_3$ Ceramic Target

Ceramic targets $Ba_{0.6}Sr_{0.4}TiO_3$ with excess 20 % BaO and 10 % SrO were prepared by a conventional solid-state reaction from $BaCO_3$, $SrCO_3$ and TiO_2 oxides of purity higher than 99.98 % and the technological details were under very careful surveillance. The starting materials in stoichiometric proportions were ball-milled for 24 h in water, dried and calcined at 1150 °C/2 h. After that, they were remixed and pressed into disk-shape pellets 90 mm in diameter, and finally sintered at 1250 °C/2 h. 3-mm-thick BST target with 75 mm in diameter was machined for sputtering. XRD results of the sputtering target were given in Fig. 3.1.

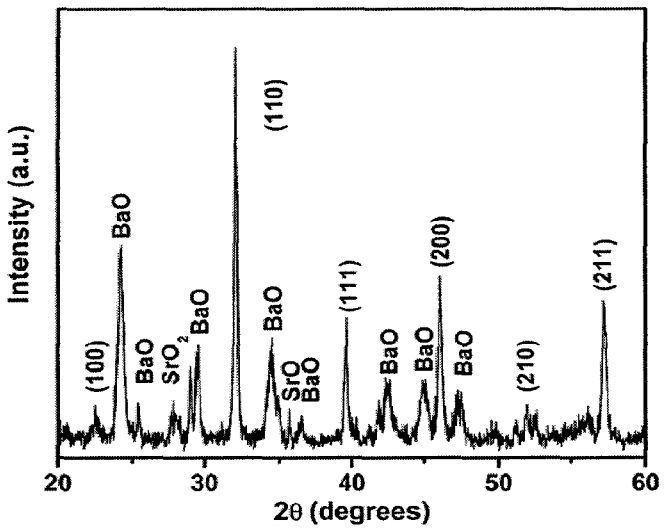

Fig. 3.1. XRD patterns of $Ba_{0.6}Sr_{0.4}TiO_3$ ceramic target with excess 20 % BaO and 10 % SrO

3.1.2 Preparation of $Bi_{1.5+x}Zn_{1.0}Nb_{1.5}O_7$ Ceramic Target

The $Bi_{1.5}Zn_{1.0}Nb_{1.5}O_7$ ceramic targets with excess 10 % Bi_2O_3 were prepared by conventional mixed oxide method from Bi_2O_3, ZnO and Nb_2O_5 oxides of purity higher than 99.99 %. The starting materials in corresponding proportions were ball-milled for 24 h in water, dried and calcined at 950 °C/2 h. After that, they were remixed and pressed into disk-shape pellets 90 mm in diameter, and finally sintered at 1050 °C/2 h. 3-mm-thick $Bi_{1.5+x}Zn_{1.0}Nb_{1.5}O_7$ target with 75 mm in diameter was machined for sputtering. XRD results of the $Bi_{1.5+x}Zn_{1.0}Nb_{1.5}O_7$ target were given in Fig. 3.2.

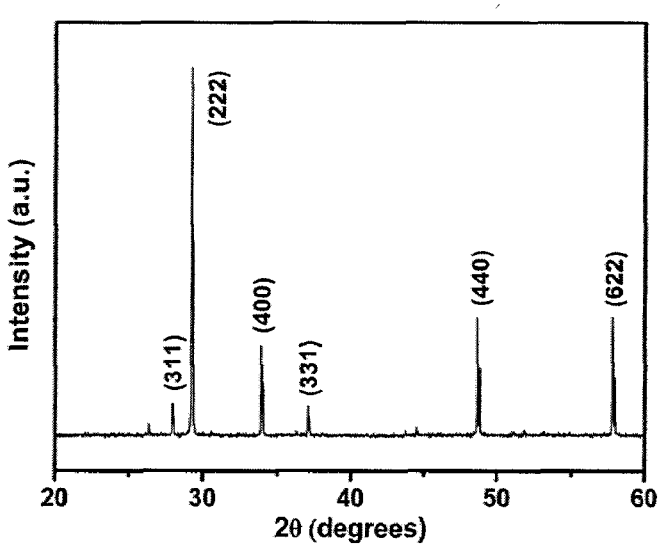

Fig. 3.2. XRD patterns of $Bi_{1.5+x}Zn_{1.0}Nb_{1.5}O_7$ ceramic target with excess 10 % Bi_2O_3 oxides

3.1.3 Ceramics Powders Used in This Thesis

Table 3.1 and 3.2 listed the main raw materials for the preparation of $Ba_xSr_{1-x}TiO_3$ and $Bi_{1.5+x}Zn_{1.0}Nb_{1.5}O_7$ targets.

Table 3.1. Main raw materials for the preparation of $Ba_xSr_{1-x}TiO_3$ ceramics

Raw materials	Molecular Formula	Specification	Company
Barium Carbonate	$BaCO_3$	99.00 %	Sinopharm Chemical Reagent Co., Ltd
Strontium Carbonate	$SrTiO_3$	99.00 %	Sinopharm Chemical Reagent Co., Ltd
Titanium Dioxide	TiO_2	99.44 %	Shanghai Titanium Dioxide Plant

Table 3.2. Main raw materials for the preparation of $Bi_{1.5+x}Zn_{1.0}Nb_{1.5}O_7$ ceramics

Raw Materials	Molecular Formula	Specification	Company
Bismuth Oxide	Bi_2O_3	99.90 %	Sinopharm Chemical Reagent Co., Ltd
Zinc Oxide	ZnO	99.50 %	Sinopharm Chemical Reagent Co., Ltd
Niobium Pentoxide	Nb_2O_5	99.99 %	Sinopharm Chemical Reagent Co., Ltd

3.2 RF Magnetron Sputtering System

Sputtering is a kind of physical vapor deposition technique which generates a glow discharge and results in a target surface being bombarded by energetic particles such as Ar ions as shown in Fig. 3.3.

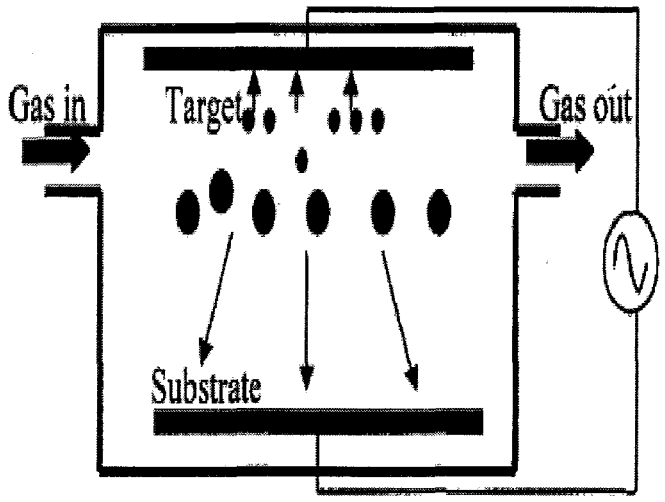

Fig. 3.3. Schematic drawing of a sputtering process

The sputtering chamber is pumped down to high vacuum first. Then a working gas such as argon is introduced into the chamber. The target is connected to a high negative voltage source, which ionizes the argon gas into positive ions and electrons. After the glow discharge occurs, the positive argon ions are accelerated towards the target and knock off clusters of atoms from the target surface. The bombarded target atoms travel through the plasma and collide with the plasma species including electrons, neutrals and gas ions and subsequently are deposited onto the substrate. The energy of the arriving atoms depends on the sputtering parameters such as power and pressure.

Both direct current (DC) and radio frequency (RF) power can be applied to the target depending on the electrically conductivity of the target. DC power can be used only for conducting targets, whereas RF power can be used for both conducting and insulating targets. Magnetron sputtering is another technique which can increase the sputtering rate and operate at lower pressure. In magnetron sputtering, a permanent magnet is installed on the backside of the cathode and generates a magnetic field to trap secondary electrons close to the target during the sputtering process. The electrons follow helical paths around the magnetic field lines and have more ionizing collisions with the neutral gas near the target than would otherwise occur. This enhances ionization of the plasma near the target and leads to a higher sputtering rate.

It also means that the plasma can be sustained at a lower pressure. The sputtered atoms are neutrally charged and so are unaffected by the magnetic trap.

The machine used for Pt and Ti deposition was a MRC system with 5"diameter commercial metal targets. The machine for $Ba_xSr_{1-x}TiO_3$ and $Bi_{1.5}Zn_{1.0}Nb_{1.5}O_3$ films was Plasyss system with a 3" ceramic target and magnetron sputtering. All the above sputtering machines use on-axis sputtering, which means the target surface is facing the substrate directly. In the Plasyss, the substrate could be heated up to 1200 °C using a copper resistance heater. The chamber was evacuated to a base pressure of 5×10^{-7} Torr using a turbo molecular pump. Then, the sputtering gas of Ar or Ar/O_2 mixture at a desired pressure was introduced into the chamber. Up to 50W RF power was applied to the target to ignite the plasma. The power, gas pressure and substrate temperature were adjusted to optimize the film quality.

3.3 Film Preparations

3.3.1 Pt Metal Electrodes

Single crystal silicon wafers with (100) orientation were cleaned using acetone, isopropanol and deionized water, then dried with a nitrogen gun and loaded into the MRC sputtering chamber, in which 5" target of Pt and Ti were installed. Pt (120nm) and TiO_x (20nm) were deposited at room temperature. After deposition, the $Pt/TiO_x/SiO_2/Si$ heterostructures were then post-annealed at 700 °C for 1 h in the conventional furnace to improve the crystallization. The X-ray diffraction (XRD) spectrum for $Pt/TiO_x/SiO_2/Si$ shows that Pt is highly (111) textured as shown in Fig. 3.4.

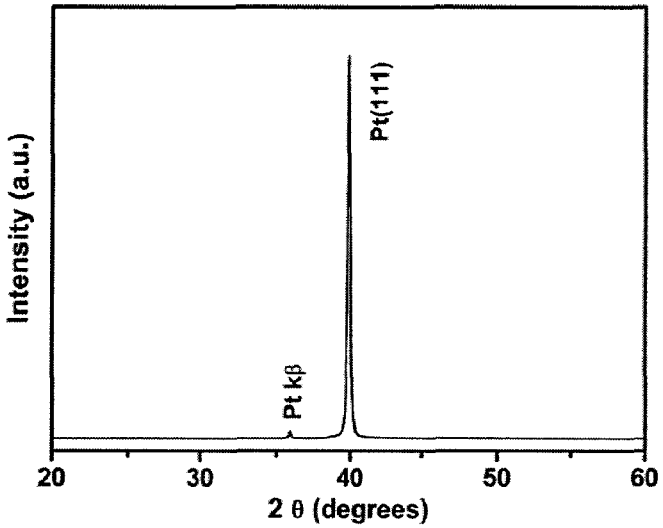

Fig. 3.4. XRD results of Pt/TiO_x/SiO_2/Si films

3.3.2 BST Thin Films Deposition

(Ba,Sr)TiO_3 (BST) thin films were *in-situ* deposited on the annealed Pt(111)/TiO_x/SiO_2/Si substrates using RF magnetron sputtering system (Plasyss). The sputtering target was ceramic $Ba_{0.6}Sr_{0.4}TiO_3$ with excess BaO and SrO which has been introduced in section of 3.1.1. Details of the BST thin films deposition conditions were tabulated in Table 3.3.

Table 3.3. Details of the BST thin films deposition conditions

Sputtering parameters	Conditions
Base pressure (Torr)	$<2\times10^{-6}$
Deposition pressure (mTorr)	15
Power density (W/cm^2)	1.58
O_2/(Ar+O_2) (%)	0; 10; 20; 30; 40; 50
Growth rate (nm/min); OMR from 0% to 50%	2.59; 1.98; 1.77; 1.50; 1.36; 1.13
Target	Ceramic $Ba_{0.6}Sr_{0.4}TiO_3$ containing excess BaO and SrO
Substrate temperature (°C)	800
Target-substrate distance (mm)	80

3.3.3 BZN Thin Films Deposition

$Bi_{1.5}Zn_{1.0}Nb_{1.5}O_7$ (BZN) thin films were *in-situ* deposited on the annealed Pt(111)/TiO_x/SiO_2/Si substrates using RF magnetron sputtering system (Plasyss). The sputtering target was ceramic $Bi_{1.5}Zn_{1.0}Nb_{1.5}O_7$ with excess Bi_2O_3 which has been introduced in section of 3.1.2. Details of the BZN thin films deposition conditions were tabulated in Table 3.4.

Table 3.4. Details of the BZN thin films deposition conditions

Sputtering parameters	Conditions
Base pressure (Torr)	$<2\times10^{-6}$
Deposition pressure (mTorr)	15
Power density (W/cm^2)	1.58
O_2/(Ar+O_2) (%)	30
Growth rate (nm/min);	3.20
Target	Ceramic containing excess Bi_2O_3
Substrate temperature (°C)	600-750
Target-substrate distance (mm)	80

3.4 Characterization Techniques

In this research work, for film microstructure and surface morphology characterization, X-ray diffraction (XRD) and Scanning electron microscopy (SEM) served as the primary tools. The electrical properties were measured using metal-insulator-metal (MIM) configuration at low frequency (< 1 MHz) and coplanar waveguide (CPW) transmission line at high frequency (1-50 GHz). The following sections provide a brief overview and description of these techniques.

3.4.1 X-Ray Diffraction (XRD) Analysis

X-ray diffractometers (Siemens D5000, München, Germany) were used to characterize ceramic targets and related thin films. All the XRD patterns were

collected using Cu Kα radiation in a step-scan mode with voltage and current at 40 kV and 40 mA. XRD patterns were obtained at a scan speed of 0.4°/min with a scan step of 0.04° over 2θ range of 20-60° for phase identification. Lattice parameters of BST films were determined using (001) and (111) peaks. After the 2θ positions were obtained, the lattice parameters were calculated using Bragg equation:

$$\lambda=2d\sin\theta \tag{3.1}$$

$$d=\frac{a}{\sqrt{h^2+k^2+l^2}} \quad \text{(for cubic structure)}$$

3.4.2 Scanning Electron Microscopy (SEM)

A high resolution scanning electron microscopy (SEM, Ultra55, Zeiss, Oberkochen, Germany) equipped with a field-emission source were used to examine the microstructure and morphology of BST and BZN thin films. Also, the thicknesses of the films were determined with FE-SEM from film cross-section observations. The acceleration voltage used was between 5-15 kV. Work distance was between 8 to 15 mm.

3.4.3 Atomic Force Microscopy (AFM)

AFM is a microscopic technique that measures the morphology and properties of surfaces on the atomic scale. It can be used to measure surface photography, surface hardness, and elastic modulus. The interaction that is monitored in AFM is the van der Waals force between the tip and the surface; this may be either the short-range repulsive force (in contact-mode) or the longer-range attractive force (in non-contact mode). For AFM, a sharp tip, typically made from Si_3N_4 or Si is placed at the end of cantilever with a very low spring constant. The nanoscope AFM head employs an optical detection system in which the tip is attached to the underside of a reflective cantilever. A diode laser is focused onto the back of a reflective cantilever. As the tip scans the surface of the sample, moving up and down with the contour of the surface, the laser beam is deflected off the attached cantilever into a dual element photodiode.

In the present work, the surface morphologies of the thin films were imaged using contact mode atomic force microscopy (AFM, Veeco, Santa Barbara, CA, USA).

3.4.4 Electrical Measurements

3.4.4.1 Metal-Insulator-Metal Structure

For electrical measurements at low frequency, metal-insulator-metal (MIM) structure capacitors were defined by standard photolithographic lift-off technique using dc magnetron sputtered 120-nm-thick Pt electrodes (A=1.766×10^{-4} cm^2) on the films surface. The capacitors were then annealed at 500 °C for 60 min in an air ambient to improve the top electrode/BST interface. The dielectric properties of the films with MIM structure were measured with an Agilent 4192A (HP, Englewood, CO, USA) precision impendance analyzer by applying 100 mV oscillating test field at frequency of 10 kHz at room temperature (RT). The MIM structure for capacitance measurement was shown in Fig. 3.5. The dielectric constant of (ε_r) the films was extracted from the capacitance by the equation: ε_r=Cd/ε_0A. Where d is the thickness of the film and A is area of the top electrode.

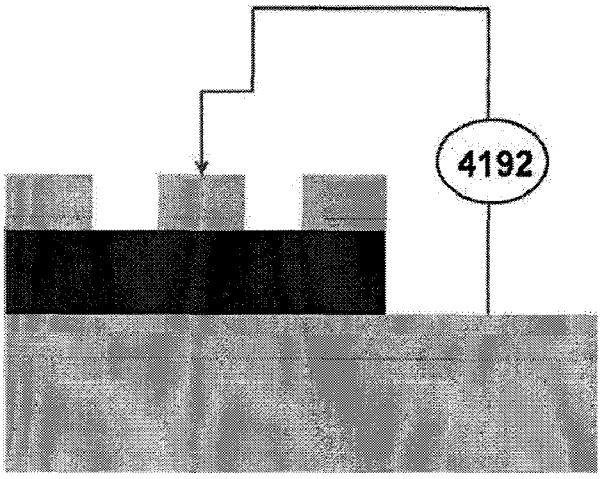

Fig. 3.5. The MIM structure for capacitance measurement

The Curie temperature (Tc) was measured by a semiconductor characterization system (Keithley, 4200-SCS, Cleveland, USA) interfaced with a temperature-controlled probe station under vacuum and cooled with liquid N_2 in a temperature range of 100-320 K.

3.4.4.2 Coplanar Waveguide Transmission Lines

For microwave properties at high frequency, coplanar waveguide (CPW) transmission lines consisting of 3 mm long fingers, 30 μm wide centre conductor, 190 μm wide ground lines with 1.0 μm finger gap (see Fig. 3.6) were defined by standard optical photolithographic lift-off technique using electron-beam evaporated Au/Ti (300-nm-thick) electrodes on both bare substrate and film surface.

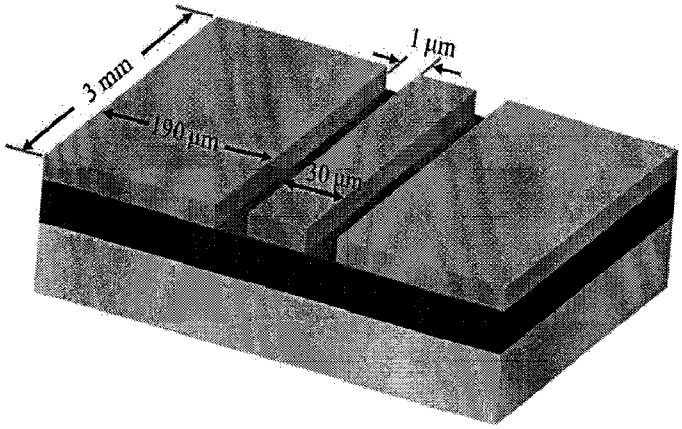

Fig. 3.6. The CPW structure for microwave measurement

The microwave dielectric properties of substrates (Sapphire, HR-Si), BST, BZN and BZN/BST films were measured as a function of frequency (1-50 GHz) and dc bias (-30-+30V) by using a ground-signal-ground microprobe (Cascade Microtech) station connected to a vector network analyzer (Agilent Technologies E8361A). First, the complex propagation constant γ ($\gamma=\alpha+j\beta$), defining microwave propagation on the transmission lines, was calculated from the scattering parameters obtained from the microwave measurements on the substrate. It is then possible to extract the complex dielectric permittivity ε ($\varepsilon=\varepsilon'-j\varepsilon''$) of the substrate and conductor losses by fitting the experimental γ using a two-dimensional tangential vector finite element method coupled with software Elfi (*JAP, 107, 054112, 2010*). It is fundamental to know these values in order to determine rigorously the main properties of the films. Finally, the intrinsic dielectric properties of the hetero structure: ε, loss, tunability was obtained by applying the same procedure.

CHAPTER 4

Growth of (001)-and (111)-Oriented BST Thin Films

This chapter is divided into two sections. In the first section (4.1) of this chapter, perfectly (001)- and (111)-oriented (Ba,Sr)TiO_3 (BST) thin films on Pt/TiO_x/SiO_2/Si without buffer layers were obtained. The second part (section 4.2) deals with the effect of ultrathin TiO_x seeding layer on crystalline orientation and electrical properties of BST thin films.

4.1 Perfectly (001)-and (111)-Oriented BST Thin Films on Pt/TiO_x/SiO_2/Si Without Buffer Layers

4.1.1 Introduction

Epitaxial and polycrystalline $Ba_xSr_{1-x}TiO_3$ (BST) thin films have been the focus for dynamic random access memories and frequency agile passive rf/microwave devices.[1,2] For high-density ferroelectric memory, the preferentially oriented films should be fabricated in order to continue scaling of ferroelectric memory devices. Epitaxial $Ba_xSr_{1-x}TiO_3$ films have been prepared, using various techniques, on different single-crystal substrates such as $LaAlO_3$ and Al_2O_3.[3,4] However, the use of these substrates is associated with major drawbacks from an industrial point of view due to their high cost and small-sized geometries (~1×1 in. pieces). Meanwhile, integrating perovskite ferroelectrics on Si technology, with its low cost, large area, and high-volume production, has intrigued great interest in order to make multifaceted devices.[5,6] Much work has been done to deposit polycrystalline ferroelectric films on platinized Si wafers for various applications.[7,8] While such an approach is quite valuable, it would also be of importance to grow an epitaxial ferroelectric layer on Si to further improve its structural and physical properties. Epitaxial growth of perovskite oxides on Si has been studied with the use of a proper buffer layer such as yttria-stabilized zirconia (YSZ), $Bi_4Ti_3O_{12}$/YSZ, and MgO.[9-11] With such a configuration, highly oriented BST was obtained and the dielectric properties were improved in comparison with polycrystalline BST. Nevertheless, the aforementioned structure is complex and a relatively simple structure is desired. Very recently, Wang *et al.*[12] fabricated (111) oriented $Ba_{0.6}Sr_{0.4}TiO_3$ film on Pt/Si(001) substrate without Ti

adhesion layer by sputtering. However, the use of Pt without Ti adhesion layer limits the versatility of this substrate. Therefore, it would be advantageous to allow growth of highly oriented BST films directly on Pt/TiO_x/SiO_2/Si substrates. In this section, $Ba_{0.6}Sr_{0.4}TiO_3$ (x=0.6, BST) thin films with different crystal orientations are deposited on Pt/TiO_x/SiO_2/Si substrates by RF magnetron sputtering without buffer layers. O_2/(Ar+O_2) mix ratios (OMR) have been used to control the crystalline properties of the BST films. This enables the growth of BST films on platinized silicon substrates without buffer layers, but with different crystallographic orientations. The effect of the orientation on the dielectric properties of BST films was also investigated.

4.1.2 Experimental Procedure

500±15 nm-thick BST thin films were *in-situ* deposited on Pt(111)/TiO_x/SiO_2/Si substrates using RF magnetron sputtering. The sputtering target was ceramic $Ba_{0.6}Sr_{0.4}TiO_3$ with excess BaO and SrO as mentioned in section 3.1.1. Details of the BST thin films deposition conditions were tabulated in Table 3.1. The structure properties and crystallinity of the BST films were characterized by an X-ray diffraction (XRD, Siemens D5000, München, Germany) with CuK_α radiation (λ=0.154 nm) using θ-2θ scan. The surface morphology and the thickness of the films were observed by scanning electron microscope (SEM; Hitachi S-4700, Tokyo, Japan). The capacitance-voltage (C-V) in the range from -400 kV/cm and 400 kV/cm were measured with an Agilent 4192A (HP, Englewood, CO, USA) precision impendance analyzer by applying 100 mV oscillating test field at frequency of 10 kHz.

4.1.3 Results and Discussions

Figure 4.1 shows the XRD patterns for BST films deposited at 800°C on Pt(111)/TiO_x/SiO_2/Si substrates with OMR ranging from 0 % to 50 %. XRD revealed that the OMR had a strong influence on the orientation and crystallization of the BST films. As shown in Fig. 4.1, films deposited with OMR=0 % were found to be single phase and perfectly oriented in the (001) direction. With increasing OMR from 10%

to 50 %, the (001) orientation was suppressed, and (111) orientation was much enhanced and completely (111)-textured BST thin films were obtained. The degree of preferred orientation, $\alpha_{(hkl)}=I(hkl)/\Sigma I(hkl)$ varies from 0 for a randomly oriented film to 1 for a completely oriented film (see Table 4.1). The BST films on $Pt/TiO_x/SiO_2/Si$ substrate show $\alpha_{(001)}$ and $\alpha_{(111)}$ of 100 % indicating perfect (001) and (111) grain orientation. The present data clearly show that the orientation of BST films could be controlled by OMR even though the dissimilarity structure between BST (pervoskite structure, a_0=3.965 Å) and Pt (fcc, a_0=3.92 Å).

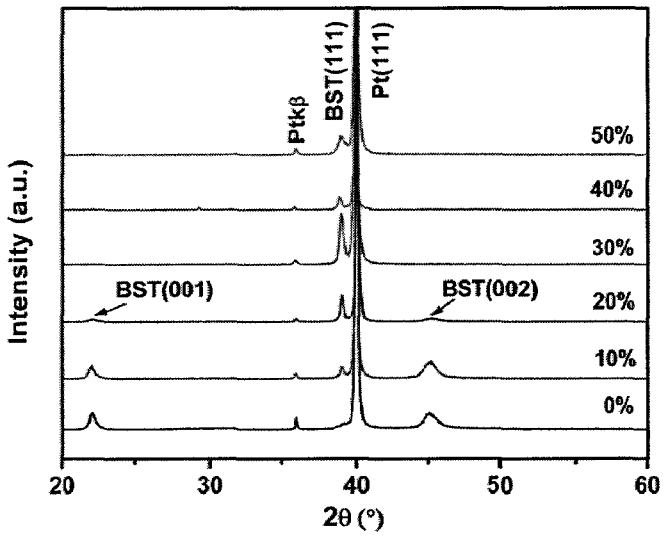

Fig. 4.1. XRD patterns of BST thin films deposited at 800°C on $Pt(111)/TiO_x/SiO_2/Si$ substrates with various OMR indicated

Table 4.1 also lists the in-plane (a), out-of-plane (c), and cubic lattice parameters (a_0) calculated by the position of (001) peak and (111) peak. The films prepared with OMR<30% exhibited out-of-plane (c>a) tetragonal lattice distortions and the cubic lattice parameters a_0 calculated for all these films were slightly larger than the bulk lattice parameter. The observations of the lattice distortion and lattice expansion may be due to lattice mismatch and thermal coefficient mismatch between film and substrate as well as oxygen vacancies in the film.[13]

Table 4.1. Lattice parameter, and the degree of orientation $\alpha_{(001)}$, $\alpha_{(111)}$ for BST thin films deposited at various OMR

OMR (%)	a (Å)	c (Å)	a_0 (Å)	$\alpha_{(001)}$ (%)	$\alpha_{(111)}$ (%)
0	_	4.017	_	100	0
10	3.980	4.024	3.995	14.36	85.64
20	3.978	4.028	3.995	9.85	90.15
30	_	_	3.995	0	100
40	_	_	4.005	0	100
50	_	_	4.007	0	100

The change of preferred orientation of BST films on $Pt/TiO_x/SiO_2/Si$ from (001) to (111) with various OMR can be explained in terms of competing surface and interface energies at the moment of nucleation. The high growth temperature (800 °C) and the high film growth rates (~2.59 nm/min, resulting from the case of OMR=0 %, see Table 3.1) probably favor the (001) nucleis by a thermodynamical mechanism due to their low surface energy.[14] However, the interface seems to dominate since oxygen presence during sputtering caused insufficient impingement of ad-atoms on the substrate (low growth rate, <2 nm/min), hence, the atoms are forced to take next energetically favorable configuration, i.e. BST(111), following the orientation of $Pt(111)/TiO_x/SiO_2/Si$ substrate.

Surface and cross-section SEM photographs of (001)-and (111)-oriented BST films deposited with OMR=0 % and 30 % are presented in Fig. 4.2. The (111)-oriented BST films had a larger grain size (~150 nm) when compared to (001)-oriented BST films of grain size 40-100 nm. An increasing in grain size of (111)-oriented BST films may be attributed to the enhanced grain growth behavior by higher OMR. Both of the cross-sectional SEM images reveal dense microstructures, a uniform thickness and sharp interface with substrate. The thickness of all BST films was carefully controlled within 500±15 nm because the dielectric permittivity of BST thin films on Pt electrodes is thickness dependent.[15]

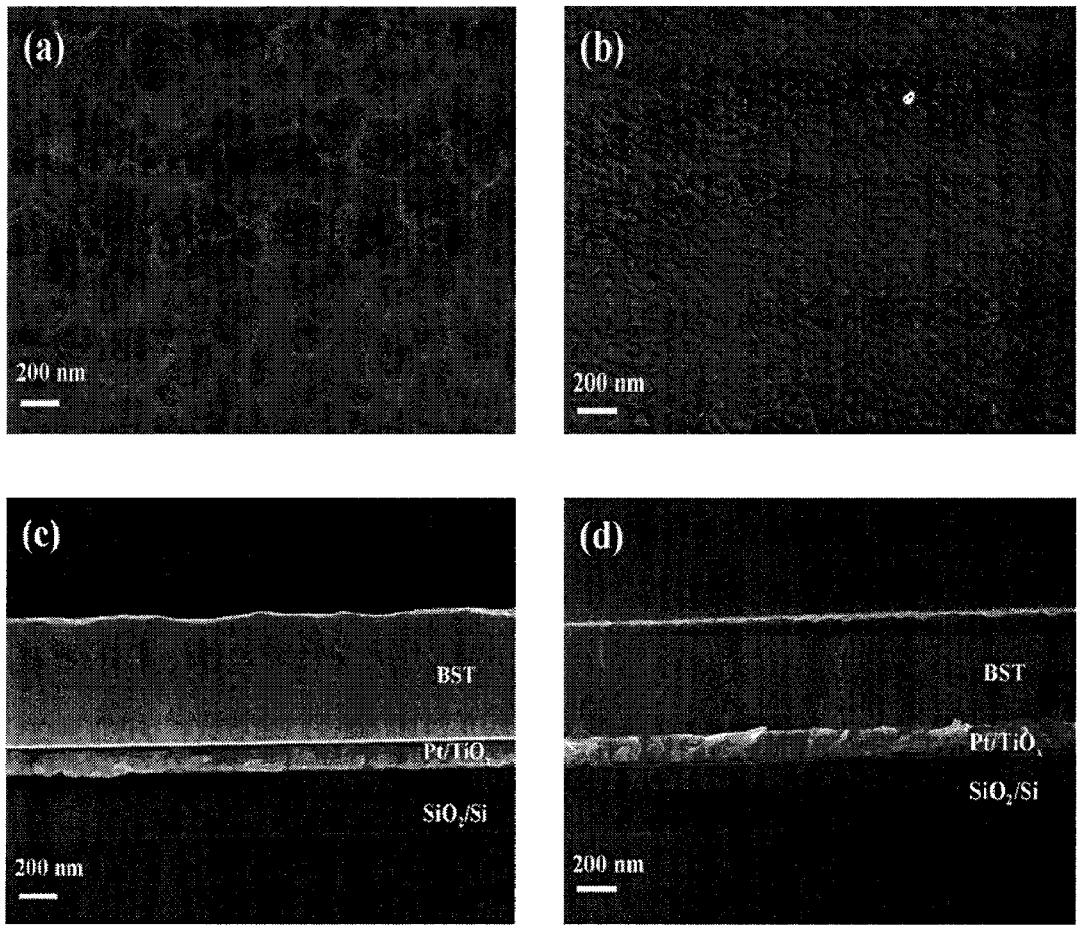

Fig. 4.2. (a) Surface and (c) cross-section SEM photographs of (001)-oriented BST thin film; (b) surface and (d) cross-section SEM photographs of (111)-oriented BST thin film deposited with OMR=0% and 30%, respectively.

Figure 4.3 shows the dielectric permittivity (ε_r) and the dielectric loss (tanδ) of BST films as a function of OMR. Depending on the degree of (111) orientation in the film (Table 4.1), each BST film shows different ε_r values. The (111)-oriented BST films always showed higher ε_r compared to the film with (001) orientation. This enhancement of ε_r was attributed to (111) orientation and the relatively larger grain size of BST films with increasing OMR. However, the decrease ε_r for the films deposited with OMR>40 % was due to relative poor crystallinity as shown in Fig. 4.1. The maximum ε_r was ~632 for (111)-oriented BST film (~332 for (001)-oriented BST film). As for tan δ of the film, a higher ε_r led to a higher tanδ, which is typical for many ferroelectric materials. The dielectric properties of BST deposited at various OMR are summarized in Table 4.2.

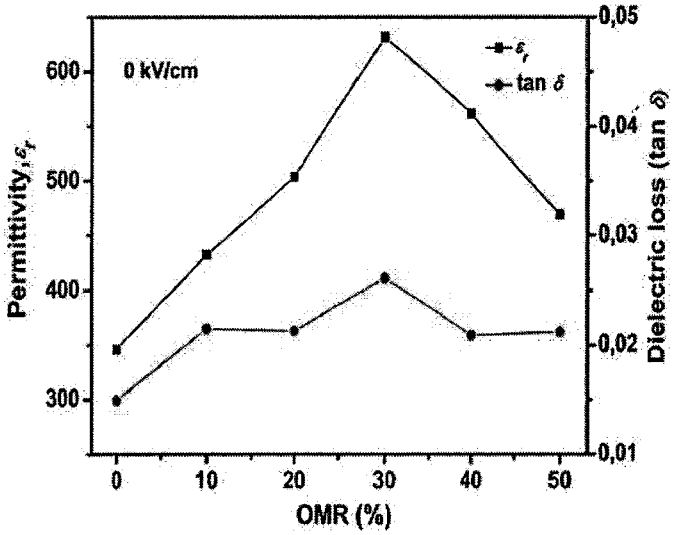

Fig. 4.3. The permittivity ε_r and the dielectric loss (tanδ) for BST thin films as a fuction of OMR, at 10 kHz frequency

Table 4.2. Summary of dielectric properties BST thin films deposited at various OMR

OMR (%)	Permittivity	tanδ at zero field	Tunability (%) at 400kV/cm	FOM
0	346.06	0.0149	52.12	34.98
10	432.34	0.0215	58.94	27.41
20	503.96	0.0213	60.56	28.43
30	631.42	0.0261	67.82	25.98
40	561.69	0.0209	62.49	29.89
50	469.21	0.0212	59.02	27.83

Figure 4.4 shows the electric field dependence of ε_r for (001)-and (111)-oriented BST films prepared with OMR=0 % and OMR=30 %, respectively. Both of the BST films exhibited clear hysteresis (butterfly curves) in the ε_r with dc bias, indicating the presence of permanent dipoles. Tunability is defined as $(\varepsilon_{r,max}-\varepsilon_{r,min})/\varepsilon_{r,max}$, is known to depend the degree of orientation.[16] The (111)-oriented BST film grown with OMR=30 % exhibited a remarkably tunability of 68 %, as compared to 52 % obtained

with the highly (001)-oriented BST film, at an applied field of ± 400 kV/cm. This value is comparable to that of polycrystalline BST thin films[8] (28 %, at 237 kV/cm), and to that of epitaxial (111)-textured BST film (49.4 %, at 455 kV/cm).[12] It is believed that the lager grains in (111)-oriented BST films deposited with OMR=30 % are also likely the source of the increased tunability.

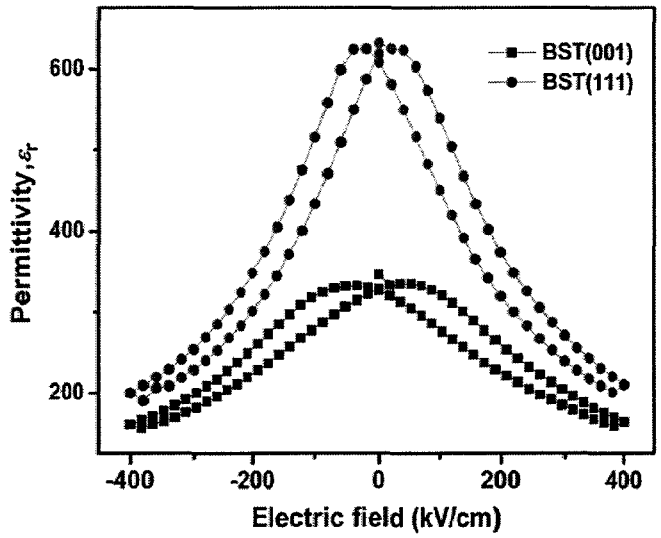

Fig. 4.4. Permittivity-electric field characteristics of (001)-and (111)-oriented of BST thin films prepared with OMR=0% and OMR=30%, respectively

4.1.4 Summary

In conclusion, perfectly (001)-and (111)-oriented $Ba_{0.6}Sr_{0.4}TiO_3$ (BST) thin films were grown on Pt (111)/TiO_x/SiO_2/Si substrates by RF magnetron sputtering without buffer layers. The oxygen presence which lowered the growth rates during sputtering have been identified as critical parameter. The perfectly (111)-oriented BST films deposited with OMR=30 % exhibited a broader grain size distribution than the (001) textured BST films. At an applied field of 400 kV/cm, high tunability of 52 % and 68 % can be achieved for (001)-and (111)-oriented BST films, respectively. This work demonstrates that the orientation of BST thin films can be controlled on Pt which should enable development of the next generation of ferroelectric devices.

4.2 Effects of Ultrathin TiO_x Seeding Layer on Crystalline Orientation and Electrical Properties of BST Thin Films

In this section, the effects of ultrathin TiO_x seeding layer on crystalline orientation and electrical properties of BST thin films have been investigated. An ultrathin TiO_x layer acts as an initial template for the BST films in the first nucleation stage, resulting in a significant influence on crystalline orientation and electrical characteristics of the resultant BST films.

4.2.1 Introduction

$Ba_xSr_{1-x}TiO_3$ (BST) thin films are being widely investigated for applications as Gbit dynamic random access memories, bypass capacitor, and tunable microwave devices because of its high dielectric constant, low dielectric loss, good thermal stability, and good high frequency characteristics.[17,18] The dielectric behaviors of BST films, including the dielectric constant, and tunability of capacitance are very sensitive to the relative crystallographic orientation, as has been observed by comparing (001), (110), (111), or randomly oriented films.[19,20] Generally, polycrystalline BST thin films are of great interest in part because of their good dielectric and electrical properties for a broader choice of device integration strategies.[7] However, randomly oriented polycrystalline films have certain limitations, and they may have unacceptable cell-to-cell variations when the lateral size of the ferroelectric cells is below 100 nm, as is required for Gbit memories.[21] The use of uniformly oriented ferroelectric films is most probably the only way to avoid such problems in high-density ferroelectric memories. Effective measures so far taken on preparing well-oriented BST thin films had been focused mainly on selection of single-crystal substrates such as Al_2O_3 and MgO, insertion of a seeding layer and/or different bottom electrodes.[20,11,22,23] Particularly, the nucleation and growth of thin films is known to be severely varied, depending on the type and material of seeding layer, which works as an initial template for the rest of the growth and determines the quality of the final film. A thin TiO_x seeding layer has been proved to play an

important role in improving electrical properties of $Pb(Zr,Ti)O_3$ films by tailoring the film orientation and acting as a barrier layer between the substrate and the film.[24,25] Moreover, the TiO_x thin film (~50 nm) also has been used as a microwave buffer layer to obtain high-tunability (33.2 %, up to 40 V) and low-microwave-loss (0.079) of BST films at 2 GHz and enables the successful integration of BST-based microwave tunable devices onto high-resistivity Si wafers.[26] However, the role of an ultrathin TiO_x seeding layer plays on structural and electrical properties of BST films on widely used Pt-coated Si substrates is unclear. In this section, we intentionally deposited ultrathin (0~12 nm) TiO_x films to investigate the effects of TiO_x seeding layers on the crystalline orientation, microstructure, and electrical characteristics of BST thin films on $Pt(111)/TiO_x/SiO_2/Si$ substrates.

4.2.2 Experimental Procedure

A series of TiO_x layers with thicknesses ranging from 0~12 nm were firstly deposited on $Pt(111)/TiO_x/SiO_2/Si$ substrates by dc magnetron reactive sputtering at room temperature using commercial Ti metal target followed by a post-anneal at 700 °C for 60 min in an air ambient. The thickness of the ultrathin TiO_x seeding layer was estimated by the deposition time according to the average growth rate of the thick TiO_x film on SiO_2/Si substrates. 600±15-nm-thick BST(x=0.4) films were then *in-situ* (800°C) deposited on TiO_x(0~12nm)/Pt(120nm)/$TiO_x/SiO_2/Si$ substrates by RF-magnetron sputtering from a stoichiometric $Ba_{0.6}Sr_{0.4}TiO_3$ ceramic target with excess BaO and SrO using an 100 % Ar sputtering gas with total pressure of 15 mTorr and a sputter power of 70 W. The distance between the target and substrate was kept 8 cm. For electrical measurements, metal-insulator-metal structure capacitors were defined by standard photolithographic lift-off technique using dc magnetron sputtered 120-nm-thick Pt electrodes (A=1.766×10^{-4}cm^2) on the BST films surface. The capacitors were then annealed at 500 °C for 60 min in an air ambient to improve the top electrode/BST interface. The structure properties and crystallinity of the BST films were characterized by an X-ray diffraction (XRD, Siemens D5000, München, Germany) with CuK_α radiation using θ-2θ scan. The surface morphology and the

thickness of the films were observed by scanning electron microscope (SEM, Ultra55, Zeiss, Oberkochen, Germany). The capacitance-voltage (C-V) were measured with an Agilent 4192A (HP, Englewood, CO, USA) precision impendance analyzer by applying 100 mV oscillating test field at frequency of 10 kHz at room temperature. The Curie temperature (*Tc*) was measured by a semiconductor characterization system (Keithley, 4200-SCS, Cleveland, USA) interfaced with a temperature-controlled probe station under vacuum and cooled with liquid N_2 in a temperature range of 100-320 K.

4.2.3 Results and Discussions

Figure 4.5 shows XRD patterns of BST thin films deposited on Pt(111)/TiO_x/SiO_2/Si substrates buffered with different thickness of TiO_x seeding layer. As shown in Fig. 4.5, the thickness of the seeding layer was varied as 0, 1.2, 5, 7, and 12 nm, and the orientation of the BST films switched from (001) to (111) preferred orientation. The degree of preferred orientation, $\alpha_{(hkl)}=I(hkl)/\Sigma I(hkl)$, where $I(hkl)$ is the relative intensity of the corresponding diffraction peaks, varies from 0 for a randomly oriented film to 1 for a completely oriented film (see inset of Figure 4.5). For example, the BST film onto 5-nm-thick TiO_x-covered Pt(111) substrate shows $\alpha_{(111)}$ of 97 % , implying that the film is highly (111)-oriented. Considering that BST film directly fabricated on bare Pt (111) substrate shows $\alpha_{(001)}$ of 100 %, the results in Fig. 4.5 clearly conclude that an ultrathin TiO_x seeding layer formed on Pt (111) surface assists the (111) growth of BST film, which is consistent with the point that an ultrathin TiO_2 layer can promote (111) growth of perovskite films such as $SrTiO_3$ and (Pb,La)(Zr,Ti)O_3 on Pt(111)[27,28]. However, TiO_x-assistant improvement in crystallinity seems to have an optimized thickness window, the increases of (111) orientation intensities concomitant with the initial increase in TiO_x thickness and show maximums at 5-nm-thick. This trend suggests that an even thicker TiO_x (e.g., 7 or 12 nm) seeding layer seems not favourable for crystallization of the BST films, which might be attributed to an excess of amount TiO_x formed at the BST/Pt interface.

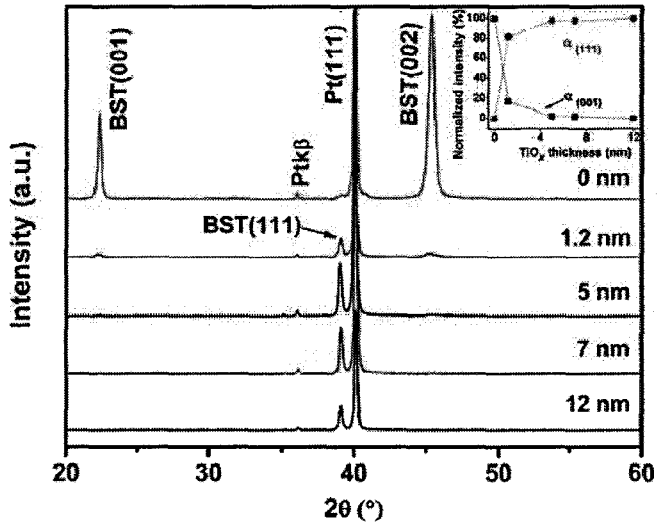

Fig. 4.5. X-ray diffraction patterns of $(Ba,Sr)TiO_3$ (BST) thin films on $Pt(111)/TiO_x/SiO_2/Si$ substrates buffered with different thickness of TiO_x seeding layer. Inset is the degree of orientation for BST films, $\alpha_{(001)}$, $\alpha_{(111)}$ as a function of TiO_x thickness.

The change in orientation and crystallinity for BST films is undoubtedly related to the growth mode of perovskite layer by the inserted TiO_x layer, in association with the expected underlying substrate and the interface properties. The additional TiO_x on Pt (111) surface serves as an initial template layer which in turn, results in minimize the surface nucleation activation energy for crystallization. Meanwhile, the TiO_x layer plays an active role in increasing the number of active sites for BST nucleation and facilitates crystallization the pervoskite phase along the orientation of $Pt(111)/TiO_x/SiO_2/Si$ substrate more easily to cause (111)-oriented BST films.

Figures 4.6 (a) and 4.6 (b) show the SEM images of the surface BST thin films on (a) 0-nm-thick and (b) 5-nm-thick TiO_x seeding layer, respectively. The 5-nm-thick TiO_x seeded BST (111) film appears to possess larger grains with better uniformity in microstructure compared to that of BST (001) on Pt directly without TiO_x layer formation. The reason for the larger grains with better uniformity for the $BST(111)/TiO_x(5nm)$ film can also be ascribed to the decrease in nucleation energy during film growth process. A similar phenomenon was also reported by Li *et al.*[29] in TiO_2 seeded $Bi_{3.15}Nd_{0.85}Ti_3O_{12}$ films.

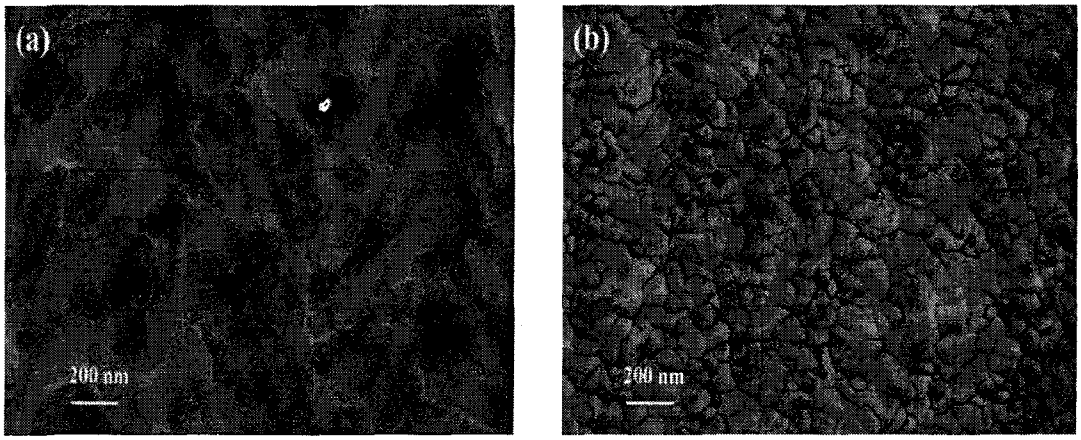

Fig. 4.6. Scanning electron microscope (SEM) photographs of the surface of (Ba,Sr)TiO_3 (BST) thin films with (a) 0-nm-thick and (b) 5-nm-thick TiOx seeding layer

Figures 4.7 (a) and 4.7 (b) depict the permittivity (ε) and loss tangent (tan δ) of the BST films with TiO_x thickness ranging from 0 to 12 nm as a function of bias field at room temperature. An outstanding improvement in dielectric characteristics of BST films was observed with the introduction of ultrathin TiO_x seeding layer. Specially, the ε at zero-bias increases initially and then decreases with increasing thickness of TiO_x seeding layer and reaches a maximum value of 504 for the BST(111)/TiO_x(5nm) film. As for tan δ shown in Fig. 4.7 (b), low values (tan δ < 0.02) are obtained for all the BST films. The tunability is defined as $\{(\varepsilon(0)-\varepsilon(E_{max})/\varepsilon(0)\}\times 100\%$, where ε(0), ε($E_{max}$) are the permittivity of BST film at zero and maximum bias field, respectively. The trends of permittivity and tunability versus TiO_x seeding layer thickness are illustrated in Fig. 4.7(c), from which a prominent enhancement tunability of 61.10 % can be achieved for the BST(111)/TiO_x(5nm) film, as compared to 50.05 % obtained with BST(001)/TiO_x(0nm) film, at an applied field of ± 400 kV/cm. This value is comparable to that of (111)-textured BST films with 10-nm-thick MgO buffer layer (30 %, at 300 kV/cm)[11] and to that of polycrystalline BST films (28 %, at 237 kV/cm).[30] These results are consistent with XRD and SEM analyses, as the dielectric properties of BST films are profoundly affected by the crystallinity, microstructure, and preferred orientation.[31,32] The hysteresis effects (butterfly curves) that are ascribed to some local ferroelectric domains existed in films[33] or induced by dead interface

layer for the BST films should be mentioned. Similar effects have not been observed obviously in BST(111)/TiO_x(5nm) films shown inset of Fig. 4.7(a), which suggested that an optimum thickness of TiO_x (5-nm-thick) seeding layer was expected to suppress the formation of the low dielectric layer at the interface. By further increasing TiO_x thickness, the interface layer might reappear thus deteriorate the permittivity and tunability value. The dielectric properties of BST films deposited with various TiO_x were summarized in Table 4.3.

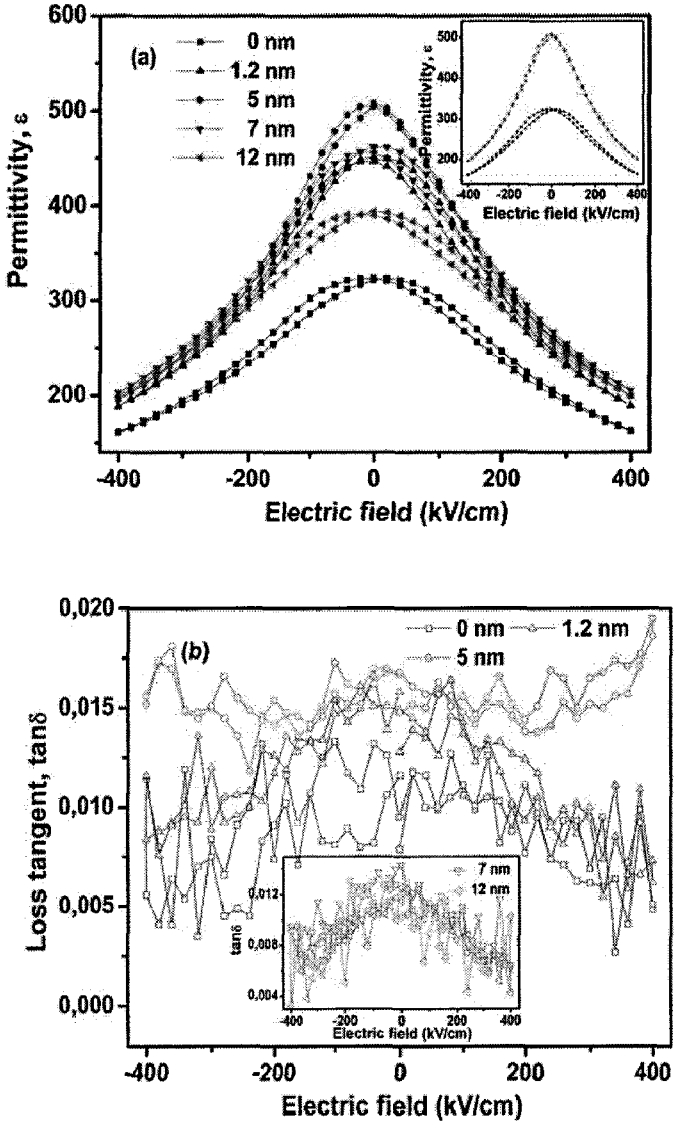

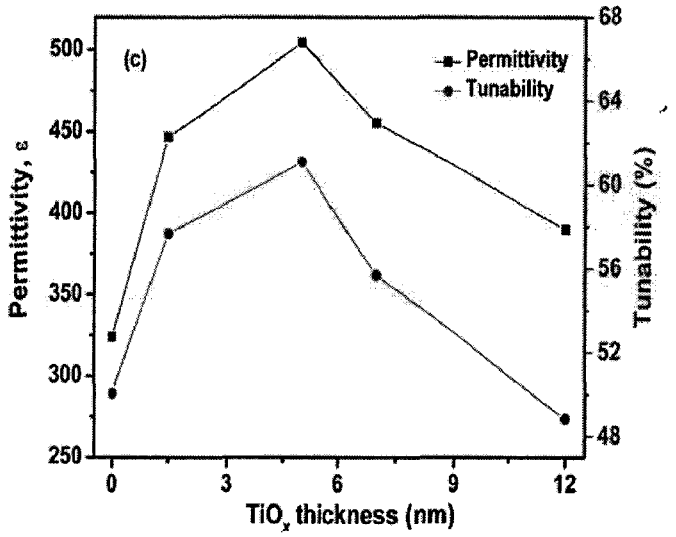

Fig. 4.7. (a) The permittivity (ε) and (b) the loss tangent (tan δ) of the (BST) thin films with TiO_x thickness ranging from 0 to 12 nm as a function of bias field, at 10 kHz frequency; [Inset is the permittivity of the BST films with 0 and 5-nm-thick TiO_x as a function of bias field]; (c) Variation of the permittivity and tunability of the BST films as a function of TiO_x seeding layer thickness.

Table 4.3. Summary of dielectric properties BST thin films deposited with various TiO_x

TiO_x (nm)	Permittivity	tanδ at zero field	Tunability (%) at 400kV/cm	FOM
0	323.76	0.0095	50.05	52.68
1.2	446.52	0.0149	57.57	38.64
5	504.51	0.0168	61.10	36.37
7	455.33	0.0143	54.94	38.42
12	389.72	0.0115	48.64	42.30

Measurement of the electrical properties over a temperature range of 100 to 320 K enabled the Curie peak at the Curie temperature (*Tc*), to be observed and also gave an idea of the possible effects of the temperature variation.

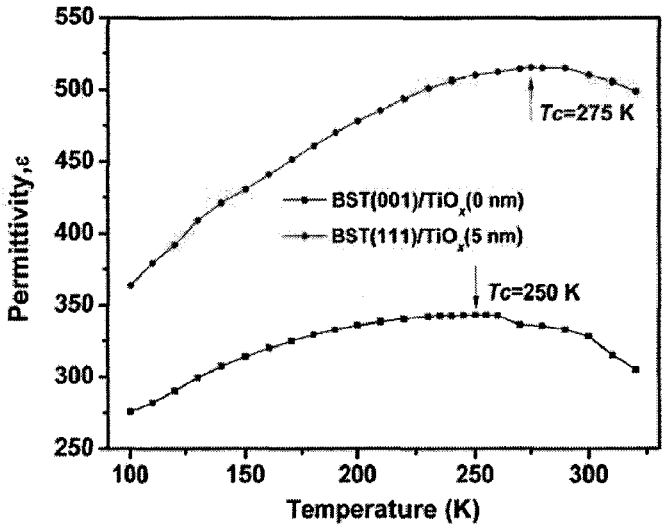

Fig. 4.8. The permittivity at zero-bias as a function of temperature at 10 kHz for (Ba,Sr)TiO_3 (BST) thin films with 0 and 5-nm-thick TiO_x seeding layer

The permittivity as a function of temperature at 10 kHz for BST films with 0 and 5-nm-thick TiO_x layer is shown in Fig. 4.8. The Curie temperature of the BST(111)/TiO_x(5nm) film [*Tc*~275K, close to that of the $Ba_{0.6}Sr_{0.4}TiO_3$ ceramic (*Tc*~278K)[34]] is about 25 K higher than that of the BST(001)/TiO_x(0nm) (*Tc*~250K), consistent with the increase in measured permittivity for BST(111)/TiO_x(5nm) films [Fig. 4.7(c)]. The shift of *Tc* in the BST(111)/TiO_x(5nm) film can be accounted by the larger grain size (as observed by SEM). On the other hand, the relieved stress resulting from thermal expansion mismatch strains with TiO_x incorporation was also believed to be one of the possible factors shifting the *Tc* of the BST(111)/TiO_x(5nm) film.

4.2.4 Summary

In conclusion, highly (001)-and (111)-oriented BST films have been fabricated on Pt and TiO_x-seeded/Pt substrates respectively by sputtering. The insertion of the ultrathin TiO_x layer changes the orientation of BST from (001) to (111) and results in a significant influence on microstructure and dielectric properties of resultant BST films. Interestingly, highly (111)-oriented BST film [$\alpha_{(111)}$ ~97%] with an optimum 5-nm-thick TiO_x seeding layer exhibits a shifted Curie temperature (*Tc*=275 K) and an enhanced tunability of 61.16 % at 400 kV/cm, when compared with (001)-oriented BST without TiO_x layer (*Tc*=250 K and tunability=50.05 %).

4.3 Reference

1. W. K. Simon, E. K. Akdogan, and A. Safari, "Misfit Strain Relaxation in $(Ba_{0.60}Sr_{0.40})TiO_3$ Epitaxial Thin Films on Orthorhombic $NdGaO_3$ Substrates," *Applied Physics Letters*, **89**(2), 022902-022904, 2006.

2. K. P. Jayadevan, C. Y. Liu, and T. Y. Tseng, "Surface Chemical and Leakage Current Density Characteristics of Nanocrystalline Ag-$Ba_{0.5}Sr_{0.5}TiO_3$ Thin Films," *Journal of the American Ceramics Society*, **88**(9), 2456-2460, 2005.

3. C. L. Chen, H. H. Feng, Z. Zhang, A. Brazdeikis, Z. J. Huang, W. K. Chu, C. W. Chu, F. A. Miranda, F. W. Van Keuls, R. R. Romanofsky, and Y. Liou, "Epitaxial Ferroelectric $Ba_{0.5}Sr_{0.5}TiO_3$ Thin Films for Room-temperature Tunable Element Applications," *Applied Physics Letters*, **75**(3), 412-414, 1999.

4. H. Li, J. Finder, Y. Liang, R. Gregory, and W. Qin, "Dielectric Properties of Epitaxial $Ba_{0.5}Sr_{0.5}TiO_3$ Films on Amorphous SiO_2 on Sapphire," *Applied Physics Letters*, **87**(7), 072905-072908, 2005.

5. C. H. Ahn, K. M. Rabe, and J. M. Triscone, "Ferroelectricity at the Nanoscale: Local Polarization in Oxide Thin Films and Heterostructures," *Science*, **303**, 488-91 (2004).

6. H. N. Lee, D. Hesse, N. Zakharov, and U. Gösele, "Ferroelectric $Bi_{3.25}La_{0.75}Ti_3O_{12}$ Films of Uniform *a*-Axis Orientation on Silicon Substrates," *Science*, **296**, 2006-2009, 2002.

7. J. Im, O. Auciello, P. K. Baumann, S. K. Streiffer, D. Y. Kaufman, and A. R. Krauss, "Composition-control of Magnetron-sputter-deposited $(Ba_xSr_{1-x})Ti_{1+y}O_{3+z}$ Thin Films for Voltage Tunable Devices," *Applied Physics Letters*, **76**(5), 625-627, 2000.

8. M. W. Cole, W. D. Nothwang, C. Hubbard, E. Ngo, and M. Ervin, "Low Dielectric Loss and Enhanced Tunability of $Ba_{0.6}Sr_{0.4}TiO_3$ Based Thin Films via Material Compositional Design and Optimized Film Processing Methods," *Journal of Applied Physics*, **93**(11), 9218-9225, 2003.

9. S. J. Jun, Y. S. Kim, J. C. Lee, and Y. W. Kim, "Dielectric Properties of Strained (Ba,Sr)TiO_3 Thin Films Epitaxially Grown on Si with Thin Yttria-stabilized Zirconia Buffer Layer," *Applied Physics Letters*, **78**(17), 2542-2544, 2001.

10. C. L. Canedy, S. Aggarwal, H. Li, T. Venkatesan, R. Ramesh, F. W. Van Keuls, R. R. Romanofsky, and F. A. Miranda, "Structural and Dielectric Properties of Epitaxial $Ba_{1-x}Sr_xTiO_3/Bi_4Ti_3O_{12}/ZrO_2$ Heterostructures Grown on Silicon," *Applied Physics Letters*, **77**(10), 1523-1525, 2000.

11. W. C. Zhu, J. R. Cheng, S. W. Yu, J. Gong, and Z. Y. Meng, "Enhanced Tunable Properties of $Ba_{0.6}Sr_{0.4}TiO_3$ Thin Films Grown on Pt/Ti/SiO_2/Si Substrates Using MgO Buffer Layers," *Applied Physics Letters*, **90**(3), 032907-032909, 2007.

12. Y. Wang, B. T. Liu, F. Wei, Z. M. Yang, and J. Du, "Fabrication and Electrical Properties of (111) Textured $(Ba_{0.6}Sr_{0.4})TiO_3$ Film on Platinized Si Substrate," *Applied Physics Letters*, **90**(4), 042905-042907, 2007.

13. W. Chang, C. M. Gilmore, W.-J. Kim, J. M. Pond, S. W. Kirchoefer, S. B. Qadri, D. B. Chirsey, and J. S. Horwitz, "Influence of Strain on Microwave Dielectric Properties of (Ba,Sr)TiO_3 Thin Films," *Journal of Applied Physics*, **87**(6), 3044-3049, 2000.

14. X. G. Tang, H. F. Xiong, L. L. Jiang, and H. L. W. Chan, "Dielectric Properties and High Tunability of (100)-and (110)-oriented $(Ba_{0.5}Sr_{0.5})TiO_3$ Thin Films Prepared by Pulsed Laser Deposition," *Journal of Crystal Growth*, **285**(4), 613–619, 2005.

15. P. Padmini, T. R. Taylor, M. J. Lefevre, A. S. Nagra, R. A. York, and J. S. Speck, "Realization of High Tunability Barium Strontium Titanate Thin Films by rf Magnetron Sputtering," *Applied Physics Letters*, **75**(20), 3186-3188, 1999.

16. W. Choi, B. S. Kang, Q. X. Jia, V. Matias, and A. T. Findikoglub, "Dielectric Properties of <001>-oriented $Ba_{0.6}Sr_{0.4}TiO_3$ Thin Films on Polycrystalline Metal Tapes Using Biaxially Oriented MgO/γ-Al_2O_3 Buffer Layers," *Applied Physics Letters*, **88**(6), 062907-062919, 2006.

17. V. N. Keis, A. B. Kozyrev, M. L. Khazov, J. Sok, and J. S. Lee, "20 GHz Tunable Filter Based on Ferroelectric (Ba,Sr)TiO_3 Film Varactors," *Electronic Letters*, **34**(11), 1107-1109, 1998.

18. P. C. Joshi and M. W. Cole, "Mg-doped $Ba_{0.6}Sr_{0.4}TiO_3$ Thin Films for Tunable Microwave Applications," *Applied Physics Letters*, **77**(2), 289-291, 2000.

19. H.-S. Kim, T.-S. Hyun, H.-G. Kim, I.-D. Kim, T.-S. Yun, and J.-C. Lee, "Orientation Effect on Microwave Dielectric Properties of Si-integrated $Ba_{0.6}Sr_{0.4}TiO_3$ Thin Films for Frequency Agile Devices," *Applied Physics Letters*, **89**(5), 052902-052904, 2006.

20. S. E. Moon, E. K. Kim, M. H. Kwak, H. C. Ryu, Y. T. Kim, K. Y. Kang, S. J. Lee, and W. J. Kim, "Orientation Dependent Microwave Dielectric Properties of Ferroelectric $Ba_{1-x}Sr_xTiO_3$ Thin Films," *Applied Physics Letters*, **83**(11), 2166-2168, 2003.

21. R. Ramesh, A. Inam, W. K. Chan, B. Wilkens, K. Myers, K. Remschnig, D. L. Hart, and J. M. Tarascon, "Epitaxial Cuprate Superconductor/Ferroelectric Heterostructures," *Science*, **252**(5008), 944-646, 1991.

22. B. Xiao, H. R. Liu, V. Avrutin, J. H. Leach, E. Rowe, H. Y. Liu, Ü. Özgür, H. Morkoç, W. Chang, L. M. B. Alldredge, S. W. Kirchoefer, and J. M. Pond, "Epitaxial Growth of (001)-oriented $Ba_{0.5}Sr_{0.5}TiO_3$ Thin Films on *a*-plane Sapphire with an MgO/ZnO Bridge Layer," *Applied Physics Letters*, **95**(21), 212901-212903, 2009.

23. K. H. Yoon, J.-H. Sohn, B. D. Lee, and D. H. Kang, "Effect of $LaNiO_3$ Interlayer on Dielectric Properties of $(Ba_{0.5}Sr_{0.5})TiO_3$ Thin Films Deposited on Differently Oriented Pt Electrodes," *Applied Physics Letters*, **81**(26), 5012-5014, 2002.

24. P. Muralt, T. Maeder, L. Sagalowicz, S. Hiboux, S. Scalaise, D. Naumovic, R. G. Agostino, N. Xanthopoulos, H. J. Mathieu, L. Patthey, and E. L. Bullock, "Texture Control of $PbTiO_3$ and $Pb(Zr,Ti)O_3$ Thin Films with TiO_2 Seeding," *Journal of Applied Physics*, **83**(7), 3835-3841, 1998.

25. R. Bouregba, G. Poullain, B. Vilquin, and H. Murray, "Orientation Control of Textured PZT Thin Films Sputtered on Silicon Substrate with TiO_x Seeding," *Materials Research Bulletin*, **35**(9), 1381-1390, 2000.

26. H.-S. Kim, H.-G. Kim, I.-D. Kim, K.-B. Kim, and J.-C. Lee, "High-tunability and Low-microwave-loss $Ba_{0.6}Sr_{0.4}TiO_3$ Thin Films Grown on High-resistivity Si

Substrates Using TiO_2 Buffer Layers," *Applied Physics Letters*, **87**(21), 212903-212905, 2005.

27. J. W. Lu, S. Schmidt, Y.-W. Ok, S. P. Keane, and S. Stemmer, "Contributions to the Dielectric Losses of Textured $SrTiO_3$ Thin Films with Pt Electrodes," *Journal of Applied Physics*, **98**(5), 054101-054109, 2005.

28. G. Leclerc, B. Domengès, G. Poullain, and R. Bouregba, "Elaboration of (111)-Oriented La-doped PZT Thin Films on Platinized Silicon Substrates," *Applied of Surface Science*, **253**(3), 1143-1149, 2006.

29. J. Li, J. Yu, G. Peng, Y. B. Wang, and W. L. Zhou, "Effects of TiO_2 Seeding Layer on Crystalline Orientation and Ferroelectric Properties of $Bi_{3.15}Nd_{0.85}Ti_3O_{12}$ Thin Films Fabricated by a Sol-Gel Method," *Journal of the American Ceramic Society*, **90**(10), 3220-3223, 2007.

30. M. W. Cole, W. D. Nothwang, C. Hubbard, E. Ngo, and M. Ervin, "Low Dielectric Loss and Enhanced Tunability of $Ba_{0.6}Sr_{0.4}TiO_3$ Based Thin Films via Material Compositional Design and Optimized Film Processing Methods," *Journal of Applied Physics*, **93**(11), 9218-9225, 2003.

31. Y. Wang, B. T. Liu, F. Wei, Z. M. Yang, and J. Du, "Effect of (Ba+Sr)/Ti Ratio on the Dielectric Properties for Highly (111) Oriented (Ba,Sr)TiO_3 Thin Films," *Journal of Alloys and Compounds*, **475**, 827-831, 2009.

32. K. B. Chong, L. B. Kong, L. F. Chen, L. Yan, C. Y. Tan, T. Yang, C. K. Ong, and T. Osipowicz, "Improvement of Dielectric Loss Tangent of Al_2O_3 Doped $Ba_{0.5}Sr_{0.5}TiO_3$ Thin Films For Tunable Microwave Devices," *Journal of Applied Physics*, **95**(3), 1416-1419, 2004.

33. G. Houzet, L. Burgnies, G. Velu, J. C. Carru, and D. Lippens, "Dispersion and Loss of Ferroelectric $Ba_{0.5}Sr_{0.5}TiO_3$ Thin Films Up to 110 GHz," *Applied Physics Letters*, **93**(5), 053507-053509, 2008.

34. H. T. Jiang, J. W. Zhai, X. J. Chou, and X. Yao, "Influence of Bi_2O_3 and CuO Addition on Low-Temperature Sintering and Dielectric Properties of $Ba_{0.6}Sr_{0.4}TiO_3$ Ceramics," *Materials Research Bulletin*, **44**(3), 566-570, 2009.

CHAPTER 5

Studies BZN/BST Composites Films for Microwave Applications

This chapter is divided into two sections. First section, section 5.1 describes the effects of substrate temperature on the crystalline of BZN thin films. In section 5.2, effect of BZN thickness on dielectric properties of (111)-oriented BST thin films for microwave device applications is described.

5.1 Effects of Substrate Temperature on the Crystalline of BZN films

5.1.1 Introduction

The rapid development of communication technologies, especially mobile communication systems, is facilitated by miniaturization of devices. Integrated decoupling capacitors and microwave resonators are of interest for such systems. Dielectric materials for these applications must possess a moderate to large dielectric constant, low loss tangent (tanδ), high dielectric quality factor Q (Q is equal to 1/tanδ), and a small temperature coefficient of resonator frequency (for resonators). Bi_2O_3-ZnO-Nb_2O_5 (BZN) pyrochlore ceramics have previously been developed for low firing temperature multilayer capacitors.[1-4] Recent studies showed that some compositions in the BZN system also exhibit excellent microwave properties.[5] BZN ceramics with dielectric constants >100, temperature coefficient of resonant frequency $|Tf|$<10 ppm/°C and microwave Qf>5000 GHz have been reported.[6] The good dielectric properties shown by the BZN system suggest that thin films of this composition are potential materials for integrated microwave resonators and decoupling capacitors. Thin films may have the advantage of lower crystallization temperatures and smaller device size than bulk ceramics and can be integrated in microelectronic devices. In this section, BZN thin films deposited on Pt/TiO_x/Si substrates by RF magnetron sputtering and the effects of substrate temperature on the crystalline of BZN thin films have been investigated.

5.1.2 Experimental Procedure

The BZN films were grown on Pt(111)/TiO_x/SiO_2/Si substrates by RF magnetron sputtering from a stoichiometric $Bi_{1.5}Zn_{1.0}Nb_{1.5}O_7$ ceramic target with excess Bi_2O_3

using an Ar/O_2 flow ratio of 70/30 sputtering gas mixture with total pressure of 15 mTorr and a sputter power of 70 W. The substrate temperature was varied and ranged from 600 °C to 750 °C (See details in Table 3.2). The structure properties and crystallinity of the BZN films were characterized by an X-ray diffraction (XRD, Siemens D5000, München, Germany) with CuK_α radiation using θ-2θ scan. The microstructure and the thickness of the films were examined using atomic force microscopy (AFM, Veeco, Santa Barbara, CA, USA) and scanning electron microscopy (SEM, Ultra55, Zeiss, Oberkochen, Germany), respectively. The capacitance-voltage (C-V) in the range from -400 kV/cm and 400 kV/cm were measured with an Agilent 4192A (HP, Englewood, CO, USA) precision impendance analyzer by applying 100 mV oscillating test field at frequency of 10 kHz.

5.1.3 Results and Discussions

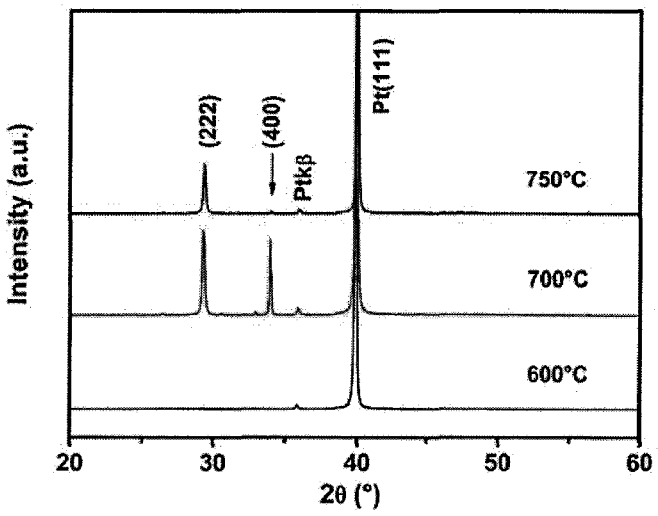

Fig. 5.1. The XRD patterns for $Bi_{1.5}Zn_{1.0}Nb_{1.5}O_7$ (BZN) films deposited on platinized silicon substrates at different substrate temperatures.

Figure 5.1 shows the XRD patterns for BZN thin films deposited on Pt(111)/TiO_x/SiO_2/Si substrates at substrate temperature 600 °C, 700 °C and 750 °C, respectively. As can be seen, the crystallization of the films strongly depends on the substrate temperature. Too low a substrate temperature (600 °C) cannot effectively convert the RF sputtered species into a crystalline structure, resulting in an amorphous

phase for the BZN films. By contrast, too high a substrate temperature (750 °C) induces vaporization loss of volatile species such as Bi and Zn, which destroys the crystallinity of the materials. Obviously, the XRD profile of the BZN films deposited at 700 °C shows a well-defined diffraction peaks. The value of lattice constant of BZN deposited at 700 °C was calculated to be 10.508 Å, which is slightly smaller than that of the bulk material (10.553 Å)[6] because of the stain effect between the BZN film and the Pt substrate.

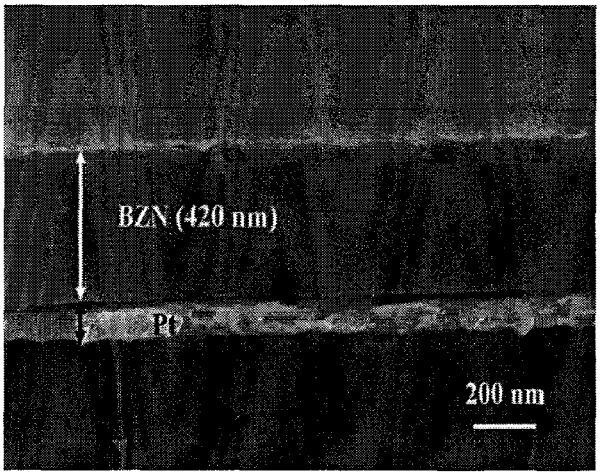

Fig. 5.2. Cross-section SEM image of BZN film deposited on platinized silicon at 700 °C

Fig. 5.2 presents the cross-section SEM image of BZN film deposited at 700 °C, from which three discernable layers were observed. The thickness of BZN layer was estimated to be ~420 nm.

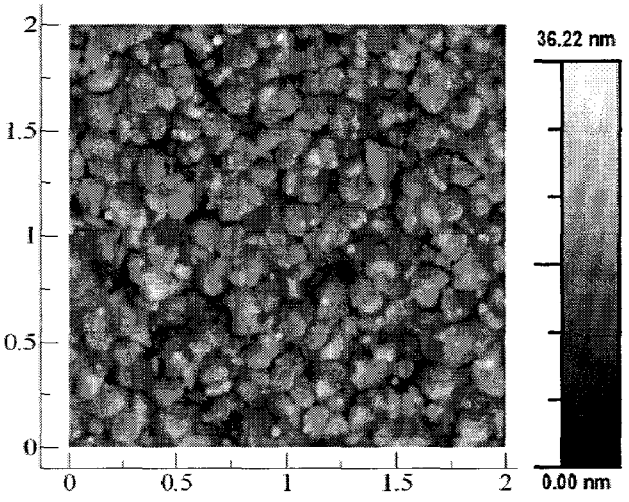

Fig. 5.3. AFM micrograph of BZN film deposited at 700 °C

The root-mean-square (rms) surface roughness of the crystalline BZN film in 2×2 μm^2 area measured by AFM was about 4.6 nm [Fig. 5.3], suggesting a very smooth thin film.

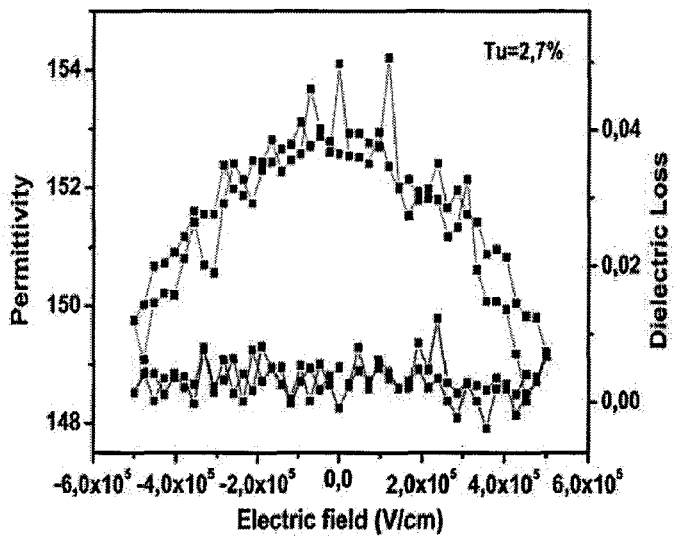

Fig. 5.4. The permittivity and loss tangent of BZN thin films deposited on Pt at 700 °C as a function of bias field at 10 kHz.

Figure 5.4 shows the permittivity and dielectric loss of BZN thin films on Pt at 700 °C as a function of bias field at frequency of 10 kHz. At zero-bias field, permittivity of ~152 and very low loss tangent of ~0.005 for BZN film can be achieved. Benefiting from extremely low loss tangent of BZN film obtaining in this study, BZN will be added as dopants to decrease the overall loss for BST thin films in the next section.

5.1.4 Summary

In summary, BZN thin films have been deposited at 600-750 °C on Pt coated Si substrate using RF magnetron sputtering. XRD, SEM and AFM analysis show that BZN deposited at 700 °C has good crystallinity and smooth surface. Electrical measurements show very low loss tangent can be achieved for BZN, thus, BZN will be used as a composite layer with BST thin films in the next section.

5.2 Improved Dielectric Properties of BZN/(111)-Oriented BST Bilayered Films for Tunable Microwave Applications

In this section, the effects of $Bi_{1.5}Zn_{1.0}Nb_{1.5}O_7$ (BZN) film thickness on dielectric properties of (111)-oriented $Ba_{0.6}Sr_{0.4}TiO_3$ (BST) thin films have been investigated. The BZN layer has played a positive role in improving the dielectric properties of the films. With the increased thickness of BZN, the dielectric loss was significantly lowered, accompanied with a tolerable reduction of tunability. The thickness effect was discussed with a series connection model of multilayered capacitors, and calculated permittivity was obtained.

5.2.1 Introduction

In recent years, much attention has been devoted to the development of tunable dielectric materials for voltage controlled, frequency-agile phase shifters and filters operating in the microwave regime.[7-9] Ferroelectrics such as $Ba_{1-x}Sr_xTiO_3$ have emerged as leading candidates for such applications due to their highly nonlinear dielectric response to an applied electric field.[10-14] The major challenge in designing material systems for tunable devices is the simultaneous requirement of high tunability (>40 %) coupled with low dielectric losses (between 3.0 and 4.0 dB in operational bandwidths ranging from several hundreds of megahertz up to 30 or more gigahertz). In the section of 4.1, we have shown that perfectly (111)-oriented $Ba_{0.6}Sr_{0.4}TiO_3$ [BST(111)] films on Pt-coated Si substrates have a dielectric permittivity of 632 with a loss tangent of 0.028 and a dielectric tunability of 67.75 % at 400 kV/cm.[15] These results are in accordance with the findings of Moon *et al.* that (111)-oriented BST thin films on MgO substrates have more advantages for microwave tunable devices application than (001)-oriented BST thin films.[16]

Compositing or introducing of BST with $Bi_{1.5}Zn_{1.0}Nb_{1.5}O_7$ (BZN) has been identified as one of the ways to reduce dielectric losses in monolithic BST films especially with low strontium content, although the addition of BZN causes a reduction in dielectric response and tunability.[17-20] For example, dielectric constant,

loss tangent, and tunability at 355 kV/cm of polycrystalline $Ba_{0.5}Sr_{0.5}TiO_3$ (400 nm) films and BZN (375 nm)/$Ba_{0.5}Sr_{0.5}TiO_3$ (300 nm) bilayered thin films were reported as 138, 0.053, and 24 % and 106, 0.011, and 10 %, respectively.[21] Thus, introducing of a low loss dielectric BZN combined with perfectly (111)-oriented BST presents an intriguing opportunity to develop materials for tunable device applications with stringent demands focused on low dielectric losses, while still maintaining moderate tunability. In this section, we present an experimental study on the addition and the thickness effect of BZN layer on dielectric properties of (111)-oriented BST thin films and show that such material systems may indeed be utilized in tunable filters for mobile communication applications such as cellular phones and handheld radios.

5.2.2 Experimental Procedure

500±15 nm-thick BZN/BST(111) bilayered thin films were deposited on Pt (120 nm)/TiO_x/SiO_2/Si substrates using RF-magnetron sputtering. The sputtering targets were ceramic $Ba_{0.6}Sr_{0.4}TiO_3$ with excess BaO and SrO and $Bi_{1.5}Zn_{1.0}Nb_{1.5}O_7$ with excess Bi_2O_3. BZN layer with various thicknesses (0; 50; 150; 250; 500 nm) were prepared on the desired BST layer thickness at a reduced temperature of 700 °C due to the lower crystallization temperature for BZN films. Details of the BST and BZN thin films deposition conditions were tabulated in Table 5.1. The structure properties and crystallinity of the bilayered thin films were characterized by an X-ray diffraction (XRD, Siemens D5000, München, Germany) with CuK_α radiation (λ=0.154 nm) using θ-2θ scan. The cross-section morphology and the thickness of the films were observed by scanning electron microscope (SEM; Hitachi S-4700, Tokyo, Japan). For electrical measurements, Metal-Insulator-Metal (MIM) structure capacitors were defined by standard photolithographic lift-off technique using dc magnetron sputtered 120-nm-thick Pt electrodes (A=1.766×10^{-4} cm^2) on the BZN/BST(111) bilayered films surface. The capacitors were then annealed at 500 °C for 60 min in an air ambient to improve the top electrode/BZN interface. The capacitance-voltage (C-V) in the range from -400 kV/cm and 400 kV/cm were measured with an Agilent 4192A (HP, Englewood, CO, USA) precision impendance analyzer by applying 100 mV

oscillating test field at frequency of 10 kHz.

Table 5.2. Details deposition conditions for BST and BZN thin films

	Films	
	BST	BZN
Base pressure (Torr)	$<2\times10^{-6}$	$<2\times10^{-6}$
Target diameter (mm)	75	75
Target-substrate distance (mm)	80	80
RF power (W)	70	70
Substrate temperature (°C)	800	700
Deposition pressure (mTorr)	15	15
Ar/O_2 flow rate ratio	70/30	70/30

5.2.3 Results and Discussions

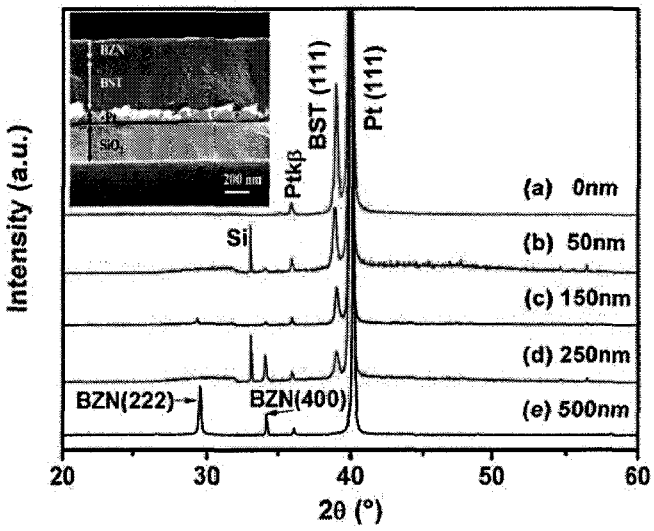

Fig. 5.5. XRD patterns of BZN/BST thin films with 0, 50, 150, 250, and 500 nm BZN thickness. Inset is the SEM cross-section image for BZN/BST with 150 nm BZN layer.

Figure 5.5 shows XRD patterns of BZN/BST bilayered thin films for different thicknesses of BZN layer. The results of the XRD indicate that the BST and BZN thin films each consist of a single phase of cubic pervoskite structure with perfect (111) orientation and cubic pyrochlore polycrystalline structure, respectively. No impurity

phases can be detected with BZN addition onto the BST layer, which excludes interdiffusion between the BZN/BST layers. The SEM cross-section image inside Fig. 5.5 shows that the BZN(150 nm)/BST(350 nm) bilayered thin films have distinct interfaces.

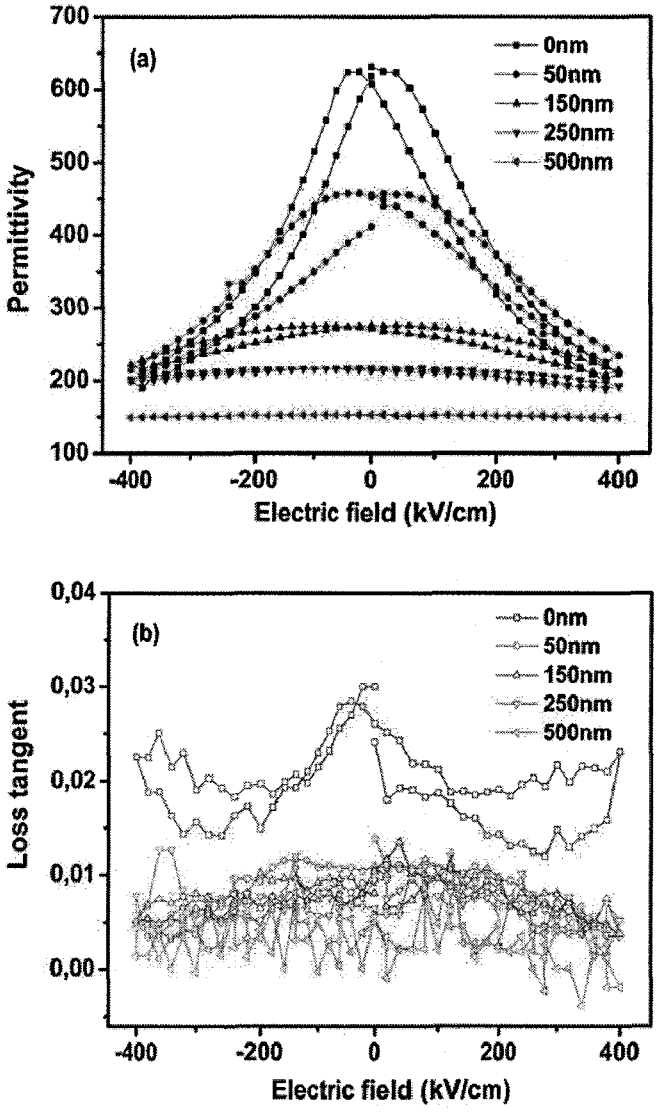

Fig. 5.6. (a) the permittivity and (b) loss tangent of BZN/BST (111) thin films with 0, 50, 150, 250, 500 nm BZN layer as a function of bias field at 10 kHz.

Figures 5.6 (a) and 5.6 (b) show the permittivity (ε) and loss tangent (tan δ) of BZN/BST (111) thin films with 0, 50, 150, 250, 500 nm BZN layer as a function of bias field. As shown in Fig. 5.6 (a), the permittivity at zero-bias electric filed of the BZN/BST(111) bilayered films decreases with increasing BZN thickness (the

permittivity values are given in Fig. 5.7). Similar phenomena were observed in SiN/$Ba_{0.5}Sr_{0.5}TiO_3$ bilayered thin films.[22] The tunability is defined as $\{(\varepsilon(0)-\varepsilon(E_{max})/\varepsilon(0)\}\times 100$ %, where $\varepsilon(0)$, $\varepsilon(E_{max})$ are the permittivity of BST thin film at zero and maximum bias field, respectively. In the meantime, the BZN/BST(111) bilayered thin films demonstrate gradually deteriorate tunability performance, which is about 67.75 %, 50.55 %, 24.64 %, 12.04 %, and 1.25 % for BZN layers of 0, 50, 150, 250 and 500 nm, respectively. A quick drop of tan δ at zero bias from 0.028 to 0.0108 with increasing in BZN thickness from 0 to 50 nm, while a slight decreasing of tan δ with further increasing in BZN thickness more than 150 nm, are observed in Fig. 5.6(b). Moreover, the tan δ of the BZN (>0 nm)/BST(111) bilayered films changed little with the downward and upward bias fields. The reduction of ε, tunability, as well as tan δ should be ascribed to the presence of BZN phase in BST. Clear hysteresis (butterflycurves) in the ε (as well as tan δ) with dc bias could be seen in Fig. 5.6. It can be attributed to the presence of permanent dipoles in the bilayered thin films or can be induced by dead interface layer. The asymmetry characteristics of the curves for the heterolayered thin films should be mentioned. Silimar asymmetry has not been observed in BZN, BST single layer or BZN/BST/BZN films with symmetry structure,[23] which suggests that the asymmetry configuration of the bilayered films should be responsible for the observed asymmetry in both curves.

The measured capacitance of the MIM structure is the series connection of the capacitance of the BST and BZN layer if the electric field is applied along the thickness direction.[17] Thus the average dielectric constant can be expressed as

$$\frac{d_{total}}{\varepsilon_{av}} = \frac{d_{BST}}{\varepsilon_{BST}} + \frac{d_{BZN}}{\varepsilon_{BZN}}, \tag{5.1}$$

where d_{total}, d_{BST}, and d_{BZN} represent the thickness of the total film, BST, and BZN, respectivley. ε_{av} is the permittivity of the bilayered film; ε_{BST}, ε_{BZN} is the permittivity of the single layer BST and BZN in our experiment, which is 632 and 152, respectively. The ε_{av} calculated from Eq. (5.1) as well as measurements of the BZN/BST(111) bilayered thin films under zero bias are presented in Fig. 5.7, which

exhibit a similar trend to the results of the experiment. Since BZN is a low dielectric layer, the decreased dielectric constant of BST thin films with increasing BZN thickness can be partially understand by Eq. (5.1). However, the difference between the calculation and measurements might actually reflect the presence interfacial capacitance. In a film, near either film-electrode interface the ionic contribution to the dielectric response is suppressed-that is, a region a few lattice constant thick acts as a low permittivity or "dead" layer.[24]

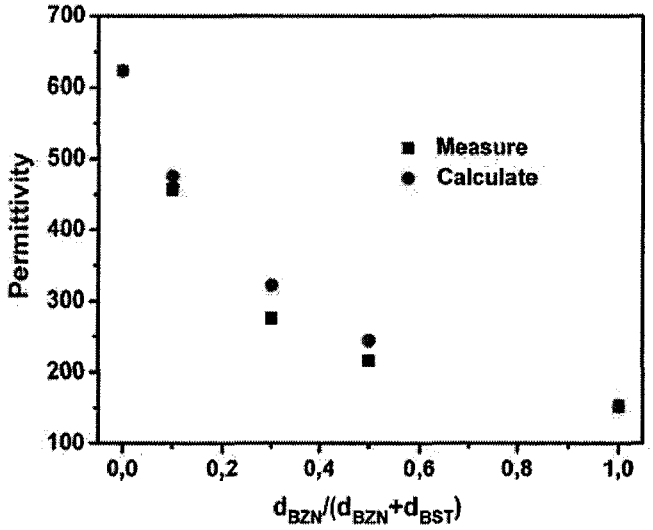

Fig. 5.7. Calculated and measured of BZN thickness dependent permittivity of BZN/BST(111) bilayered thin films using the series connection model of multilayered capacitors

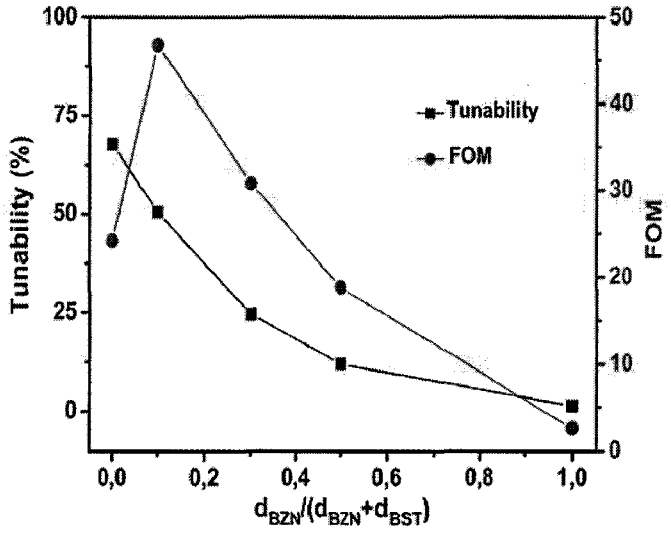

Fig. 5.8. BZN thickness dependent tunability and FOM of BZN/BST(111) bilayered thin films

The figure of merit (FOM) defined as FOM=tunability/tan δ is frequently used to characterize the quality of tunable materials, which is a balanced combination of tunability and dielectric loss. Figure 5.8 summarizes the tunability and FOM of BZN/BST(111) bilayered thin films as a function of the thickness ratio of $d_{BZN}/(d_{BST}+d_{BZN})$. As mentioned above, the tunability decreases with the increase in BZN thickness. However, the BZN/BST(111) bilayered thin films at a thickness ratio $d_{BZN}/(d_{BST}+d_{BZN})$ of 0.1 give the largest FOM of 46.8, at which the tunability and dielectric loss exhibit an optimum balance. This experimental result shows a better dielectric properties behavior than that in BST thin films with MgO buffer layer[25] and demonstrates an attractive prosper for the tunable microwave device applications.

5.2.4 Summary

Our results show that introducing of a low loss dielectric BZN combined with perfectly (111)-oriented BST is a promising tool to achieve desired material properties required for specific tunable device applications. For example, for phase shifters, one would require a large tunability. In that case, highly (111)-oriented BST thin films would be an appropriate choice. On the other hand, for frequency-agile filters operating in the microwave regime, low dielectric losses are a premium. Therefore, BZN combined with highly (111)-oriented BST would yield significantly better loss properties with a reasonable dielectric tunability. Our findings indicate than BZN/BST (111) bilayered films are promising materials for such tunable device applications which advocate stringent demands of reduced dielectric loss while maintaining moderate tunability.

5.3 Reference

1. M. F. Yan, H. C. Ling, and W. W. Rhodes, "Low-Firing, Temperature-Stable Dielectric Composition Based on Bismuth Nickel Zinc Niobates," *Journal of the American Ceramic Society*, **73**(4), 1106-1107, 1990.

2. D. Liu, Y. Liu, S. Huang, and X. Yao, "Phase structure and Dielectric Properties of Bi_2O_3-ZnO-Nb_2O_5-Based Dielectric Ceramics," *Journal of the American Ceramic Society*, **76**(8), 2129-2132, 1993.

3. D. P. Cann, C. A. Randall, and T. R. Shrout, "Investigation of the Dielectric Properties of Bismuth Pyrochlores," *Solid State Communications*, **100**(7), 529-534, 1996.

4. X. Wang, H. Wang, and X. Yao, "Structure, Phase Transformation and Dielectric Properties of Pyrochlores Containing Bismuth," *Journal of the American Ceramic Society*, **80**(10), 2745-2748, 1997.

5. H. Kagata, T. Inoue, J. Kato, and I. Kameyama, "Low-Fire Bismuth-Based Dielectric Ceramics for Microwave Use," *Japanese of Journal Applied Physics Part 1*, **31**, 3152-3155, 1992.

6. Q. Wang, H. Wang, and X. Yao, "Structure, Dielectric and Optical Properties of $Bi_{1.5}ZnNb_{1.5-x}Ta_xO_7$ Cubic Pyrochlores," *Journal of Applied Physics*, **101**(10), 104116-104120, 2007.

7. M. W. Cole, E. Ngo, S. Hirsch, M. B. Okatan, and S. Alpay, "Dielectric Properties of MgO-doped Compositionally Graded Multilayer Barium Strontium Titanate Films," *Applied Physics Letters*, **92**(7), 072906-072908, 2008.

8. K. P. Jayadevan, C. Y. Liu, and T. Y. Tseng, "Surface Chemical and Leakage Current Density Characteristics of Nanocrystalline Ag–$Ba_{0.5}Sr_{0.5}TiO_3$ Thin Films," *Journal of the American Ceramic Society*, **88**(9), 2456-2460, 2005.

9. F. A. Miranda, G. Subramanyam, F. W. van Keuls, R. R. Romanofsky, J. D. Warner, and C. H. Mueller, "Design and Development of Ferroelectric Tunable Microwave Components for *Kμ*- and *K*-Band Satellite Communication Systems," *IEEE Transaction Microwave Theory Techniques*, **48**(7), 1181-1189, 2000.

10. M. W. Cole, E. Ngo, S. Hirsch, J. D. Demaree, S. Zhong, and S. P. Alpay, "The Fabrication and Material Properties of Compositionally Multilayered $Ba_{1-x}Sr_xTiO_3$ Thin Films for Realization of Temperature Insensitive Tunable Phase Shifter Devices," *Journal of Applied Physics*, **102**(3), 034104-034114, 2007.

11. X. G. Tang, H. F. Xiong, L. L. Jiang, and H. L. W. Chan, "Dielectric Properties and High Tunability of (100)-and (110)-oriented $(Ba_{0.5}Sr_{0.5})TiO_3$ Thin Films Prepared by Pulsed Laser Deposition," *Journal of Crystal Growth*, **285**(4), 613-619, 2005.

12. Z. Yuan, Y. Lin, J. Weaver, X. Chen, C. L. Chen, G. Subramanyam, J. C. Jiang, and E. I. Meletis, "Large Dielectric Tunability and Microwave Properties of Mn-doped (Ba,Sr)TiO_3 Thin Films," *Applied Physics Letters*, **87**(15), 152901-152903, 2005.

13. S. G. Lu, X. H. Zhu, C. L. Mak, K. H. Wong, H. L. W. Chan, and C. L. Choy, "High Tunability in Compositionally Graded Epitaxial Barium Strontium Titanate Thin Films by Pulsed-Laser Deposition,"*Applied Physics Letters*, **82**(17), 2877-2879, 2003.

14. H. Shen, Y. H. Gao, P. Zhou, J. H. Ma, J. L. Sun, X. J. Meng, and J. H. Chu, "Effect of Oxygen to Argon ratio on Properties of (Ba,Sr)TiO_3 Thin Films Prepared on $LaNiO_3$/Si Substrates," *Journal of Applied Physics*, **105**(6), 061637-061640, 2009.

15. L. H. Yang, G. S. Wang, D. Rémiens, and X. L. Dong, "Perfectly (001)-and (111)-Oriented (Ba,Sr)TiO_3 Thin Films Sputtered on Pt/TiO_x/SiO_2/Si Without Buffer Layers," *Journal of the American Ceramic Society*, **93**(2), 350-352, 2010.

16. S. E. Moon, E. K. Kim, M. H. Kwak, H. C. Ryu, Y. T. Kim, K. Y. Kang, S. J. Lee, and W. J. Kim, "Orientation Dependent Microwave Dielectric Properties of Ferroelectric $Ba_{1-x}Sr_xTiO_3$ Thin Films," *Applied Physics Letters*, **83**(11), 2166-2168, 2003.

17. S. X. Wang, M. S. Guo, X. H. Guo, X. H. Sun, T. Liu, M. Y. Li, and X. Z. Zhao, "Tunable, Low Loss $Bi_{1.5}Zn_{1.0}Nb_{1.5}O_7/Ba_{0.6}Sr_{0.4}TiO_3/Bi_{1.5}Zn_{1.0}Nb_{1.5}O_7$ Sandwich Films," *Applied Physics Letters*, **89**(21), 212907-212909, 2006.

18. L. Yan, L. B. Kong, L. F. Chen, K. B. Chong, C. Y. Tan, and C. K. Ong,

"$Ba_{0.5}Sr_{0.5}TiO_3$–$Bi_{1.5}Zn_{1.0}Nb_{1.5}O_7$ Composite Thin Films with Promising Microwave Dielectric Properties for Microwave Device Applications," *Applied Physics Letters*, **85**(16), 3522-3524, 2004.

19. W. Y. Fu, L. Z. Cao, S. F. Wang, Z. H. Sun, B. L. Cheng, Q. Wang, and H. Wang, "Dielectric Properties of $Bi_{1.5}Zn_{1.0}Nb_{1.5}O_7$/Mn-doped $Ba_{0.6}Sr_{0.4}TiO_3$ Heterolayered Films Grown by Pulsed Laser Deposition," *Applied Physics Letters*, **89**(13), 132908-132910, 2006.

20. H. Y. Tian, Y. Wang, D. Y. Wang, J. Miao, J. Q. Qi, H. L. W. Chan, and C. L. Choy, "Dielectric Properties and Abnormal *C-V* Characteristics of $Ba_{0.5}Sr_{0.5}TiO_3$-$Bi_{1.5}ZnNb_{1.5}O_7$ Composite Thin Films Grown on MgO (001) Substrates by Pulsed Laser Deposition," *Applied Physics Letters*, **89**(14), 142905-142907, 2006.

21. X. Yan, W. Ren, P. Shi, X. Q. Wu, X. F. Chen, and X. Yao, "$Ba_{0.5}Sr_{0.5}TiO_3$/$Bi_{1.5}Zn_{1.0}Nb_{1.5}$ Multilayer Thin Films Prepared by Sol-gel Method," *Applied Surface Science*, **255**, 2129-2132, 2008.

22. N. D. Xiong, S. W. Jiang, Y. R. Li, L. F. Tan, and R. G. Li, "Dielectric Properties of $Ba_{0.5}Sr_{0.5}TiO_3$/SiN Bilayered Thin Films Grown on Pt-coated Sapphire Substrates," *Applied Physics Letters*, **93**(23), 232905-232907, 2008.

23. I. D. Kim, H. L. Tuller, H. S. Kim, and J. S. Park, "High Tunability (Ba,Sr)TiO_3 Thin Films Grown on Atomic Layer Deposited TiO_2 and Ta_2O_5 Buffer Layers," *Applied Physics Letters*, **85**(20), 4705-4707, 2004.

24. T. M. Shaw, Z. Suo, M. Huang, E. Liniger, R. B. Laibowitz, and J. D. Baniecki, "The Effect of Stress on the Dielectric Properties of Barium Strontium Titanate Thin Films," *Applied Physics Letters*, **75**(14), 2129-2131, 1999.

25. W. C. Zhu, J. R. Cheng, S. W. Yu, J. Gong, and Z. Y. Meng, "Enhanced Tunable Properties of $Ba_{0.6}Sr_{0.4}TiO_3$ Thin Films Grown on Pt/Ti/SiO_2/Si Substrates Using MgO Buffer Layers," *Applied Physics Letters*, **90**(3), 032907-032909, 2007.

CHAPTER 6

Thickness Effects and Interfacial Properties for BST(111) Thin Films

In this chapter, the variations in the permittivity with film thickness and measurement temperature of perfectly (111)-oriented $Ba_{0.6}Sr_{0.4}TiO_3$ (BST) thin films with thicknesses ranging from 45 to 800 nm were investigated. All the films showed elongations in the lattice parameter, suggesting the presence of residual strains but which were insensitive to film thickness. Temperature-dependent measurement of the permittivity revealed unusual Curie point independent of thickness, about 305±5 K, where the phase transition appeared frustrated. The thickness-dependent permittivity at a given temperature was explained by using the previously reported interfacial intrinsic low-permittivity layer model.

6.1 Introduction

Ferroelectric materials offer an enticing prospect for incorporation into frequency-agile microwave electronic components, including phase shifters, varactors, tunable filters, and antennas.[1,2] Ultimately, these materials are envisioned to enter into microwave integrated circuits for possible insertion in satellite and wireless communication platforms.[3,4] In this area, $(Ba,Sr)TiO_3$-based ceramic thin films are considered as leading candidates for room-temperature (RT) applications.[5,6] $(Ba,Sr)TiO_3$ solid solutions exhibit a large permittivity that can be as large as 10 000 for bulk samples in the vicinity of the paraelectric-to-ferroelectric phase transformation temperature T_C which can be controlled via the composition [e.g., the bulk T_C of $Ba_{0.6}Sr_{0.4}TiO_3$ (BST) is close to room temperature (5 °C)].[7] Tuning applications rely on the nonlinear dielectric response of ferroelectric materials, which can be maximized close to T_C.[4] So, if the T_C can be modulated to be closer to the operation temperature (*i.e.*, RT), higher tunability could be obtained. However, an almost universal issue is present: the inability to reproduce the properties of bulk ceramics or single crystals in thin-film forms, most probably due to the interfacial intrinsic low-permittivity layer,[8-10] electrode polarization,[11,12] defects and film stress.[4,13] Generally, as film thickness is reduced: catastrophic reductions in dielectric constant are observed;[8,14] "Curie anomalies" in dielectric constant normally seen in bulk and single crystal are progressively suppressed, and increase in diffuseness;[15,16]

The T_C temperature at which the dielectric constant is at a maximum can change dramatically.[15-17] For example, studies by Paker *et al.*[15] have been shown that the maximum permittivity of BST films decreased from 662 to 168, and T_C shifted from 269 to 102 K with decreasing thickness from 580 to 40 nm. This shift of T_C to low values reduces the performances of the material at RT, making it less attractive to integrate into commercial devices.

While in section 4.1 our studies have shown that perfectly (111)-oriented BST films on Pt(111)/TiO_x/SiO_2/Si substrates exhibited excellent dielectric properties, which have more advantages for microwave tunable devices application than (001)-oriented BST films.[18] Thus, accurately quantifying the characteristics of the temperature-dependent dielectric response that change with thickness in such perfectly (111)-oriented BST thin films is of great practical and theoretical importance. In this section, the variations in permittivity of perfectly (111)-oriented BST films with film thicknesses ranging from 45 to 800 nm in a wide range of 77-320 K were studied in order to give insight into the dielectric behavior of the bulk layer and the nature of the low dielectric interfacial component.

6.2 Experimental Procedure

A series of (111)-oriented BST thin films with thicknesses ranging from 45 to 800 nm were *in-situ* (800 °C) deposited on Pt(120nm)/TiO_x/SiO_2/Si substrates by RF magnetron sputtering from a stoichiometric $Ba_{0.6}Sr_{0.4}TiO_3$ ceramic target with excess BaO and SrO under conditions listed in Table 3.1. For electrical measurements, metal-insulator-metal structure capacitors were defined by standard photolithographic lift-off technique using dc magnetron sputtered 120-nm-thick Pt electrodes(A=1.766×$10^{-4}$$cm^2$) on the BST film surface. The capacitors were then annealed at 500 °C for 60 min in an air ambient to improve the top electrode/BST interface. The structure properties and crystallinity of the BST films were characterized by an X-ray diffraction (XRD, Siemens D5000, München, Germany) with CuK_α radiation (λ=0.154 nm) using θ-2θ scan. The surface morphology and the

thicknesses of the films were observed by scanning electron microscope (SEM, Ultra55, Zeiss, Oberkochen, Germany). The T_C was measured by a semiconductor characterization system (Keithley, 4200-SCS, Cleveland, USA) interfaced with a temperature-controlled probe station under vacuum and cooled with liquid N_2 in a temperature range of 77-320 K.

6.3 Results and Discussions

Figure 6.1 shows the SEM images of the surface BST thin films with various thicknesses. The grain size was found to increase with increasing film thickness which has also been observed by other researchers.[19]

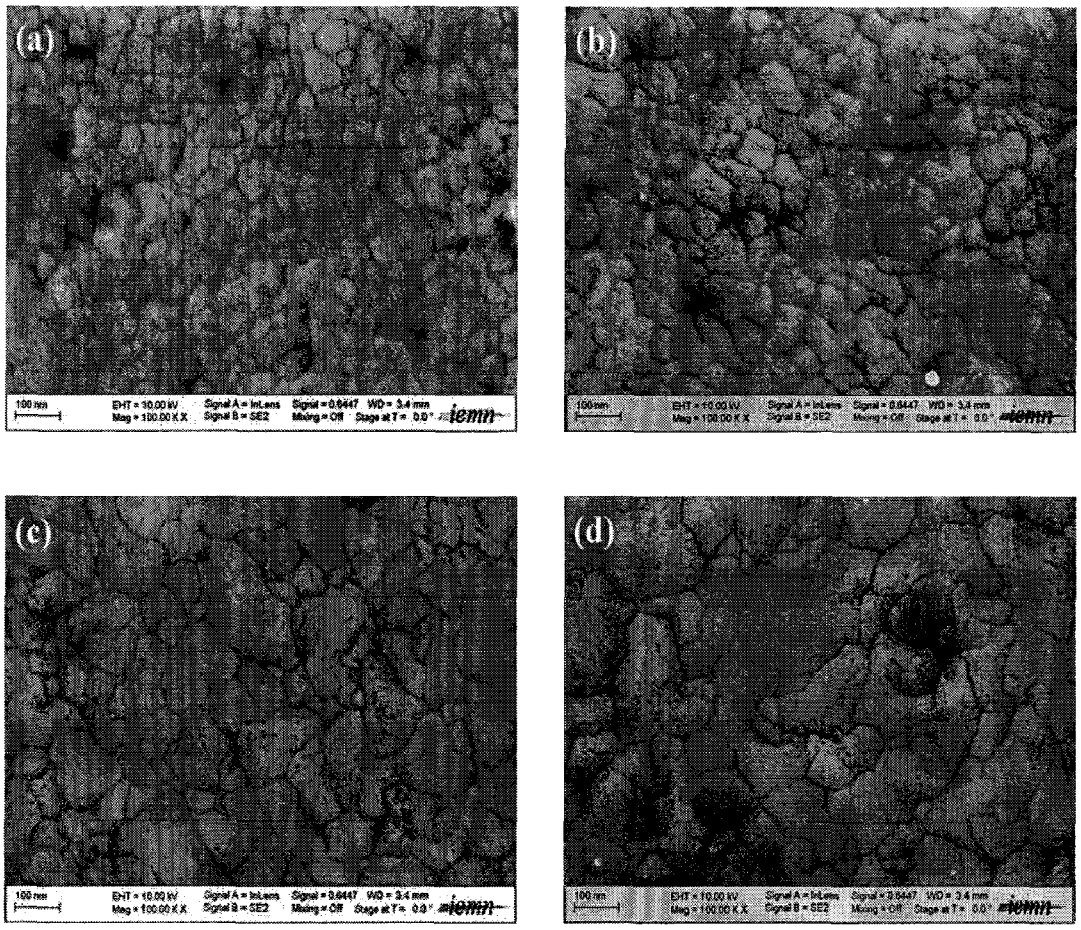

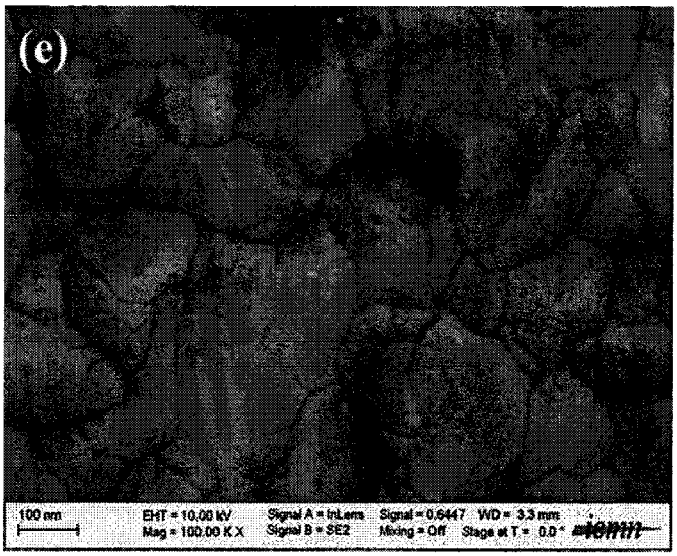

Fig. 6.1. Scanning electron microscope (SEM) photographs of the surface of (Ba,Sr)TiO_3 (BST) thin films: (a) 45 nm, (b) 100 nm, (c) 200 nm, (d)415 nm, and (e) 800 nm, respectively.

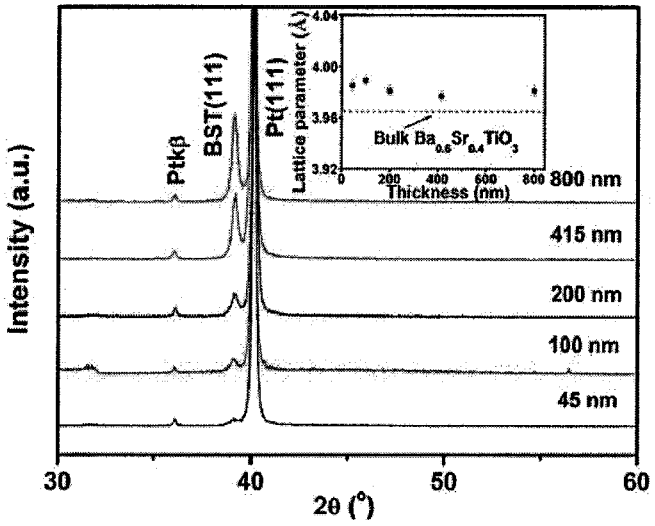

Fig. 6.2. XRD patterns of BST thin films on Pt(111)/TiO_x/SiO_2/Si substrates with thicknesses ranging from 45 to 800 nm. Inset is the lattice parameter as a function of BST film thickness. The straight dashed line represents the lattice parameter of the bulk $Ba_{0.6}Sr_{0.4}TiO_3$ material (3.965 Å).

XRD patterns for a representative set of BST films with thicknesses ranging from 45 to 800 nm are shown in Fig. 6.2. It can be seen that all the films exhibited single pervoskite structure with perfectly (111) orientation, and the intensity of (111) peak increases with increasing thickness, which is consistent with increasing grain size as displayed in Fig. 6.1. The lattice parameters calculated assuming cubic crystal

symmetry of the BST films shown inset of Fig. 6.2 are slightly larger than that of the bulk $Ba_{0.6}Sr_{0.4}TiO_3$ material (3.965 Å, JCPDS Card No. 34-0411) and almost independent of the film thickness, probably due to the residual strains inside all the films are similar. Strains in BST (111) films result from either intrinsic (growth stresses), $u_{Intrinsic}$, or lattice mismatch, $u_{Lattice}$, and thermal mismatch, $u_{Thermal}$:

$$u_{Residual} = u_{Intrinsic} + u_{Lattice} + u_{Thermal}, \tag{6.1}$$

Various reasons exist for the development of intrinsic stress, including grain coalescence, oxygen vacancies and/or other defects during film growth. The lattice and thermal mismatch strains are given by:

$$u_{Lattice} = \frac{a_{Pt} - a_{BST}}{a_{Pt}},^{20} \tag{6.2}$$

$$u_{Thermal} = \int_{T1}^{T2} (\alpha_{BST} - \alpha_{Si}) dT,^{21} \tag{6.3}$$

Based on the lattice parameter of bulk BST higher than that of Pt (3.923 Å, JCPDS Card No.04-0802), we would expect compressive in-plane strains within the film, which were relaxed in a continuous fashion as the thickness increased.[4] The tensile strains developing due to the difference in the thermal expansion between the film and the underlying substrate (α_{BST}=10×10^{-6}/K and α_{Si}=2.5×10^{-6}/K, respectively)[21]were estimated to be similar and of opposite sign as the films cooling from T_1=800 °C to T_2=25 °C. Here the α_{BST} of different thicknesses of BST(111) films was assumed to be the same as that of $Ba_{0.6}Sr_{0.4}TiO_3$ reported in literature[21]. As the film thickness increased from 45 to 800 nm in our work, the potential sources of intrinsic stress may become influential, which compensates with the relaxed compressive strains and makes the lattice insensitive to film thickness.

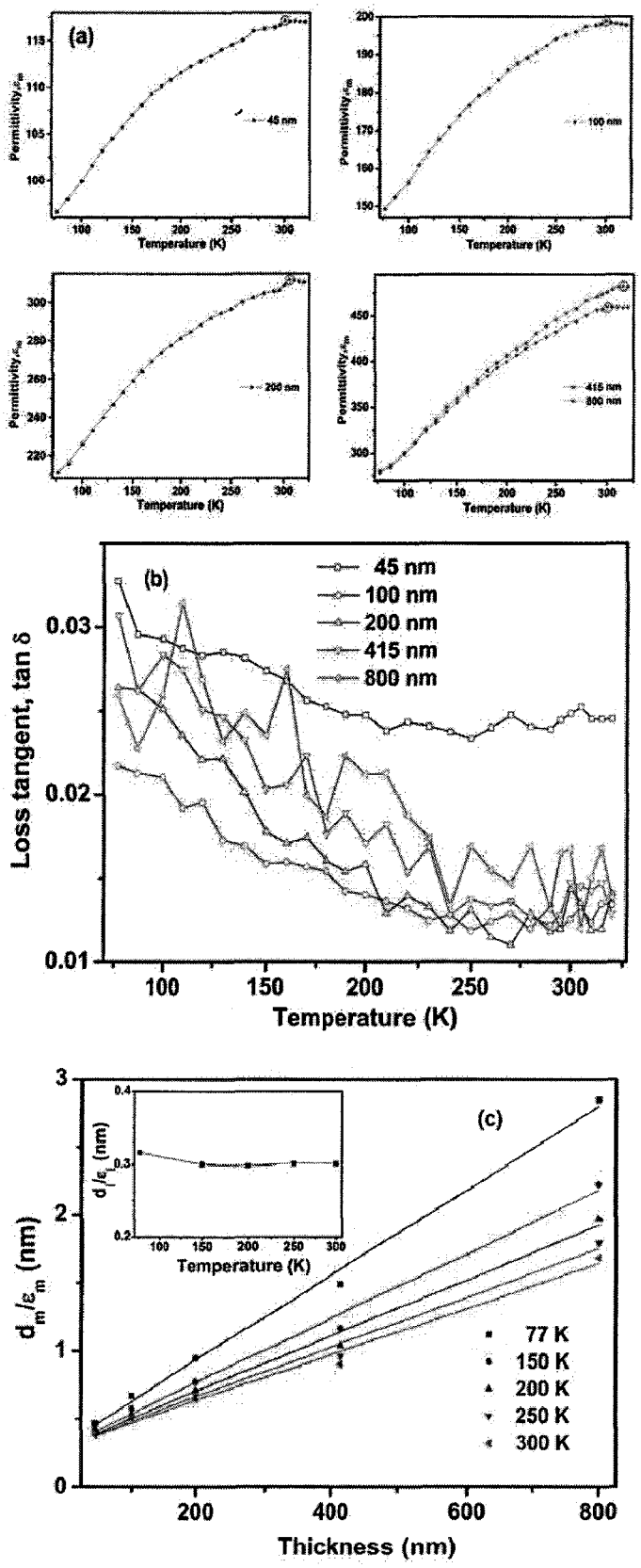

Fig. 6.3. Temperature dependence of the measured relative permittivity (ε_m) (a) and dielectric loss tangent (b) at zero field for the BST(111) films of different thicknesses, at 10 kHz frequency. (b) Inverse capacitance (d_m/ε_m) versus the film thickness of BST (111) films with varying temperature.

Measurement of the electrical properties over a temperature range of 77 to 320 K enabled the Curie peak at the *Tc*, to be observed and also gave an idea of the possible effects of the temperature variation. The temperature dependent the measured relative permittivity (ε_m) for the BST (111) thickness series are shown in Fig. 6.3 (a). It was found that (1) all the BST films exhibit a broad ferroelectric-to-paraelelctric phase transition which can be explained as the results of nanoscaled grain size of the films. (2) The value ε_m of the films increases with increasing film thickness and reaches a saturation value at thickness of ~ 415 nm but is always much smaller than that of the ceramics. (3) The T_C marked by open circles is almost independent of film thickness, about 305±5 K. We owe the unusual *Tc* independence of thickness behavior for our (111)-oriented BST films caused by the insensitive lattice parameter with film thickness as discussed above. With respect to the phase transition behavior, the residual strain has been related to the shift in the temperature, change of the order of the transition and increase of the diffuseness.[22] Figure 6.3(b) shows the variation of the dielectric loss with temperature, the room temperature dielectric loss was found to lie between 0.012 and 0.025 depending on the thickness of the film.

The experimentally observed reduction in ε_m for BST capacitors can be explained by the existence of interfacial "dead-layer" at electrode-dielectric boundaries with poor properties. They might arise from the oxygen interdiffusion, chemical reaction, or structural defects at the interfaces. The measured capacitance, C_m, may then be expressed as an interfacial capacitance, C_i, and the bulk film capacitance C_b, connected in series:

$$\frac{1}{C_m}=\frac{1}{C_b}+\frac{1}{C_i}, \tag{6.4}$$

$$\text{or} \quad \frac{d_m}{\varepsilon_m}=\frac{d_b-d_i}{\varepsilon_b}+\frac{d_i}{\varepsilon_i}=\frac{d_b}{\varepsilon_b}+\frac{d_i}{\varepsilon_i}, \tag{6.5}$$

where d_m, d_b, d_i are the thickness and $\varepsilon_m, \varepsilon_b, \varepsilon_i$ are the permittivity of the BST (111) film, bulk BST dielectric layer and the interfacial layer, respectively. Eq. (6.5) has been widely used to model thickness dependent dielectric properties.[8,12,13,16,17] The last

term of Eq. (6.5) is obtained assuming either $\varepsilon_b >> \varepsilon_i$ or $d_b >> d_i$,[8] giving a linear relationship between d_m / ε_m and d_m with a gradient of $1/\varepsilon_b$ and y-axis intercept of d_i / ε_i. This is done for our BST (111) films with thicknesses from 45 to 800 nm at various temperatures as shown in Fig. 6.3 (c), from which the deviations between the fitting and measurements ascribed to the size effect could be observed, and d_i / ε_i as a function of temperature is shown in the inset of Fig. 6.3 (c). It is interesting to note that the d_i / ε_i values are almost constant in the whole temperature region. This T-independent d_i / ε_i shows an important implication on the nature of the interfacial capacitance component as previously discussed by Park[12] and Hwang[16] (~0.3 nm, which is quite reasonable value). The d_i / ε_i ratio is relatively large (compared with 0.05 nm for $Pt/Ba_{0.5}Sr_{0.5}TiO_3/Pt$,[19] 0.12 nm for $Pd/Ba_{0.5}Sr_{0.5}TiO_3/Au/Ti$,[23] whereas a little lower than 0.40 nm for the $SrRuO_3/Ba_{0.5}Sr_{0.5}TiO_3/Au$[24]), and the effect of low dielectric interfacial component is, therefore, apparent even in relatively thick films. However, the fact that d_i and ε_i are inseparable in the conventional series capacitor model means that neither the dead-layer thickness nor the permittivity is well defined.

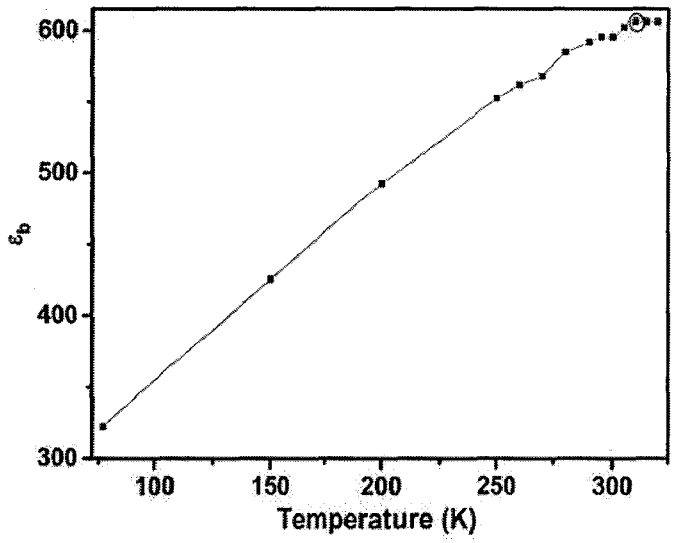

Fig. 6.4. Variations in the bulk permittivity (ε_b) of BST (111) films as a function of temperature.

The ε_b extracted from the inverse slopes of linear graphs as a function of

temperature is plotted in Fig. 6.4, showing that the ε_b of the BST films increases with temperature and reaches a maximum value at 310 K, although the temperature dependence of ε_b is weak than that of the single crystal, further reflecting the size effects in ferroelectric materials. Since the interfacial layer is independent of temperature, the unusual *Tc* independence of BST film thickness can also be partially understand by the contribution of bulk BST component.

6.4 Summary

In summary, we have studied the variations in the permittivity with film thickness and measurement temperature of sputtered BST (111) thin films on $Pt/TiO_x/SiO_2/Si$ substrates with thicknesses ranging from 45 to 800 nm. All the films showed elongations in the lattice parameter insensitive to film thickness. Temperature-dependent measurements of the permittivity in our BST (111) films revealed unusual Curie point independent of thickness, about 305±5 K, at which the phase transition became more diffuse. A model incorporating a bulk film and an interfacial capacitance was employed to explain the thickness-dependent permittivity at the given temperature.

6.5 Reference

1. B. A. Baumert, L. H. Chang, A. T. Matsuda, C. J. Tracy, N. G. Cave, R. B. Gregory, and P. L. Fejes, "A Study of Barium Strontium Titanate Thin Films for Use in Bypass Capacitors," *Journal of Materials Research,* **13**(1), 197-204, 1998.

2. J. Im, O. Auciello, P. K. Baumann, S. K. Streiffer, D. Y. Kaufman, and A. R. Krauss, "Composition-control of Magnetron-sputter-deposited $(Ba_xSr_{1-x})Ti_{1+y}O_{3+z}$ Thin Films for Voltage Tunable Devices," *Applied Physics Letters*, **76**(5), 625-627, 2000.

3. D. Collier, "Ferroelectric Phase Shifters for Phased Array Radar Applications," *Integrated Ferroelectrics*, **4**(2), 113-119, 1994.

4. C. L. Canedy, H. Li, S. P. Alpay, L. Salamanca-Riba, A. L. Roytburd, and R. Ramesh, "Dielectric Properties in Heteroepitaxial $Ba_{0.6}Sr_{0.4}TiO_3$ Thin Films: Effect of Internal Stresses and Dislocation-type Defects," *Applied Physics Letters*, **77**(11), 1695-1697, 2000.

5. C. M. Carlson, T. V. Rivkin, P. A. Parilla, J. D. Perkins, D. S. Ginley, A. B. Kozyrev, V. N. Oshadchy, and A. S. Pavlov, "Large Dielectric Constant ($\varepsilon/\varepsilon_0$>6000) $Ba_{0.4}Sr_{0.6}TiO_3$ Thin Films for High-performance Microwave Phase Shifters," *Applied Physics Letters*, **76**(14), 1920-1922, 2000.

6. W. Chang, C. Gilmore, W. Kim, J. Pond, S. Kirchoefer, S. Qadri, D. Chrisey, and J. Horwitz, "Influence of Strain on Microwave Dielectric Properties of (Ba,Sr)TiO_3 Thin Films," *Journal of Applied Physics*, **87**(6), 3044-3049, 2000.

7. M. W. Cole, C. V. Weiss, E. Ngo, S. Hirsch, L. A. Coryell, and S. P. Alpay, "Microwave Dielectric Properties of Graded Barium Strontium Titanate Films," *Applied Physics Letters*, **92**(18), 182906-182908, 2008.

8. B. T. Lee and C. S. Hwang, "Influences of Interfacial Intrinsic Low-dielectric Layers on the Dielectric Properties of Sputtered (Ba,Sr)TiO_3Thin Films," *Applied Physics Letters*, **77**(1), 124-126, 2000.

9. C. Zhou and D. M. Newns, "Intrinsic Dead Layer Effect and the Performance of Ferroelectric Thin Film Capacitors," *Journal of Applied Physics*, **82**(6), 3081-3088,

1997.

10. X. L. Li, B. Chen, H. Y. Jing, H. B. Lu, B. R. Zhao, Z. H. Mai, and Q. J. Jia, "Experimental Evidence of the "Dead Layer" at Pt/$BaTiO_3$ Interface," *Applied Physics Letters*, **87**(22), 222905-222907, 2005.

11. M. Dawber and J. F. Scott, "Models of Electrode-dielectric Interfaces in Ferroelectric Thin-film Devices," *Japanese Journal of Applied Physics*, Part 1 **41**, 6848-6851, 2002.

12. C. S. Hwang, "Thickness-dependent Dielectric Constants of (Ba,Sr)TiO_3 Thin Films with Pt or Conducting Oxide Electrodes," *Journal of Applied Physics*, **92**(1), 432-437, 2002.

13. W. Y. Park, K. H. Ahn, and C. S. Hwang, "Effects of In-plane Compressive Stress on Electrical Properties of (Ba,Sr)TiO_3 Thin Film Capacitors Prepared by on- and off-axis rf Magnetron Sputtering," *Applied Physics Letters*, **83**(21), 4387-4389, 2003.

14. C. Basceri, S. K. Streiffer, A. I. Kingon, and R. Waser, "The Dielectric Response as a Function of Temperature and Film Thickness of Fiber-textured (Ba,Sr)TiO_3 Thin Films Grown by Chemical Vapor Deposition," *Journal of Applied Physics*, **82**(5), 2497-2504, 1997.

15. C. B. Paker, J. P. Maria, and A. I. Kingon, "Temperature and Thickness Dependent Permittivity of (Ba,Sr)TiO_3 Thin Films," *Applied Physics Letters*, **81**(2), 340-342, 2002.

16. W. Y. Park and C. S. Hwang, "Film-thickness-dependent Curie-Weiss Behavior of (Ba,Sr)TiO_3 Thin-film Capacitors Having Pt Electrodes," *Applied Physics Letters*, **85**(22), 5313-5315, 2004.

17. R. Plonka, R. Dittmann, N. A. Pertsev, E. Vasco, and R. Waser, "Impact of the Top-electrode Material on the Permittivity of Single-crystalline $Ba_{0.7}Sr_{0.3}TiO_3$ Thin Films," *Applied Physics Letters*, **86**(20), 202908-202910, 2005.

18. L. H. Yang, G. S. Wang, D. Rémiens, and X. L. Dong, "Perfectly (001)-and (111)-Oriented (Ba,Sr)TiO_3 Thin Films Sputtered on Pt/TiO_x/SiO_2/Si Without Buffer Layers," *Journal of the American Ceramic Society*, **93**(2), 350-352, 2010.

19. W. J. Lee, H. G. Kim, and S. G. Yoon, "Microstructure Dependence of Electrical

Properties of $(Ba_{0.5}Sr_{0.5})TiO_3$ Thin Films Deposited on $Pt/SiO_2/Si$," *Journal of Applied Physics*, **80**(10), 5891-5894, 1996.

20. K. Venkata Saravanan, M. Ghanashyam Krishna, and K. C. James Raju, "Effect of Misfit Strain and Surface Roughness on the Tunable Dielectric Behavior of $Ba_{0.5}Sr_{0.5}TiO_3$ Thin Films," *Journal of Applied Physics*, **106**(11), 114102-114408, 2009.

21. T. R. Taylor, P. J. Hansen, B. Acikel, N. Pervez, R. A. York, S. K. Streiffer, and J. S. Speck, "Impact of Thermal Strain on the Dielectric Constant of Sputtered Barium Strontium Titanate Thin Films," *Applied Physics Letters*, **80**(11), 1978-1980, 2002.

22. N. A. Pertsev, A. G. Zembilgotov, and A. K. Tagantsev, "Effect of Mechanical Boundary Conditions on Phase Diagrams of Epitaxial Ferroelectric Thin Films," *Physical Review Letters*, **80**(9), 1988-1991, 1998.

23. S. Yamamichi, H. Yabuta, T. Sakuma, and Y. Miyasaka, "(Ba+Sr)/Ti Ratio Dependence of the Dielectric Properties for Thin Films Prepared by Ion Beam Sputtering," *Applied Physics Letters*, **64**(13), 1644-1646, 1994.

24. L. J. Sinnamon, R. M. Bowman, and J. M. Gregg, "Investigation of Dead-layer Thickness in $SrRuO_3/Ba_{0.5}Sr_{0.5}TiO_3/Au$ Thin-film Capacitors," *Applied Physics Letters*, **78**(12), 1724-1726, 2001.

CHAPTER 7
Microwave Properties of BST Films up to 50 GHz

This chapter is divided into two sections. In the first section (7.1) of this chapter, epitaxial (111)-oriented $Ba_{0.6}Sr_{0.4}TiO_3$ (BST) films on sapphire were obtained and microwave properties of BST films were evaluated. The second part (section 7.2) describes the microwave properties of BZN-BST bilayered thin film on high resistivity Si substrates.

7.1 Microwave Properties of Epitaxial BST (111) Thin Films on Al_2O_3 (0001) up to 40 GHz

Perovskite $Ba_{0.6}Sr_{0.4}TiO_3$ (BST) thin films have been synthesised on Al_2O_3(0001) substrates without/with inserting an ultrathin TiO_x seeding layer by RF-magnetron sputtering. X-ray diffraction and pole figure studies suggest that the film with the TiO_x layer (12-Å-thick) is highly oriented along the (111) direction, and exhibits a good in-plane relationship of BST(111)||Al_2O_3(0001). The high frequency (1-40 GHz) dielectric measurements demonstrate that the complex permittivity ($\varepsilon=\varepsilon'-j\varepsilon''$) is well described by a Curie-von Scheidler power law with an exponent of 0.40. Moreover, the high permittivity (~428) combined with a high tunability (~40.88%, 300kV/cm) up to 40 GHz suggest that epitaxial (111)-oriented BST thin film could be well suited for microwave tunable devices.

7.1.1 Introduction

$Ba_xSr_{1-x}TiO_3$ (BST) is a material with enormous potential for the application in capacitors of dynamic random access memories,[1,2] tunable microwave devices/radio frequency components,[3-5] and power-supply decoupling[6] because of its high permittivity and large electric-field-dependent tunability and relatively low dielectric loss. Among the various applications of BST thin films, the application as tunable devices for telecommunications which are operated in the microwave range (300 MHz to 300 GHz) requires detailed knowledge of the microwave dielectric constant, tunability, and the microwave loss in the high-frequency domain.[7,8] Therefore, determining dielectric properties in the high-frequency domain is vital to fully

characterize BST films. Although ferroelectric materials in thin-film form often show inferior properties (lower dielectric constant and higher loss) as compared to bulk ceramics, it has been demonstrated that high quality epitaxial films generally have much better properties than polycrystalline films. [9-11]

Very recently, it was shown that by depositing epitaxial (111)-oriented BST films employing an ultrathin (9-Å-thick) TiN layer as a template on Al_2O_3 (0001) substrates, it is possible to obtain higher tunability while keeping the microwave loss low compared to polycrystalline BST films directly deposited on the substrates.[12] Xiao *et al.* also reported that epitaxial (001)-oriented BST thin films on MgO/ZnO/Al_2O_3 (1120) substrates revealed a very high dielectric tunability of up to 84 % at 1 MHz in 5 μm gap interdigital capacitor.[13] The improvement in tunability was attributed, in part, to a buffer layer-dependent strain relaxation of epitaxial BST films correlating with higher permittivity. All the above recent advancements have certainly paved the way for the realization of high frequency microwave applications based on the epitaxial-BST thin film capacitors. Benefiting from their work, we recently attempted to adopt an ultrathin (12-Å-thick) TiO_x buffer layer to obtain epitaxial (111) BST films on *c*-plane sapphire substrate, *i.e.*, Al_2O_3 (0001) and have systematically investigated their corresponding physical properties. Here, we present our recent achievements of the microwave dielectric properties of the highly epitaxial as well as polycrystalline BST thin films on Al_2O_3 (0001) over a wide range of microwave frequencies (1-40 GHz), rather than at the lower, narrower frequency ranges ($\leq$ 10 GHz) more commonly studied.[14]

7.1.2 Experimental Procedure

An ultrathin TiO_x layer with thickness ~12 Å was firstly deposited on Al_2O_3 (0001) substrates by dc magnetron reactive sputtering at room temperature using commercial Ti metal target followed by a post-anneal at 700 °C for 60 min in an air ambient. The thickness of the ultrathin TiO_x layer was estimated by the deposition time according to the average growth rate of the thick TiO_x film on SiO_2/Si substrates.

450-nm-thick BST (x=0.6) films were then *in-situ* (800°C) deposited on Al_2O_3 (0001) and TiO_x-buffered/Al_2O_3(0001) substrates by RF-magnetron sputtering from a stoichiometric $Ba_{0.6}Sr_{0.4}TiO_3$ ceramic target with excess BaO and SrO using an Ar/O_2 flow ratio of 70/30 sputtering gas mixture with total pressure of 15 mTorr and a sputter power of 70 W, similar to the conditions described in chapter 6. The structure properties, crystallinity, and epitaxial behavior of BST films were characterized by an X-ray diffraction (XRD) with CuK_α radiation using θ-2θ scan and pole figure. The cross section and thickness of the films were conformed by scanning electron microscope (SEM). For microwave properties, coplanar waveguide (CPW) transmission lines consisting of 3 mm long fingers, 30 μm wide center conductor, 190 μm wide ground lines with 1 μm finger gap [illustrated in Fig. 7.1(a)] were defined by standard photolithographic lift-off technique using electron-beam evaporated Au/Ti (300-nm-thick) electrodes on both bare Al_2O_3 substrate and BST film surface. The microwave dielectric properties of BST films were measured as a function of frequency (1-40GHz) and dc bias (-30-30V) by using a ground-signal-ground microprobe (Cascade Microtech) station connected to a vector network analyzer (Agilent Technologies E8361A). Details have been described in section of 3.4.4.2.

7.1.3 Results and Discussions

Figure 7.1(b) shows the XRD θ-2θ patterns of BST films grown on Al_2O_3 (0001) covered without/with TiO_x layer (12-Å-thick). As can be seen inset of Fig. 7.1(b), the film directly grown on Al_2O_3 (0001) shows a distinctly polycrystalline nature. On the other hand, the film on TiO_x-covered Al_2O_3(0001) surface shows a completely different growth behavior. Only very strong (111) peak without any peaks originating from other orientations can be found. Pole figure [Fig. 7.1(c)] studies have been done to understand the quality of the epitaxy and to determine the in-plane relationship between the (111)-oriented BST film and the Al_2O_3 (0001) substrate. The six-fold symmetry reflections from the {100}, {110}, and {111} poles can be clearly seen in the Fig. 7.1(c). Following the conclusion of Yamada *et al.*,[12] this six-fold symmetry corresponds to two in-plane variants of the three-fold (111) orientation. The in-plane

orientation relationship has been determined to be BST(111)||Al_2O_3(0001), from which only 3 % of mismatch between d_{220}-BST and d_{300}-Al_2O_3 can be achieved.

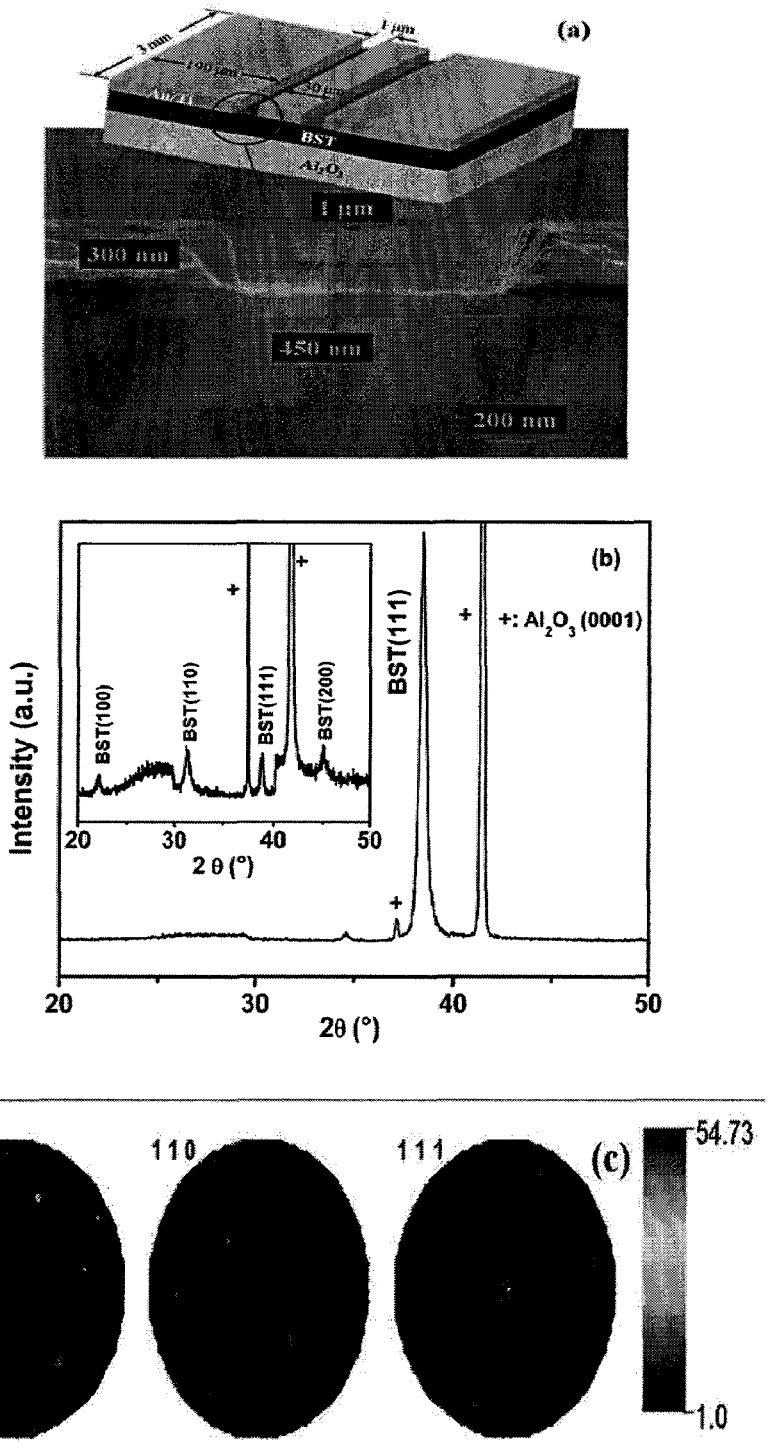

Fig. 7.1(a). Schematic representation of the coplanar waveguide (CPW) transmission lines structure and Cross-sectional of SEM images for BST film with CPW on sapphire substrate. (b) XRD θ-2θ patterns of the 450-nm-thick BST films on Al_2O_3(0001) with 12-Å-thick TiO_x layer; and (c): {100}, {110} and {111} pole figures of BST thin films on TiO_x/Al_2O_3(0001).

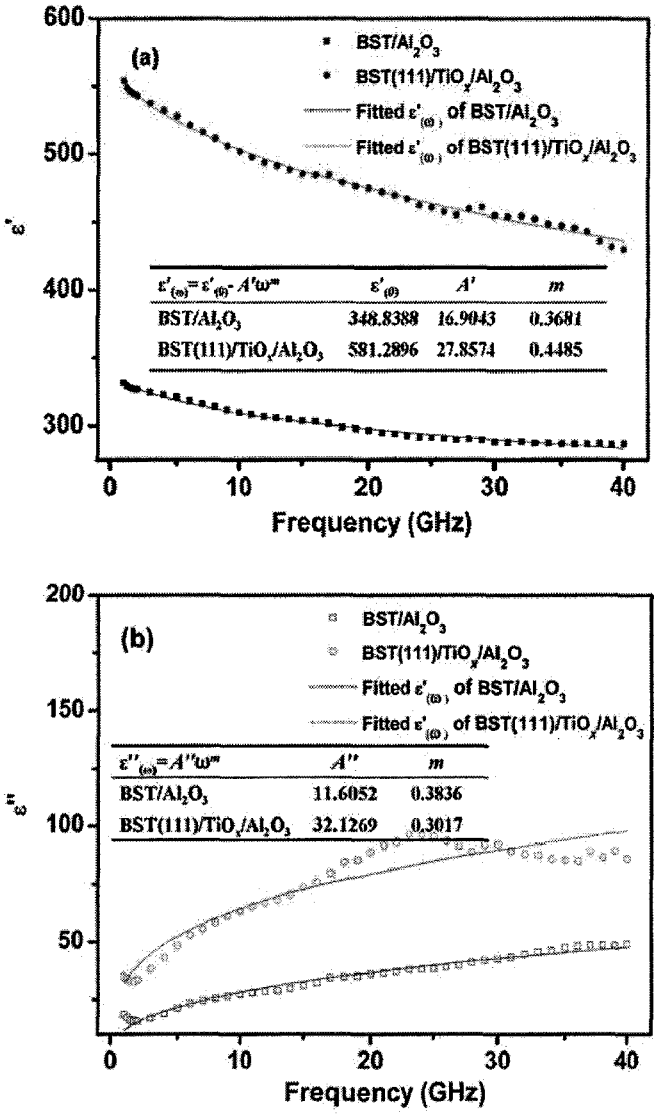

Fig. 7.2. Frequency spectrum of (a) real part of permittivity (ε′) and (b) imaginary part of permittivity (ε″) for BST thin films grown on Al_2O_3(0001) covered without/with 12-Å-thick TiO_x layer. Data follow a Curie-von Schweidler power law.

Figures 7.2(a) and 7.2(b) show real (ε′) and imaginary part of permittivity (ε″) of BST thin films grown on Al_2O_3 (0001) covered without/with 12-Å-thick TiO_x layer as a function of frequency. As shown in Fig. 7.2(a), it is found that ε′ of both BST thin films slightly decreased over the measured frequency range, and the enhanced dielectric properties for the BST(111)/TiO_x/Al_2O_3 film are observed in the measured frequency range. The large observed ε′ can be attributed to largely (111)-oriented domain structure and the high crystallinity of the film. On the other hand, a power-law dispersion of ε′ and ε″ is noted. The empirical dispersion is given by the Curie-von

Schweidler relationship:[17]

$$\varepsilon'_{(\omega)} = \varepsilon'_{(0)} - A'\omega^m, \quad (7.1)$$

$$\varepsilon''_{(\omega)} = A''\omega^m. \quad (7.2)$$

In these expressions, ω and $\varepsilon'_{(0)}$ are the angular frequency and the static dielectric constant, respectively, and A', A'', and m are constants. The fitting curve in Fig. 7.2 is calculated by fitting the complex permittivity of the dispersion curve to obtain $\varepsilon'_{(0)}$, A', A'', and m which are listed inset of Figs. 7.2(a) and 2(b). Values for the exponent m are in the range of 0.3–0.5, which is comparable to the values reported for the frequency range of 1 mHz to 20 GHz.[18] Our fitting curves provided $\varepsilon'_{(0)}$ of 581 and 349 for BST(111)/TiO_x/Al_2O_3 and BST/TiO_x/Al_2O_3, respectively. The elevated static dielectric constant can be attributed to the strain-modified in the epitaxial film due to the introduction of TiO_x buffer layer. The Curie-von Schweidler behavior is in consistent with observations in epitaxial and polycrystalline $BaTiO_3$, and has been reported to persist up to GHz range.[19]

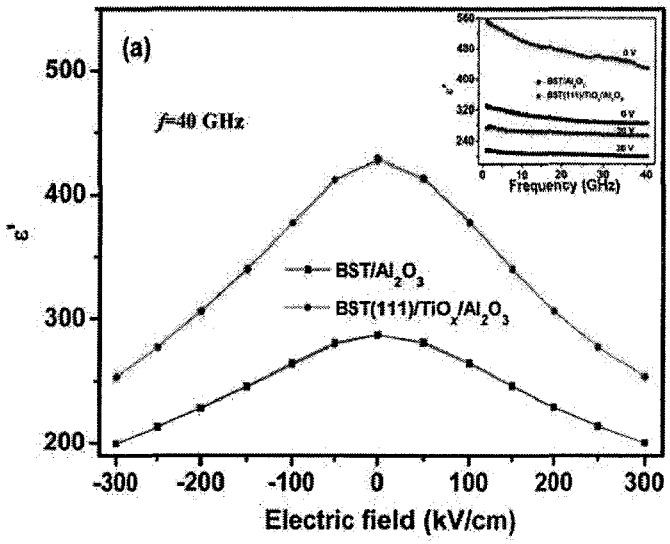

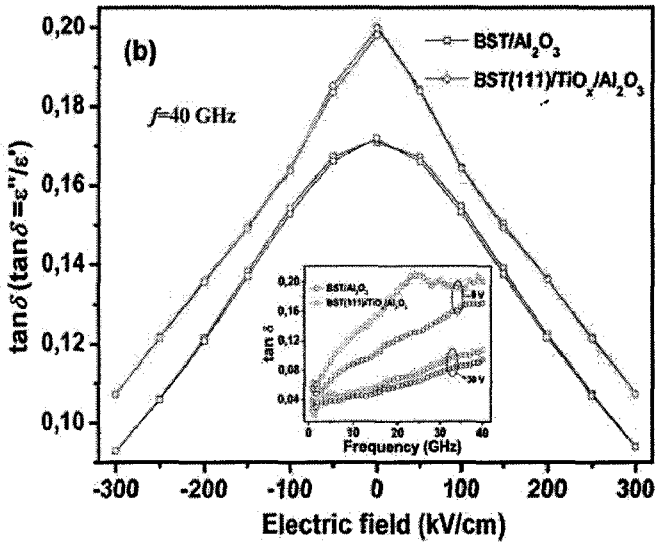

Fig. 7.3. The electric field dependence of (a) ε′ and (b) loss tangent (tan δ= ε″/ ε′) of BST thin films deposited on with and without the insertion of the TiO_x buffer layer at 40 GHz, respectively.

Figure 7.3 shows the electric field dependence of (a) ε′ and (b) loss tangent (tan δ= ε″/ ε′) of BST thin films deposited on without and with the insertion of the TiO_x buffer layer at 40 GHz, respectively. The zero-bias ε′ of BST(111)/TiO_x/Al_2O_3 is ~ 428, and a significantly decrease in ε′ (~ 287) is observed for BST/Al_2O_3 film. The tunability, defined as $\{(\varepsilon'(0)-\varepsilon'(V_{max})/\varepsilon'(0)\}\times 100\%$, where ε′(0), ε′($V_{max}$) are the ε′ of BST film at zero and the maximum applied voltage, respectively. The trends of ε′(40V) and tan δ(40V) versus frequency for both epitaxial and polycrystalline BST films are illustrated inset of Fig. 7.3(a) and (b), respectively. Thus, a prominent enhancement tunability of 40.88 % can be achieved for the BST(111)/TiO_x/Al_2O_3 film, as compared to 30.54 % obtained with BST/Al_2O_3 film, at frequency of 40 GHz with an applied field of ± 300 kV/cm. In a previously published result for an epitaxial (111)-oriented $Ba_{0.3}Sr_{0.7}TiO_3$ (250-nm-thick) thin film with TiN buffer layer on *c*-plane sapphire, the tunability was ~33.87 % at 8 GHz with an applied field of 200 kV/cm.[12] While polycrystalline $Ba_{0.5}Sr_{0.5}TiO_3$ film showed a tunability of 26 % (20 GHz, 200 kV/cm) was reported in Ref. 20. The dielectric loss tangent, tan δ (tan δ= ε″/ε′) was also obtained as a function of bias at microwave frequency (40 GHz) which is shown in Fig. 7.3(b) for BST/Al_2O_3 and BST(111)/TiO_x/Al_2O_3 films. At zero-bias voltage, the tan δ for BST/Al_2O_3 and BST(111)/TiO_x/Al_2O_3 film is 0.16 and 0.20, respectively.

Similar behavior was also observed for BST thin films on Pt-coated sapphire substrates with somewhat higher permittivity and higher loss tangent at low frequency. While both values are significantly larger than the dielectric loss at 100 kHz (~0.015),[21] indicating further investigations are needed to lower the tan δ. The increase in tan δ in the microwave frequency range can be thought of to be due to a number of reasons, both of intrinsic (due to the interaction of the ac field phonons, including quasi-Debye losses) and of extrinsic (e.g., mobile charged defects, such as oxygen vacancies) nature.[22] Besides, no hysteresis in ε' (as well as tan δ) versus dc bias is displayed in any of the films shown in Fig. 7.3, although we have reported hysteretic effects for similar BST thin films with metal-insulator-metal (MIM) capacitors, where hysteresis was explained by presence of permanent dipoles or dead interfacial layers.[15] Compare to MIM structure, the CPW configuration avoids the most of the parasitic components of the circuit and also the low-permittivity dead layer occurs at the interface of ferroelectric film/electrode. Overall, the microwave properties of BST thin films suggest that the high quality of the epitaxial films have excellent microwave performance for the development of high frequency tunable microwave elements operating at room temperature.

7.1.4 Summary

In conclusion, the (111) epitaxial growth of BST films on sapphire was achieved using an ultrathin TiO_x seeding layer deposited by RF magnetron sputtering. A six-fold symmetry of epitaxial BST on sapphire suggesting the presence of 60° rotation domains was observed by XRD pole figure analysis. The frequency dependence obeys a Curie-von Schweidler law over a frequency range of 1 to 40 GHz. The tunability in an epitaxial (111)-textured BST film on TiO_x buffered sapphire was approximately 40.88 %, which was enhanced by 34 %, compared to that in a BST film directly on sapphire. For applications such as phase shifters, the benefits of high tunability dominate over the drawbacks of increased film loss, making our epitaxial films well suited to such applications.

7.2 Microwave Properties of BZN/BST Bilayered Thin Films Directly Deposited on High Resistivity Si Toward 50 GHz

Perovskite $Ba_{0.6}Sr_{0.4}TiO_3$ (BST), pyrochlore $Bi_{1.5}Zn_{1.0}Nb_{1.5}O_7$ (BZN) and hetero-structures BZN/BST thin films have been grown directly on high-resistivity (HR)-Si substrates by RF-magnetron sputtering. The microwave properties (toward 50 GHz) of all the films are evaluated by fabricating coplanar waveguide configuration. The dielectric dispersion demonstrates that the complex permittivity ($\varepsilon=\varepsilon'-j\varepsilon''$) is well described by a Curie-von Scheidler power law. Experimental results showed that the BZN helped in tailoring the dielectric constant and reducing the loss tangent significantly. Moreover, the low microwave loss (~0.167) combined with a high tunability (~7.7 %, 200 kV/cm) until 50 GHz suggest that BZN/BST/HR-Si films could be well suited for integrated into microwave tunable devices.

7.2.1 Introduction

Ferroelectric materials have been extensively studied for many decades owing to their outstanding ferroelectric, piezoelectric, and pyroelectric properties offering great promise for various applications. A potential application of ferroelectric materials is in microwave tunable devices, including tunable mixers, delay lines, filters, and phase shifters for steerable antennas.[22,23] Barium strontium titanate ($Ba_xSr_{1-x}TiO_3$ or BST) has become the leading materials system for these devices due to its high dielectric response and its tunability near the ferroelectric phase transformation temperature T_C which can be controlled via adjusting composition [e.g., the bulk T_C of $Ba_{0.6}Sr_{0.4}TiO_3$ is close to room temperature (5 °C)].[24] By adjusting the composition of BST films, the transition temperature and, hence, the dielectric properties and its tunability can be tailored but the loss still keep high. Therefore, several compositions of BST thin films have been studied in great detail for use in tunable microwave devices using a variety of different fabrication methods and substrates.[25-27]

To be utilized in such devices, thin films of BST must have a high tunability, a

low loss tangent in the microwave regime, and good insulating properties, accompanied by the integration with large-area, low-cost, and microwave-friendly substrates such as high resistivity (HR)-Si. Addition of moderate dielectric constant and low loss materials $Bi_{1.5}Zn_{1.0}Nb_{1.5}O_7$ (BZN) in synthesizing the composite BST has been indentified an attractive approach to achieve the desirable dielectric properties suitable for microwave devices.[28-31] To date, BST-BZN composite thin films with promising microwave dielectric properties for microwave device applications have been deposited on $LaAlO_3$, $SrTiO_3$, and MgO single substrates.[32] However, these substrates are not widely used in making integrated devices due to their high cost and small-size-geometry availability ($50-$100 for ~1×1-in^2. pieces). Thus, introducing of a low loss dielectric BZN combined with high permittivity BST on HR-Si presents an intriguing opportunity to develop materials for tunable integrated circuit device applications with stringent demands focused on low dielectric losses, while still maintaining moderate tunability. Indeed, we have recently fabricated and optimized BZN with BST on Pt coated Si substrate in metal-insulator-metal (MIM) configuration and large and simultaneous improvements in tunability and loss tangent are achieved.[33] Since tunable devices for telecommunications are operated in the microwave range (300 MHz to 300 GHz), it is important to test the dielectric properties of these materials at higher frequencies. Thus the primary objective of this work was to develop the integration strategy and the associated industry standard processing science protocols to fabricate BZN/BST composite bilayer heterostructure on HR-Si substrates at gigahertz frequency in the coplanar device design configuration for tunable phase-shift applications. Our results showed that the BZN/BST composite thin films demonstrated low dielectric loss tangent while retaining reasonably high dielectric constant and dielectric tunability, making them excellent candidates for integration into tunable microwave devices.

7.2.2 Experimental Procedure

The BST, BZN and BZN/BST thin films were *in-situ* deposited directly on high resistivity (HR)-Si substrates using RF-magnetron sputtering. The sputtering targets

were ceramic $Ba_{0.6}Sr_{0.4}TiO_3$ with excess BaO and SrO and $Bi_{1.5}Zn_{1.0}Nb_{1.5}O_7$ with excess Bi_2O_3. Details of the pure BST (~600 nm), pure BZN (~550 nm) and BZN(~300 nm)/BST(~300 nm) bilayered thin films deposition conditions have been described in section of 5.2. The structure properties and crystallinity of thin films were characterized by an X-ray diffraction (XRD, Siemens D5000, München, Germany) with CuK_α radiation (λ=0.154 nm) using θ-2θ scan. The surface and the cross-section morphology of the films were observed by scanning electron microscope (SEM; Ultra55, Zeiss, Oberkochen, Germany). For microwave properties, coplanar waveguide (CPW) transmission lines consisting of 3 mm long fingers, 30 μm wide center conductor, 190 μm wide ground lines with 1.5 μm finger gap were defined by standard photolithographic lift-off technique using electron-beam evaporated Au/Ti (300-nm-thick) electrodes on both bare HR-Si substrate and film surface. The microwave dielectric properties of HR-Si, BST, BZN and BZN/BST films were measured as a function of frequency (1-50 GHz) and dc bias (-30-+30V) by using a ground-signal-ground microprobe (Cascade Microtech) station connected to a vector network analyzer (Agilent Technologies E8361A). Details have been described in section of 3.4.4.2.[16]

7.2.3 Results and Discussions

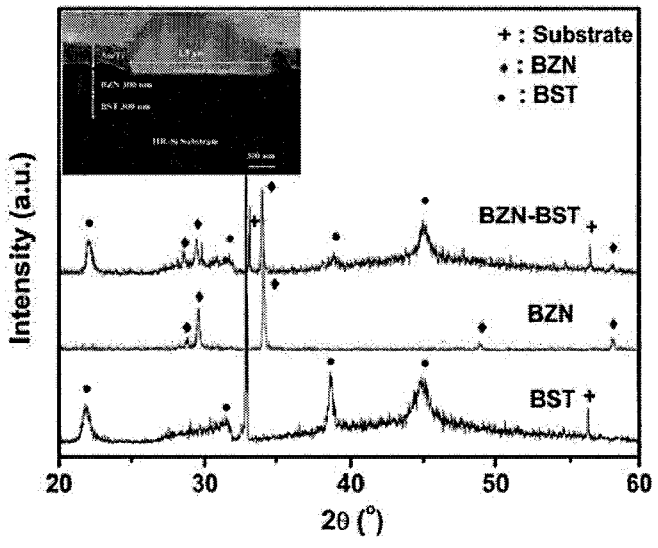

Fig. 7.4. XRD patterns of BST, BZN, BZN/BST heterolayered thin films on HR-Si substrates.

Figure 7.4 shows XRD patterns of BST, BZN, BZN/BST heterolayered thin films on HR-Si substrates. The results showed that pure BST films were cubic perovskite polycrystalline structure, and pure BZN films were cubic pyrochlore polycrystalline structure, respectively. There was no preferential orientation for both two films. No impurity phases can be detected with BZN addition onto the BST layer, which excludes interdiffusion between the BZN/BST layers. The SEM cross-section image inside Fig. 7.4 shows that the BZN(300nm)/BST(300nm) bilayered thin films have distinct interfaces.

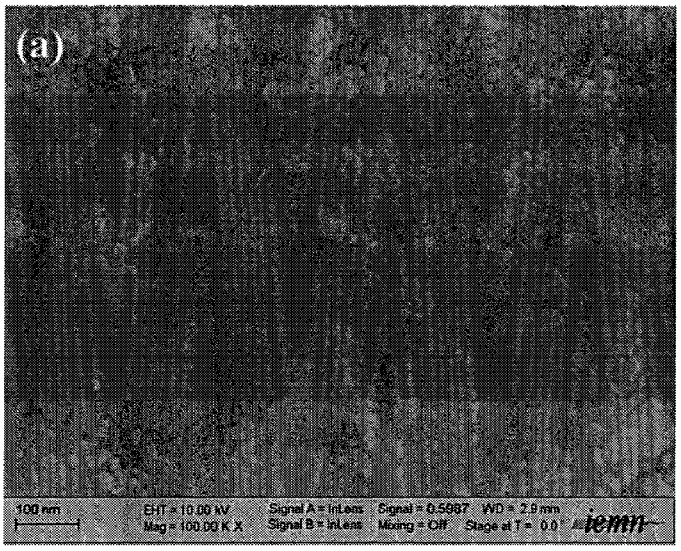

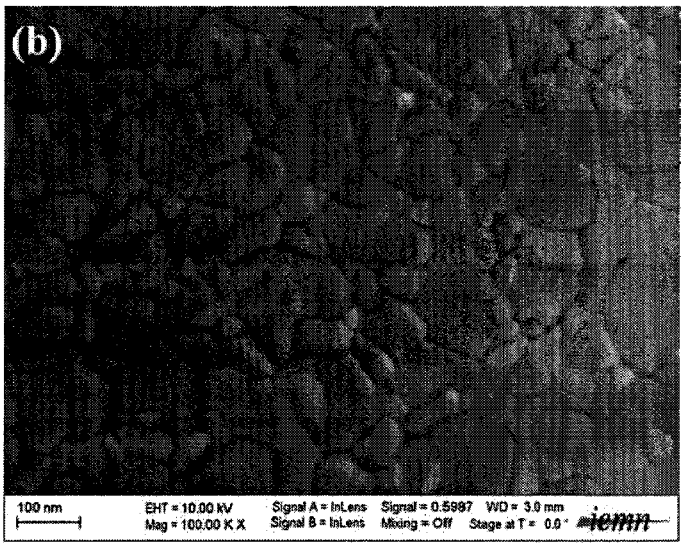

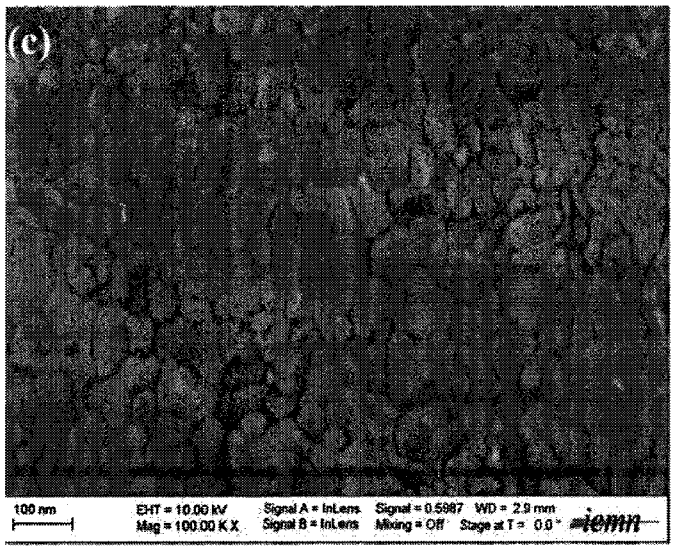

Fig. 7.5. SEM images of BST, BZN, and BZN/BST thin films on HR-Si substrate: (a) BST thin films, (b) BZN thin films, and (c) BZN/BST thin films.

Figs. 7.5(a)-(c) show the surface morphology images of pure BST, pure BZN, and BZN/BST thin films on HR-Si substrates, respectively. It can be seen that the average grain size of BZN films is around 100 nm, which is larger than that of BST films (~30 nm). The key reason should be the lower crystallization temperature for BZN films comparing with the relative higher of BST films, resulting in better crystallization of BZN thin films, although the deposition temperature for BZN (700°C) was lower than that of BST (800°C). The morphology of the BZN/BST bilayered thin films is different from that of pure BZN thin films, since they were deposited on different substrates (The BZN layer within the bilayer thin film was deposited on the BST layer, and pure BZN thin films were deposited on HR-Si substrate.), which can cause the BZN grain different growth mechanism. Moreover, the interfaces in the bilayer thin film can affect the BZN grain growth. Similar phenomenon have also been observed by other researchers.[29]

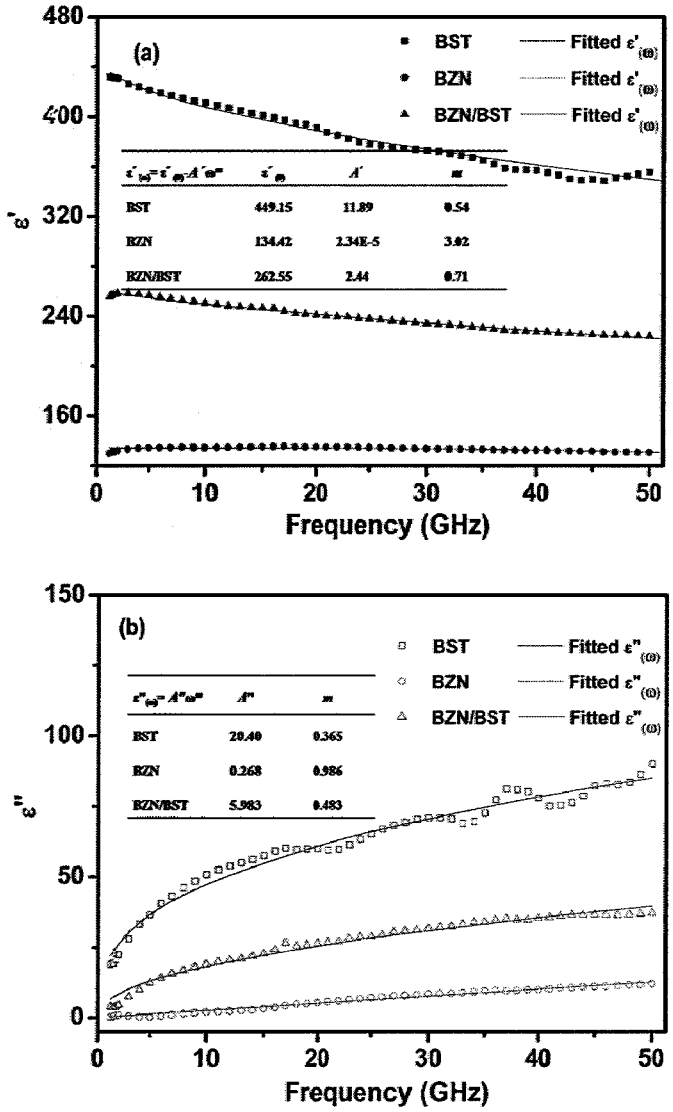

Fig. 7.6. Frequency spectrum of (a) real part of permittivity (ε′) and (b) imaginary part of permittivity (ε″) for BST, BZN, and BZN/BST thin films. Data follow a Curie-von Schweidler power law.

Figures 7.6(a) and 7.6(b) show real (ε′) and imaginary part of permittivity (ε″) of BST, BZN, and BZN/BST thin films as a function of frequency. As shown in Fig. 7.6(a), it is found that ε′ for BST, BZN and BZN/BST thin films slightly decreased over the measured frequency range, and the moderate dielectric constants for the BZN/BST bilayered films are observed, which can be attributed to combined effects of high permittivity of BST with low permittivity of BZN. On the other hand, a power-law dispersion of ε′ and ε″ is noted. The empirical dispersion is given by the Curie-von Schweidler relationship:[17]

$$\varepsilon'_{(\omega)} = \varepsilon'_{(0)} - A'\omega^m, \tag{7.3}$$

$$\varepsilon''_{(\omega)} = A''\omega^m. \tag{7.4}$$

In these expressions, ω and $\varepsilon'_{(0)}$ are the angular frequency and the static dielectric constant, respectively, and A', A'', and m are constants. The fitting curve in Fig. 7.6 is calculated by fitting the complex permittivity of the dispersion curve to obtain $\varepsilon'_{(0)}$, A', A'', and m which are listed inset of Figs. 7.6(a) and 7.6(b). Our fitting curves provided $\varepsilon'_{(0)}$ of 449, 134 and 262 for BST, BZN and BZN/BST films, respectively. The Curie-von Schweidler behavior is in consistent with observations in thin film polycrystalline BST and $BaTiO_3$, and has been reported to persist up to GHz range.[17,18,34]

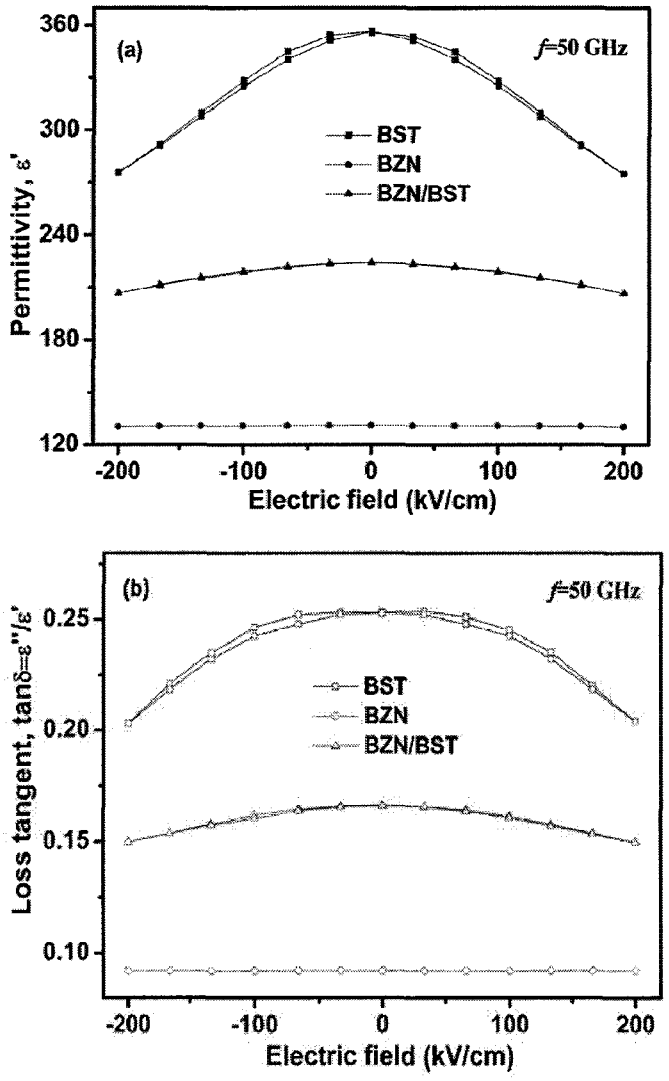

Fig. 7.7. The electric field dependence of (a) ε' and (b) loss tangent (tan $\delta=\varepsilon''/\varepsilon'$) of BST, BZN, and BZN/BST thin films at frequency of 50 GHz, respectively.

Figure 7.7 shows the electric field dependence of (a) ε′ and (b) loss tangent (tan δ= ε″/ε′) for BST, BZN and BZN/BST thin films at 50 GHz, respectively. The zero-bias ε′ for BST, BZN and BZN/BST is 356, 130 and 224, respectively. The tunability, defined as $\{(\varepsilon'(0)-\varepsilon'(V_{max})/\varepsilon'(0)\}\times 100\%$, where ε′(0), ε′($V_{max}$) are the ε′ of the films at zero and the maximum applied voltage, respectively. Thus, dielectric tunability is about 22.89 %, 0.5 % and 7.7 %, respectively; at frequency of 50 GHz with an applied field of ± 200 kV/cm. This is expected as BZN addition is known to lower the dielectric constant and tunability, as shown by Wang *et al.*[7] and Yan *et al.*[8] in BZN/BST multilayer films at low frequency. In a previously published result for a polycrystalline $Ba_{0.5}Sr_{0.5}TiO_3$-$Bi_{1.5}Zn_{1.0}Nb_{1.5}O_7$ composite thin film on $LaAlO_3$(100) substrate, the tunability was ~6.2 % at 7.7 GHz with an applied field of 8.1 kV/cm.[11] The dielectric loss tangent, tan δ (tan δ= ε″/ε′) was also obtained as a function of bias at microwave frequency (50 GHz) which is shown in Fig. 4(b) for BST, BZN and BZN/BST films. At zero-bias voltage, the tan δ for BST, BZN and BZN/BST film is 0.253, 0.092 and 0.166, respectively. The sudden decrease in tan δ for BZN/BST film was undoubtedly ascribed to the presence of low loss BZN phase in BST, which is similar to that observed in the case of BST doped with other dielectrics.[35] The tan δ value for BZN/BST film at 50 GHz is significantly larger than the dielectric loss at 10 kHz (~0.010),[33] but still is within acceptable tolerances for tunable devices. The increase in tan δ in the microwave frequency range can be thought of to be due to a number of reasons, both of intrinsic (due to the interaction of the ac field phonons, including quasi-Debye losses) and of extrinsic (e.g., mobile charged defects, such as oxygen vacancies) nature.[22] Besides, no hysteresis in ε′ (as well as tan δ) versus dc bias is displayed in any of the films shown in Fig. 7.7, although we have reported hysteretic effects for similar BST, BZN and BZN/BST thin films with metal-insulator-metal (MIM) capacitors, where hysteresis was explained by presence of permanent dipoles or dead interfacial layers.[33] Compare to MIM structure, the CPW configuration avoids the most of the parasitic components of the circuit and also the low-permittivity dead layer occurs at the interface of ferroelectric film/electrode.

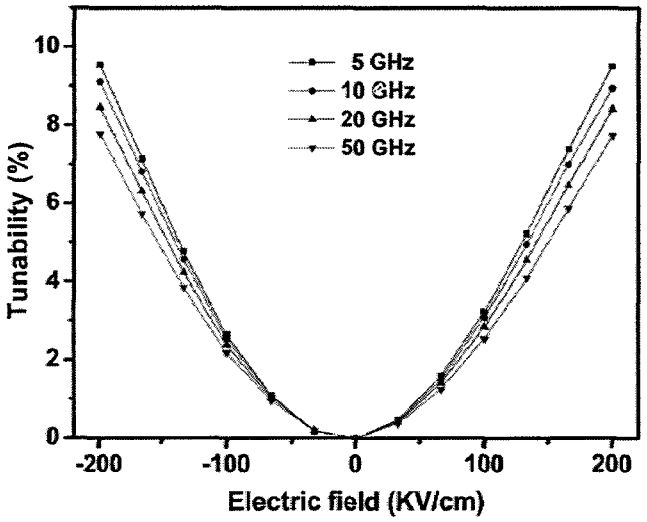

Fig. 7.8. High frequency tunability as a function of electric field at 5, 10, 20, and 50 GHz for BZN/BST bilayered thin films.

Figure 7.8 shows the dielectric tunability as a function of electric field at 5, 10, 20, and 50 GHz for BZN/BST bilayered thin films. The tunability of BZN/BST bilayered thin films displays little frequency dependence. For example, the tunability decreases only from 9.5 % at 5 GHz to 7.7 % even at 50 GHz. There is a substantial decline in the tunability for all the samples at gigahertz frequencies compared to the previous report where the electrical measurements were carried out at 10 kHz.[33] This behavior may not be entirely intrinsic. It is well known that one can expect a precipitous fall in the dielectric response (and hence its tunability) at higher frequencies for materials where the significant portion of the polarization is due to ionic displacements and/or molecular rearrangement in the presence of an external field. However, the decrease in the tunability in the current study and the one previously reported at 10 kHz can also be related to completely different device geometries (CPW versus MIM structure). Since the device geometry is coplanar, the tunability that is reported here for gigahertz frequencies is actually the lower limit since only a portion (typically less than 50%) of the field is confined within the film.[25]

7.2.4 Summary

Perovskite $Ba_{0.6}Sr_{0.4}TiO_3$ (BST), pyrochlore $Bi_{1.5}Zn_{1.0}Nb_{1.5}O_7$ (BZN) and hetero-structures BZN/BST thin films have been grown directly on high-resistivity (HR)-Si substrates by RF-magnetron sputtering. Experimental results showed that the BZN helped in tailoring the dielectric constant and reducing the loss tangent significantly. Moreover, the low microwave loss (~0.167) combined with a high tunability (~7.7 %, 200 kV/cm) until 50 GHz suggest that BZN/BST/HR-Si films could be well suited for integrated into tunable microwave devices.

7.3 Reference

1. D. E. Kotecki, "A Review of High Dielectric Materials for DRAM Capacitors," *Integrated Ferroelectrics*, **16**, 1-19, 1997.

2. C. S. Hwang, S. O. Park, H.-J. Cho, C. S. Kang, H. K. Kang, S. I. Lee, and M. Y. Lee, "Deposition of Extremely Thin (Ba,Sr)TiO_3 Thin Films for Ultra-large-scale Integrated Dynamic Random Access Memory Application," *Applied Physics Letters*, **67**(19), 2819-2921, 1995.

3. J. Im, O. Auciello, and S. K. Streiffer, "Layered $(Ba_xSr_{1-x})Ti_{1+y}O_{3+z}$ Thin Films for High Frequency Tunable Devices," *Thin Solid Films*, **413**(1-2), 243-247, 2002.

4. D. Dimos and C. H. Mueller, "Perovskite Thin Films for High-frequency Capacitor Applications," *Annual Review of Materials Science*, **28**, 397-419, 1998.

5. M. W. Cole, P. C. Joshi, M. Ervin, M. Wood, and R. L. Pfeffer, "Evaluation of Ta_2O_5 as a Buffer Layer Film for Integration of Microwave Tunable $Ba_{1-x}Sr_xTiO_3$ Based Thin Films with Silicon Substrates," *Journal of Applied Physics*, **92**(7), 3967-3973, 2002.

6. D. S. Jeong, C. S. Hwang, J. D. Baniecki, T. Shioga, K. Kurihara, N. Kamehara, and M. Ishii, "Dielectric Constant Dispersion of Yttrium-doped (Ba,Sr)TiO_3 Films in the High-frequency (10 kHz-67 GHz) Domain," *Applied Physics Letters*, **87**(23), 232903-232905, 2005.

7. I. P. Koutsaroff, T. A. Bernacki, I, M. Zelner, A. Cervin-Lawry, T. Jimbo, and K. Suu, "Characterization of Thin-Film Decoupling and High-Frequency (Ba,Sr)TiO_3 Capacitors on Al_2O_3 Ceramic Substrates," *Japanese Journal of Applied Physics, Part 1*, **43**, 6740-6745, 2004.

8. S. H. Kim and J. H. Koh, "The Microwave Properties of Li Doped 0.7(Ba,Sr)TiO_3-0.3MgO Thick Film Interdigital Capacitors on the Alumina Substrates," *Microelectronic Engineering*, **87**, 79-82, 2010.

9. S. W. Liu, Y. Lin, J. Weaver, W. Donner, X. Chen, C. L. Chen, J. C. Jiang, E. I. Meletis, and A. Bhalla, "High-dielectric-tunability of ferroelectric (Pb,Sr)TiO_3 thin films on (001) $LaAlO_3$," *Applied Physics Letters*, **85**(15), 3202-3204, 2004.

10. T. Yamada, K. F. Astafiev, V. O. Sherman, A. K. Tagantsev, P. Muralt, and N. Setter, "Strain Relaxation of Epitaxial $SrTiO_3$ Thin Films on $LaAlO_3$ by Two-step Growth Technique," *Applied Physics Letters*, **86**(14), 142904-142906, 2005.

11. W. Chang, S. W. Kirchoefer, J. M. Pond, J. S. Horwitz, and L. Sengupta, "Strain-relieved $Ba_{0.6}Sr_{0.4}TiO_3$ Thin Films for Tunable Microwave Applications," *Journal of Applied Physics*, **92**(3), 1528-1535, 2002.

12. T. Yamada, P. Muralt, V. O. Sherman, C. S. Sandu, and N. Setter, "Epitaxial Growth of $Ba_{0.3}Sr_{0.7}TiO_3$ Thin Films on Al_2O_3(0001) Using Ultrathin TiN Layer as a Sacrificial Template," *Applied Physics Letters*, **90**(14), 142911-142913, 2007.

13. B. Xiao, H. R. Liu, V. Avrutin, J. H. Leach, E. Rowe, H. Y. Liu, Ü. Özgür, H. Morkoç, W. Chang, L. M. B. Alldredge, S. W. Kirchoefer, and J. M. Pond, "Epitaxial Growth of (001)-oriented $Ba_{0.5}Sr_{0.5}TiO_3$ Thin Films on *a*-plane Sapphire with an MgO/ZnO Bridge Layer," *Applied Physics Letters*, **95**(21), 212901-212903, 2009.

14. M. W. Cole, C. V. Weiss, E. Ngo, S. Hirsch, L. A. Coryell, and S. P. Alpay, "Microwave dielectric properties of graded barium strontium titanate films," *Applied Physics Letters*, **92**(18), 182906-182908, 2008.

15. L. H. Yang, G. S. Wang, D. Rémiens, and X. L. Dong, "Perfectly (001)-and (111)-Oriented (Ba,Sr)TiO_3 Thin Films Sputtered on Pt/TiO_x/SiO_2/Si Without Buffer Layers," *Journal of the American Ceramic Society*, **93**(2), 350-352, 2010.

16. F. Ponchel, J. Midy, J. F. Legier, C. Soyer, D. Rémiens, T. Lasri, and G. Guéguan, "Dielectric microwave characterizations of (Ba,Sr)TiO_3 film deposited on high resistivity silicon substrate: Analysis by two-dimensional tangential finite element method," *Journal of Applied Physics*, **107**(5), 054112-054116, 2010.

17. B. H. Hoerman, G.M. Ford, L.D. Kaufmann, and B. W. Wessels, "Dielectric Properties of Epitaxial $BaTiO_3$ Thin Films," *Applied Physics Letters*, **73**(16), 2248-2250, 1998.

18. J. D. Baniecki, R. B. Laibowitz, T. M. Shaw, P. R. Duncombe, D. A. Neumayer, D. E. Kotecki, H. Shen, and Q. Y. Ma, "Dielectric Relaxation of $Ba_{0.7}Sr_{0.3}TiO_3$ Thin Films From 1 mHz to 20 GHz," *Applied Physics Letters*, **72**(4), 498-500, 1998.

19. T. Hamano, D. J. Towner, and B. W. Wessels, "Relative Dielectric Constant of

Epitaxial $BaTiO_3$ Thin Films in the GHz Frequency Range," *Applied Physics Letters*, **83**(25), 5274-5276, 2003.

20. J.-Y. Kim and A. M. Grishin, "Processing and on-wafer test of ferroelectric film microwave varactors," *Applied Physics Letters*, **88**(19), 192905-192907, 2006.

21. N. D. Xiong, S. W. Jiang, Y. R. Li, L. F. Tan, and R. G. Li, "Dielectric Properties of $Ba_{0.5}Sr_{0.5}TiO_3$/SiN Bilayered Thin Films Grown on Pt-coated Sapphire Substrates," *Applied Physics Letters*, **93**(23), 232905-232907, 2008.

22. A. K. Tagantsev, V. O. Sherman, K. F. Astafiev, J. Venkatesh, and N. Setter, "Ferroelectric Materials for Microwave Tunable Applications," *Journal Electroceramics*, **11**, 5-66, 2003.

23. M. J. Lancaster, J. Powell and A. Porch, "Thin-film Ferroelectric Microwave Devices," *Superconductor Science and Technology*, **11**(11), 1323-1334, 1998.

24. P. Bao, T. J. Jackson, X. Wang, and M. J. Lancaster, "Barium Strontium Titanate Thin Film Varactors for Room-temperature Microwave Device Applications," *Journal of Physics D: Applied Physics*, **41**(6), 063001, 2008.

25. M. W. Cole, C. V. Weiss, E. Ngo, S. Hirsch, L. A. Coryell, and S. P. Alpay, "Microwave Dielectric Properties of Graded Barium Strontium Titanate Films," *Applied Physics Letters*, **92**(18), 182906-182908, 2008.

26. M. Jain, S. B. Majumder, R. S. Katiyar, A. S. Bhalla, F. A. Miranda, and F. W. Van Keuls, "Investigations of Sol-gel-derived Highly (100)-oriented $Ba_{0.5}Sr_{0.5}TiO_3$:MgO Composite Thin Films for Phase-shifter Applications," *Applied Physics A: Materials Science & Processing*, **80**(3), 645-647, 2005.

27. J. Sigman, P. G. Clem, C. D. Nordquist, J. J. Richardson, and J. T. Dawley, "Effect of Microstructure on the Dielectric Properties of Compositionally Graded (Ba,Sr)TiO_3 Films," *Journal of Applied Physics*, **102**(5), 054106-054112, 2007.

28. S. X. Wang, M. S. Guo, X. H. Guo, X. H. Sun, T. Liu, M. Y. Li, and X. Z. Zhao, "Tunable, Low Loss $Bi_{1.5}Zn_{1.0}Nb_{1.5}O_7/Ba_{0.6}Sr_{0.4}TiO_3/Bi_{1.5}Zn_{1.0}Nb_{1.5}O_7$ Sandwich Films," *Applied Physics Letters*, **89**(21), 212907-212909, 2006.

29. X. Yan, W. Ren, P. Shi, X. Q. Wu, X. F. Chen, and X. Yao, "$Ba_{0.5}Sr_{0.5}TiO_3/Bi_{1.5}Zn_{1.0}Nb_{1.5}$ Multilayer Thin Films Prepared by Sol-gel Method,"

Applied Surface Science, **255**(5), 2129-2132, 2008.

30. W. Y. Fu, L. Z. Cao, S. F. Wang, Z. H. Sun, B. L. Cheng, Q. Wang, and H. Wang, "Dielectric Properties of $Bi_{1.5}Zn_{1.0}Nb_{1.5}O_7$/Mn-doped $Ba_{0.6}Sr_{0.4}TiO_3$ Heterolayered Films Grown by Pulsed Laser Deposition," *Applied Physics Letters*, **89**(13), 132908-132910, 2006.

31. W. Y. Fu, H. Wang, L. Z. Cao, and Y. L. Zhou, "$Bi_{1.5}Zn_{1.0}Nb_{1.5}O_7$/Mn-doped $Ba_{0.6}Sr_{0.4}TiO_3$ Heterolayered Thin Films with Enhanced Tunable Performance," *Applied Physics Letters*, **92**(18), 182910-182912, 2008.

32. L. Yan, L. B. Kong, L. F. Chen, K. B. Chong, C. Y. Tan, and C. K. Ong, "$Ba_{0.5}Sr_{0.5}TiO_3$-$Bi_{1.5}Zn_{1.0}Nb_{1.5}O_7$ Composite Thin Films with Promising Microwave Dielectric Properties for Microwave Device Applications," *Applied Physics Letters*, **85**(16), 3522-3524, 2004.

33. L. H. Yang, G. S. Wang, D. Rémiens, and X. L. Dong, "Improved Dielectric Properties of $Bi_{1.5}Zn_{1.0}Nb_{1.5}O_7$/(111)-Oriented $Ba_{0.6}Sr_{0.4}TiO_3$ Bilayered Films for Tunable Microwave Applications," *Journal of American Ceramic Society*, 93(5),1215-1217, (2010).

34. T. Horikawa, T. Makita, T. Kuriowa, and N. Mikami, "Dielectric Relaxation of (Ba,Sr)TiO_3 Thin Films," *Japanese Journal of Applied Physics*, **34**, 5478-5482, 1995.

35. M. W. Cole, C. Hubbard, E. Ngo, M. Ervin, M. Wood, and R. G. Geyer, "Structure-property Relationships in Pure and Acceptor-doped $Ba_{1-x}Sr_xTiO_3$ Thin Films for Tunable Microwave Device Applications," *Journal of Applied Physics*, **92**(1), 475-483, 2002.

CHAPTER 8
Conclusions and Future Work

8.1 Conclusions

This thesis discussed the deposition and characterization of perovskite (Ba,Sr)TiO_3 (BST) films using RF magnetron sputtering with the goal of studying the feasibility of fabricating high quality BST films in an economical manner for tunable microwave devices applications. Several variable parameters like oxygen partial pressure, TiO_x seeding layer, low loss material $Bi_{1.5}Zn_{1.0}Nb_{1.5}O_7$ (BZN), film thickness and substrate, which generally influence the orientation and dielectric behavior of BST films were studied. Some of the main findings are listed below:

(1) The growth and control of crystal orientation of (001)-and (111)-oriented BST films on the same Pt(111)/TiO_x/SiO_2/Si substrates has been achieved. There are some important conclusions that we can draw from this study. Growth of oriented BST film is predominantly dictated by the orientation of the substrate or by the crystallization kinetics. For example, by controlling the O_2/(Ar+O_2) ratios in the sputtering and the deposition rates, we can stabilize the thermodynamically favored equilibrium phase of BST (001) orientation. Very high oxygen partial pressure followed by relatively slow growth rate was found to yield a BST (111) film on Pt (111). At an applied field of 400 kV/cm, high tunability of 52 % and 68 % can be achieved for (001)-and (111)-oriented BST films, respectively. Such achievements demonstrated that the orientation of BST thin films can be controlled on Pt which should enable development of the next generation of ferroelectric devices.

(2) Highly (111)-oriented BST films can also been fabricated on TiO_x-seeded/Pt(111)/TiO_x/SiO_2/Si substrates. The insertion of the ultrathin TiO_x layer changes the orientation of BST from (001) to (111) and results in a significant influence on microstructure and dielectric properties of resultant BST films. Interestingly, highly (111)-oriented BST film [$\alpha_{(111)}$ ~97%] with an optimum5-nm-thick TiO_x seeding layer exhibits a shifted Curie temperature (*Tc*=275 K) and an enhanced tunability of 61.16 % at 400 kV/cm, when compared with (001)-oriented BST without TiO_x layer (*Tc*=250 K and tunability=50.05 %).

(3) Since it is important in microwave devices to have desirable dielectric constant of the material while having at the same time low loss and high tuning and figure of merit, an approach to composite with perfectly (111)-oriented BST thin film with low loss BZN material was made. Introducing of a low loss dielectric BZN combined with perfectly (111)-oriented BST films are demonstrated to be a promising tool to achieve desired material properties required for specific tunable device applications. In the BZN/BST(111) bilayered thin films, the effects of the BZN layer thicknesses were studied. It was observed that the layer thicknesses play an important role in the dielectric properties. The significantly improved figure of merit of 46.8 was obtained as compared to 24.5 for pure BST films deposited by the same conditions. Our findings indicate than BZN/BST (111) bilayered films are promising materials for such tunable device applications which advocate stringent demands of reduced dielectric loss while maintaining moderate tunability.

(4) Based on that perfectly (111)-oriented BST films exhibited excellent dielectric properties, which have more advantages for microwave tunable devices application than (001)-oriented BST films. We have studied the variations in the permittivity with film thickness and measurement temperature for such perfectly (111)-oriented BST thin films on Pt/TiO_x/SiO_2/Si substrates with thicknesses ranging from 45 to 800 nm. All the films showed elongations in the lattice parameter insensitive to film thickness. Temperature-dependent measurements of the permittivity in our BST (111) films revealed unusual Curie temperature independent of thickness, about 305±5 K, at which the phase transition became more diffuse. The interfacial capacitance (d_i / ε_i~0.3 nm) was found to be almost constant in the whole temperature range (77~320 K) and the bulk permittivity ε_b reaches a maximum value at 310 K, suggesting that the unusual *Tc* independence of BST film thickness can also be partially understand by the contribution of bulk BST component.

(5) High (111) epitaxial growth of BST films on sapphire was achieved using an ultrathin (~1.2 nm) TiO_x seeding layer. XRD and pole figure studies suggest that the film with the TiO_x layer (12-Å-thick) is highly oriented along the (111) direction, and

exhibits a good in-plane relationship of BST(111)||Al_2O_3(0001). The frequency dependence obeys a Curie-von Schweidler law over a frequency range of 1 to 40 GHz. The tunability in an epitaxial (111)-textured BST film on TiO_x buffered sapphire was approximately 40.88 %, which was enhanced by 34 %, compared to that in a BST film directly on sapphire. For applications such as phase shifters, the benefits of high tunability dominate over the drawbacks of increased film loss, making our epitaxial films well suited to such applications.

(6) Benefiting from the work that composite BST film with low loss BZN material, the characterizations BZN/BST films on HR-Si at microwave frequency also have been carried out. By employing the same measurement technique on BZN/BST heterostructures, experimental results showed that the BZN helped in tailoring the dielectric constant and reducing the loss tangent significantly. As a result, the moderate permittivity (~224), low microwave loss (~0.167) combined with a high tunability (~7.7 %, 200 kV/cm) until 50 GHz suggest that BZN/BST/HR-Si films have demonstrated a great promise for application in the tunable microwave devices.

8.2 Future Work

Based on the previous experimental results and discussions, this work has opened up several directions and avenues where the materials can be improved and also further studies can be carried out to enhance the importance of the present work in the microwave and related fields of research. Some topics are described briefly below:

(1) The approach of making composites using low dielectric constant and low loss material presented in the present thesis can be applied to other materials ($MgTiO_3$, MgO), where the specific needs of tailoring the losses and dielectric constants are desirable. The multilayer deposition technique presented in this thesis will definitely be useful for many other applications (such as in ferroics and antiferroics), where properties of the two phases are antagonist and the phases maintain their separate identity.

(2) TiO_x buffer layer thickness strongly affects the properties of subsequent layer in the heteroepitaxial growth of a lattice-mismatched structure. The losses in the epitaxial BST (111) thin films are still moderate than the desirable losses for the good microwave devices at high frequencies. Thus, the effect of TiO_x buffer layer thickness on the BST (111) top layer needs to be further investigated in order to optimize the properties of epitaxial films.

(3) TiO_x buffered sapphire substrates make it possible to growth epitaxial BST thin films on big lattice mismatched substrates. Based on the deposition parameters for epitaxial growth BST on sapphire, BST could be grown on TiO_x buffered Si. Thus, crystalline substrates (MgO, $LaAlO_3$, Sapphire), which have been extensively considered for fabrication of tunable ferroelectric devices can be replaced.

Other ideas besides the ones listed above will undoubtedly emerge as one continues the research in these directions. It is the wish of the author that this work has paved the way for future work which will eventually bring the high dielectric constant materials to technological as well as commercial maturity for use in tunable microwave applications.

List of Publications

1. **Lihui Yang**, Genshui Wang, Chaoliang Mao, Yuanyuan Zhang, Ruihong Liang, Caroline Soyer, Denis Rémiens, Xianlin Dong, "Orientation Control of $LaNiO_3$ Thin Films by RF Magnetron Sputtering with Different Oxygen Partial Pressure," ***J. Cryst. Growth***, 311, 4241-4246 (2009).

2. **Lihui Yang**, Genshui Wang, Denis Rémiens, and Xianlin Dong, "Perfectly (001)-and (111)-Oriented (Ba,Sr)TiO_3 Thin Films Sputtered on Pt Without Buffer Layers," ***J. Am. Ceram. Soc.***, **93** [2] 350-352 (2010).

3. **Lihui Yang**, Genshui Wang, Denis Rémiens, and Xianlin Dong, "Improved Dielectric Properties of $Bi_{1.5}ZnNb_{1.5}O_7$/(111)-oriented $Ba_{0.6}Sr_{0.4}TiO_3$ Bilayered Films For Tunable Microwave Applications," ***J. Am. Ceram. Soc.***, **93** [5] 1215-1217 (2010).

4. **Lihui Yang**, Genshui Wang, Denis Rémiens, and Xianlin Dong, "Effects of Ultrathin TiO_x Seeding Layer on Crystalline Orientation and Electrical Properties of Sputtered (Ba,Sr)TiO_3 Thin Films," ***J. Am. Ceram. Soc.***, DOI: 10.1111/j.1551-2916.2010.03677.x, (2010).

5. **Lihui Yang**, Genshui Wang, Denis Rémiens, and Xianlin Dong, "Unusual Curie temperature Independence of Thickness and Interfacial Properties for Perfectly (111)-Oriented $Ba_{0.6}Sr_{0.4}TiO_3$ Thin Films," ***J. Am. Ceram. Soc.***, DOI.10.1111/j.1551-2916.2010.03877.x, (2010).

6. **Lihui Yang**, Freddy Ponchel, Genshui Wang, Denis Rémiens, Jean-Fançois Légier and Xianlin Dong, "Microwave Properties of Epitaxial (111)-oriented $Ba_{0.6}Sr_{0.4}TiO_3$ Thin Films on Al_2O_3 (0001) up to 40 GHz," (Under Review).

7. **Lihui Yang**, Freddy Ponchel, Genshui Wang, Denis Rémiens, Jean-Fançois Légier and Xianlin Dong, "Microwave properties of $Bi_{1.5}Zn_{1.0}Nb_{1.5}O_7$/$Ba_{0.6}Sr_{0.4}TiO_3$ bilayered thin films directly on Si toward 50 GHz," (Prepared).

8. Shu-Tao Chen, Gen-Shui Wang, Yuan-Yuan Zhang, **Li-Hui Yang**, and Xian-Lin

Dong, "Orientation Control Growth of Lanthanum Nickelate Thin Films Using Chemical Solution Deposition," ***J. Am. Ceram. Soc.***, 90 [11] 3635-3637 (2007).

9. Yuanyuan Zhang, Genshui Wang, Ying Chen, Fei Cao, **Lihui Yang**, and Xianlin Dong, "Effect of Donor, Acceptor, and Donor–Acceptor Codoping on the Electrical Properties of $Ba_{0.6}Sr_{0.4}TiO_3$ Thin Films for Tunable Device Applications," ***J. Am. Ceram. Soc.***, 92 [11] 2759-2761 (2009).

10. Yuanyuan Zhang, Genshui Wang, Ying Chen, **Lihui Yang**, Fei Cao, Xianlin Dong, Xiangjian Meng, and Jing Yang, "Highly Temperature Stable Dielectric Properties of Nanograin Barium Strontium Titanate Thin Films Grown on Silicon Substrate," ***J. Am. Ceram. Soc.***, 92 [11] 2795-2797 (2009).

11. Zhiyong Zhou, Yuchen Li, **Lihui Yang**, and Xianlin Dong, "Effect of Annealing on Dielectric Behavior and Electrical Conduction of W^{6+} Doped Bi_3TiNbO_9 Ceramics," ***Appl. Phys. Lett.***, 90 [21] 212908-212910 (2007).

12. R. H. Liang, D. Rémiens, D. Deresmes, C. Soyer, D. Troadec, X. L. Dong, **L. H. Yang**, R. Desfeux, J. F. Blach, "Enhancement in Nanoscale Electrical Properties of Lead Zirconic Titanate Island Fabricated by Focused Ion Beam," ***J. Appl. Phys.***, 105 [4] 044101-044107 (2009).

UNIVERSITE DE VALENCIENNES ET DU HAINAUT CAMBRESIS
LE MONT HOUY - 59313 VALENCIENNES CEDEX 9

THESE DE DOCTORAT
N° ORDRE : 10/19
DISCIPLINE : Electronique

OM DU CANDIDAT : YANG Lihui

ITRE : **INVESTIGATIONS OF SPUTTERED (Ba,Sr)TiO3 THIN FILMS FOR TUNABLE MICROWAVE PPLICATIONS.**

ETUDES DES DEPOTS DE FILMS MINCES DE BASRTIO3 PAR PULVERISATION CATHODIQUE OUR DES APPLICATIONS D'ACCORDABILITE EN MICRO ONDES.

URY :

I. Robert Plana , Prof. LAAS, Toulouse, rapporteur
I. Gérard Tanné, Prof. Lab STICC, Brest, rapporteur
I. Wang Genshui, Prof. SICCAS, examinateur
I. D. Lippens , Prof. IEMN, examinateur
I. Velu Gabriel, MdC habilité, LEMCEL, examinateur
I. Légier Jean-Francois, MdC IEMN, examinateur
I. Dong Xianlin, Prof. SICCAS, Directeur de thèse
I. Rémiens Denis, Prof. IEMN – DOAE, Directeur de thèse

ESUME :

Cette thèse porte sur l'étude des conditions de dépôt et la caractérisation de films minces de $(Ba,Sr)TiO_3$ (BST) ; la chnique de dépôt mise en œuvre est la pulvérisation cathodique magnétron radiofréquence. Ce travail a pour objectif essentiel : démontrer la faisabilité de la fabrication de films de BST de haute qualité et de manière économique, i.e. en utilisant les uipements de la micro électronique (production de masse & bas coût) pour des applications dans le domaine des dispositifs icro-ondes accordables. Nous avons optimisé les paramètres de pulvérisation pour synthétiser parfaitement des couches inces de BST orientées (001) et (111) directement sur des substrats $Pt(111)/TiO_x/SiO_2/Si$ en plasma réactif ou non ; la mpérature de croissance optimale est de 800°C. Ces résultats nous ont permis d'étudier et de comparer les performances ectriques de ces films et de tirer les lois de variation de l'accordabilité en fonction de l'orientation préférentielle du film. ans le cadre de cette étude nous avons fabriqué des films de BST épitaxiés en introduisant une couche d'ensemencement trafine de TiO_2 entre le film et le substrat. Différents type de substrats ont été utilisés : $Si/SiO_2/TiO_x/Pt$, Sapphire et Si haute sistivité. Nous avons obtenu les meilleures propriétés diélectriques possibles pour les dispositifs micro-ondes accordables visagés : forte accordabilité. Le BST est certes le matériau de choix en termes d'accordabilité mais il présente des pertes électriques importantes. A ce titre, afin de diminuer les pertes sans pour autant dégrader les performances de tunabilité, nous ons fabriqué des hétéro structures BST/BZN. Le BZN est très intéressant car les pertes diélectriques sont très faibles mais la nabilité fortement atténuée par rapport au BST. C'est la raison pour laquelle nous avons réalisé des hétéro structures ST/BZN ; l'épaisseur des films de BZN est variable. Nous avons démontré que pour une épaisseur de couche de BZN bien écifique, le facteur de mérite de l'hétéro structure est nettement meilleur que celui d'une mono couche de BST. L'ensemble s caractérisations électriques ont été effectuées en température et en fréquence dans la bande [1 – 60 GHz].

---

outenance prévue le : 28 juin [illegible] **Amphi LCI, Villeneuve d'ascq**